Turbulence Statistics and Eddy Convection in Heated Supersonic Jets

Tobias Ecker

Dissertation submitted to the faculty of the
Virginia Polytechnic Institute and State University
in partial fulfillment of the requirements for the degree of

Doctor of Philosophy
in
Aerospace Engineering

K. Todd Lowe, Chair
William J. Devenport
Lin Ma
Wing F. Ng
Joseph A. Schetz

March 20th, 2015
Blacksburg, Virginia

Keywords: Doppler global velocimetry, supersonic jets, jet noise, compressible shear layers, eddy convective velocity, radiation efficiency

Turbulence Statistics and Eddy Convection in Heated Supersonic Jets

Tobias Ecker

(ABSTRACT)

Supersonic hot jet noise causes significant hearing impairment to the military workforce and results in substantial cost for medical care and treatment. Detailed insight into the turbulence structure of high-speed jets is central to understanding and controlling jet noise. For this purpose a new instrument based on the Doppler global velocimetry technique has been developed. This instrument is capable of measuring three-component velocity vectors over extended periods of time at mean data-rates of 100 kHz. As a demonstration of the applicability of the time-resolved Doppler global velocimetry (TR-DGV) measurement technique, statistics of three-component velocity measurements, full Reynolds stress tensors and spectra along the stream-wise direction in a cold, supersonic jet at exit Mach number $M_j = 1.4$ (design Mach number $M_d = 1.65$) are presented. In pursuance of extending the instrument to planar operation, a rapid response photomultiplier tube, 64-channel camera is developed. Integrating field programmable gate array-based data acquisition with two-stage amplifiers enables high-speed flow velocimetry at up to 10 MHz. Incorporating this camera technology into the TR-DGV instrument, an investigation of the perfectly expanded supersonic jet at two total temperature ratios ($TTR = 1.6$ and $TTR = 2.0$) was conducted. Fourth-order correlations — which have direct impact on the intensity of the acoustic far-field noise — as well as convective velocities on the lip line at several stream-wise locations were obtained. Comprehensive maps of the convective velocity and the acoustic Mach number were determined. The spatial and frequency scaling of the eddy convective velocities within the developing shear layer were also investigated. It was found that differences in the radial diffusion of the mean velocity field and the integral eddy convective velocity creates regions of locally high convective Mach numbers after the potential core. This, according to acoustic analogies, leads to high noise radiation efficiency. The spectral scaling of the eddy convective velocity indicates intermittent presence of large-scale turbulence structures, which, coupled with the emergence of Mach wave radiation, may be one of the main driving factors of noise emission observed in heated supersonic jets.

(337 words)

Acknowledgments

A dissertation is a long, but by no means a lonely journey. Many people have helped and made it possible for me to reach my goals.

First of all, I want to thank my advisor Dr. Todd Lowe, who supported me continuously throughout my development as a graduate student and provided guidance whenever needed. I would like to thank my dissertation committee members Dr. William Devenport, Dr. Lin Ma, Dr. Wing Ng, and Dr. Joseph Schetz for their support and advice over the past years, during which my dissertation research took shape. Especially Dr. Wing Ng has supported my research and ensured that I never lost the 'big picture' of my research out of sight.

I would like to thank my fellow research group students—those who have completed their studies and those just beginning—for their support during my time at Virginia Tech, especially Donald Brooks, Pietro Maisto, and Dan Cadel. Further I would like to acknowledge Isaac Yeaton, AJ Wickersham, David Owens, Tamy Guimarães, Caroline Kirk, Mike Nelson, Brian Petrosky, Alex Schneider, Tyler Englerth, Will O'Connor, Ryan Meritt, Patrick Seiler, and all the others who made my graduate school experience the exciting life period it was.

Further I would like to thank the Office of Naval Research and the research staff at NASA Glenn research center for the financial support and expertise that made this work possible.

I would like to thank the AOE shop and the AOE administrative staff without whom nothing in the department would ever work. At last I want to thank my family and my girlfriend Chrisy Button for their unwavering support during my studies.

Tobias Ecker

March 2015

Contents

List of Figures

List of Tables

Attributions

Several colleagues and mentors aided in the research and writing contained in this dissertation. A brief description of their contributions is included below.

Dr. K. Todd Lowe is the primary adviser and committee chair for this research. He provided extensive guidance on the research plan and provided editorial revisions and advice on the analysis of the experimental data on all manuscripts.

Dr. Wing F. Ng is a committee member and Co-PI for this research. He provided extensive guidance on the research plan and provided editorial revisions on all manuscripts.

Donald R. Brooks has been a valued colleague and provided support for portions of the measurement campaigns described in part III and V of this dissertation. Further, he recorded the laser Doppler velocimetry data analyzed in part **V**.

Part I.

Introduction

Supersonic jet noise — its effect on health and the physics involved in its generation — has been a subject of investigation almost as long as the study of the jet engine technologies that produces it. While from a biomedical point of view the detrimental effects of jet noise on human hearing are of utmost interest (NARC, 2009), the understanding of the multi-faceted physics involved in the noise generation are directly applicable to the development of noise reduction strategies.

On aircraft carriers the noise on the flight deck exceeds safe sound pressure levels by a large degree and reaches peak levels as high as 155 dB. As a result, the U.S. Department of Veterans Affairs (VA) spends almost a billion dollars a year on veteran disability benefits for veterans with hearing loss as the primary disability (NARC, 2009). The Office of Naval Research (ONR) has recently introduced the Noise-Induced Hearing Loss (NIHL) program which aims at optimizing aircraft performance while minimizing noise-induced hearing loss. As part of the NIHL program a Basic Research Challenge (BRC), which included an advanced instrumentation development component, was introduced. Within this framework, this dissertation shows the development of new advanced laser diagnostics for time-resolved velocimetry and new fluid dynamics insights from measurements in supersonic heated jets.

Non-intrusive optical investigation of compressible flows originated in the late 19th century, when Schlieren photography enabled the first qualitative flow field studies (Mach and Salcher, 1890). The introduction of laser technology in the 1970s has provided many new experimental techniques and a corresponding breakthrough in the fundamental understanding of many aspects of flow physics. Experimental techniques like laser Doppler velocimetry (LDV) and particle image velocimetry (PIV) have previously been used to obtain time-resolved and whole flow field data, respectively. The technique used in this dissertation is called Doppler global velocimetry (DGV) and is based on the Doppler effect. When this technique was patented in 1990, its main intent was to provide a whole flow field alternative to PIV, particularly well suited for high-speed flow applications. In this work the first three-component time-resolved implementation of this technique, and its application to supersonic cold and heated jets at conditions relevant to military aircraft jet exit plumes, is presented.

1. Structure and contents

This dissertation is divided into several self-contained parts:

Part I provides prefatory information to the main topics of this dissertation.

Part II contains a brief literature review with a focus on the the aspects not covered in the main manuscript chapters.

Part III is the first research study published as "Development and application of a point Doppler velocimeter featuring two-beam multiplexing for time-resolved measurements of high speed flow" in Experiments in Fluids (2014) (55:1819, DOI 10.1007/s00348-014-1819-0). This paper contains an in-depth study on uncertainties of the time-resolved DGV (TR-DGV) technique, as well as the application of a new point Doppler velocimeter (pDV) to a cold, screeching, supersonic jet. Mean flow velocities and full Reynolds stress tensors along the streamwise direction near the jet centerline are presented. The capability to record time-resolved, long duration, three-component velocity data is leveraged by determining the spatial development of velocity auto- and cross-correlations, as well as auto and cross-spectra. From cross-correlations, the screech tone feedback mechanism is revealed as a phase-coordinated shock motion, having direct impact onto the radial/azimuthal shear stress production.

Part IV is a technical design study, "A rapid response 64-Channel photomultiplier tube camera for high-speed flow velocimetry" published in Meas. Sci. Technol. 26 (2015) 027001 (6pp) (DOI 10.1088/0957-0233/26/2/027001). This brief technical communication contains the technical details on the development of a new, rapid response photomultiplier camera system which enables optical flow observations at 64 points in a plane at up to 10 MHz. This camera system is an enabling technology and the basis for the instrumentation described and applied in the chapters to follow.

Part V is the second research study, "Eddy Convection and Statistical Correlations in the Developing Shear Layers of Heated Supersonic Jets". In this study TR-DGV is extended onto a plane with 32 measurement points, recording data in a supersonic, perfectly expanded and heated jet at two total temperature ratios. Limited data exist on the behavior of eddy convection in high Reynolds number, supersonic plumes, particularly for heated jets. From the experimental data, second and fourth order space-time correlations, integral time-scales and convection velocities on the lip line, at different streamwise locations, are found. LDV data were used to elaborate the importance of the fourth order correlation in the region of immediate interface between the potential core and the shear layer. Maps of the integral convective velocity and acoustic Mach number were generated, indicating significant changes in jet spreading similar to heated subsonic jets for density ratios below unity.

Part VI contains a study on the distribution and scaling of convective wave speeds in the shear layers of heated, supersonic jets. The convective wave speeds, and their scaling with density ratios at conditions similar to operating conditions of tactical aircraft jet plumes, are of special interest as they hold direct impact on the peak radiation of the noise emission. The results are analyzed for cases of varying total temperature ratio to establish

stream-wise scaling and development of the eddy convective speeds and their spectral behavior. The presented data at several locations in the shear layer and near the centerline indicate the presence of high momentum, high velocity, large-scale eddies in regions of locally reduced mean velocities. The difference in the radial diffusion of the mean velocity field and the integral eddy convective velocity along the streamwise coordinate creates regions of locally high convective Mach numbers leading to high convective amplification factors. Based on the presented data it is hypothesized that the intermittent presence of large-scale turbulent structures in regions after and surrounding the potential core leads to an increase in radiation efficiency, which coupled with the emergence of Mach wave radiation is one of the key drivers of noise emission observed in heated supersonic jets.

Part VII contains a summary of the conclusions of this dissertation and additionally brief outlook identifies future work to be done.

Formatting of each chapter contents and citations style may deviate due to the different publication guidelines of the journal in which they are intended to be published.

2. Achievements

Some primary accomplishments of this work include:

- A new time-resolved DGV variant has been established and supported by substantial analysis on uncertainty and dynamic range. Application to a cold, supersonic and screeching jet has proven its real-world applicability and indicated new information about the radial/azimuthal shear stress generation due to the acoustic feedback mechanism.

- The point technique was advanced to a planar variant using a newly developed photomultiplier camera with 32/64 points. Experimental time-resolved velocimetry data at 250 kHz have been successfully demonstrated.

- Experiments in a perfectly expanded supersonic jet at total temperature ratios of 1.6 and 2.0 have been performed. The data were used to obtain integral time-scales, second- and fourth-order correlation coefficients and space-time peak correlations maps. Further, the data were analyzed for the spatial distribution of integral eddy convective velocities and acoustic Mach numbers.

- The spectral scaling of the eddy convective velocity is used to develop a conceptual mechanism explaining the dominant drivers in hot supersonic jet noise.

References

E. Mach and P. Salcher. Optische Untersuchung der Luftstrahlen. *Annalen der Physik und Chemie*, 277(9):144–150, 1890. doi: 10.1002/andp.18902770910.

NARC. *Report on Jet Engine Noise Reduction*. Naval Research Advisory Committee, April 2009.

Part II.

Literature survey

1. The supersonic jet

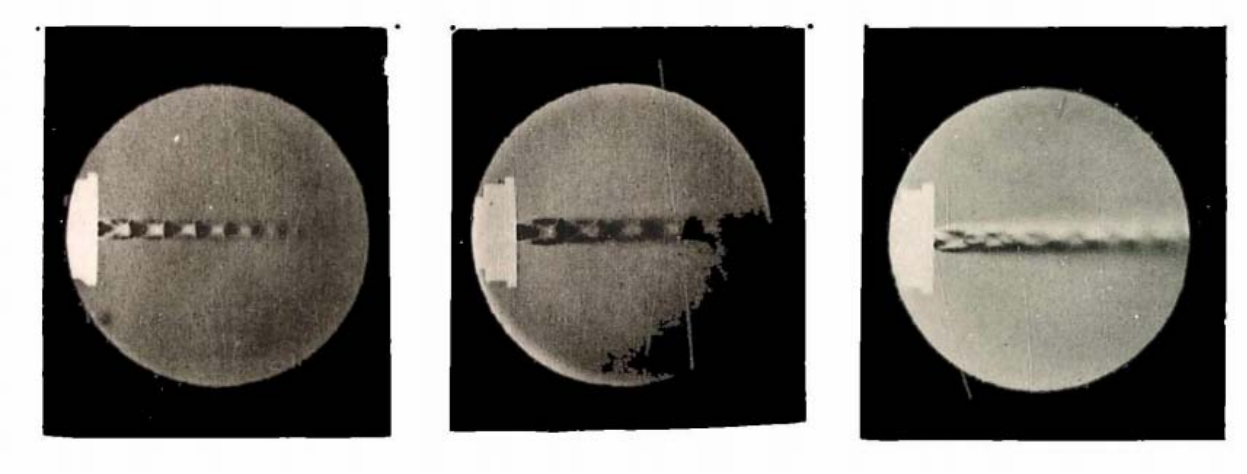

Figure 1.1: Schlieren photographs recorded by Mach and Salcher (1890)

Supersonic jets are present in many technical and natural processes, ranging from military supersonic aircraft, to supersonic coating nozzles, and to volcano eruptions. Research on the supersonic jet first started at the end of the 19th century when Austrian scientists Mach and Salcher (Mach and Salcher, 1890) described for the first time the structure of a sonic jet flow in their 1890 paper on optical measurements in jets, a work following on their work on ballistic projectiles (Mach and Salcher, 1889a,b). Part of the Schlieren photographs published by Mach and Salcher (1890) are shown in figure 1.1; the shock cell structure of the sonic jet is clearly visible. Supersonic jets are very different from their subsonic counterparts. They exhibit a distinct cell shock structure with a complex flow geometry of compression and expansion waves. Apart from the perfectly expanded situation ($p_e = p_a$), the cases of the over-expanded ($p_e < p_a$) and under-expanded ($p_e > p_a$) jet exist.

A special technical occurrence of supersonic jets is at the nozzle exit of supersonic tactical aircraft. Very rarely is a supersonic jet expanded perfectly — while a jet engine exhaust nozzle at sea level usually is over-expanded, at high altitudes it often is operated at under-expanded conditions (Ennix et al., 2012; Holzman et al., 1996). In order to reduce off-design operation, variable geometry nozzles are used in this type of aircraft (Gamble, 2004).

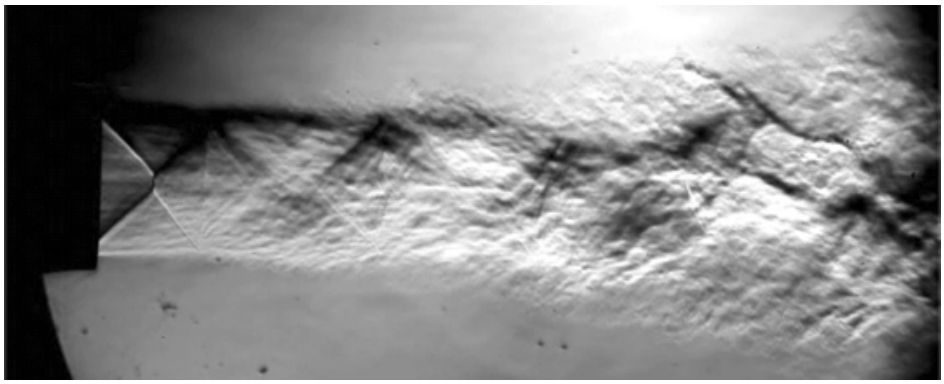

$NPR = 3.2, TTR = 1$

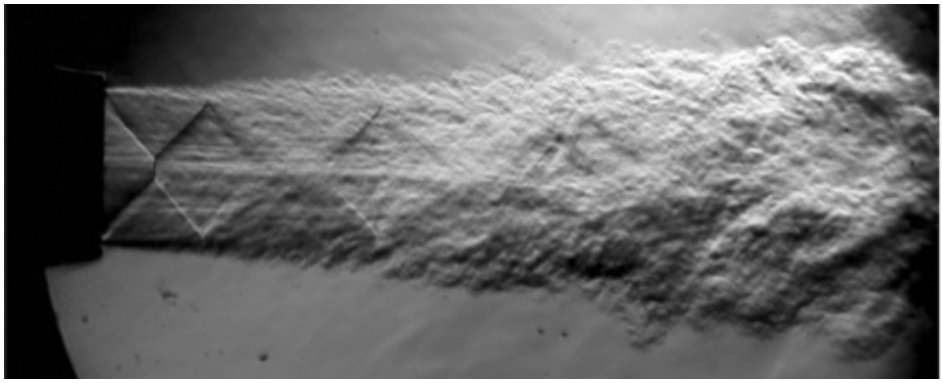

$NPR = 3.2, TTR = 2$

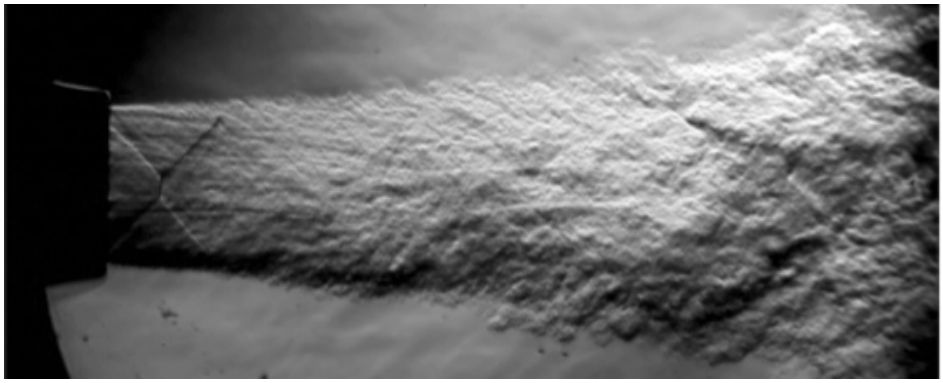

$NPR = 3.2, TTR = 3$

Figure 1.2: Schlieren photographs of an over-expanded supersonic jet at different TTR conditions in the VT hot jet facility

For F-16XL (Holzman et al., 1996) and F-18 (Ennix et al., 2012) tactical aircraft, detailed studies on operating conditions of the GE F110 at sea-level/flight deck and the GE F404 engine at various altitudes have been published. On the ground deck the F-16XL was operated at total temperature ratios (TTR) between 1.65 and 2.75 at nozzle pressure ratios (NPR) between 1.02 and 2.57. At 3800 ft TTRs up to 3.3 andNPRs up to 5 were reached when operating at intermediate power.

Schlieren photographs of an over-expanded supersonic jet at various TTR conditions are shown in figure 1.2. At over-expanded conditions the pressure at the exhaust plane is lower than the ambient pressure; this causes an oblique shock wave as well as a normal shock disc in the center to form. After this, the shock wave reflects of the free jet boundary and a series of expansion fans follow. If it were not for viscous and instability effects this structure would be repeated indefinitely. The stresses on the interface between the jet and its surrounding eventually lead to a breakdown of the nominally irrotational region called the potential core. More details on the development of the mean velocity and the normal and shear stresses in the cold, screeching jet can be found in part III. Increasing the TTR leads to significantly increased shear layer growth and supersonically convecting eddies.

1.1. Compressible mixing and shear layers

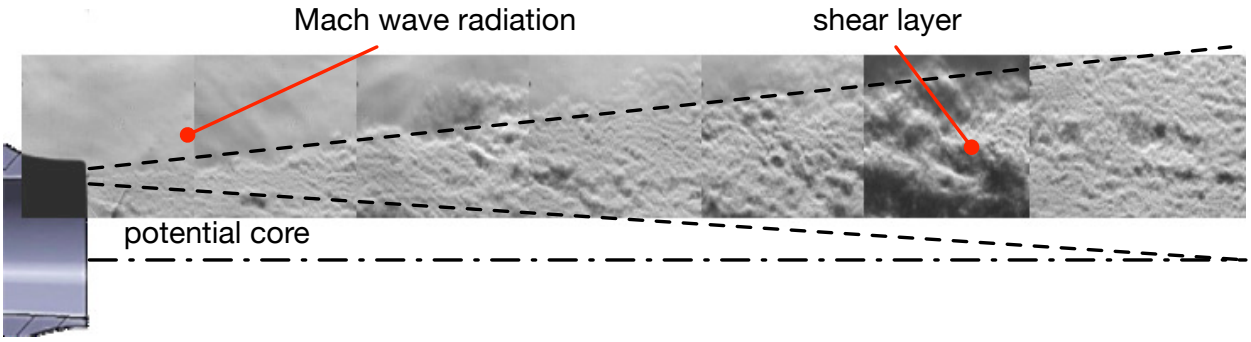

Figure 1.3: Composite Shadowgraph/Schlieren of the shear layer development in a heated supersonic jet

Mixing and shear layers are generated at the interface between two fluids moving at different velocities. They are generally defined by the difference in velocity, density and molecular composition. A composite image of several Shadowgraph/Schlieren images along the shear layer of a supersonic heated jet is shown in figure 1.3. It can be seen clearly that the growth of the shear layer coincides with the development of large scale turbulent structures, entraining and mixing fluid from the colder fluid at rest.

A study on the influence of density and compressibility onto the large structures in turbulent mixing layers was presented by Brown and Roshko (1974b). One of the fundamental insights of this study was the indication that compressibility effects seem to be dominant over density effects in the growth of turbulent shear layers at very high density ratios. Their analysis showed that at low Mach numbers turbulent mixing is incompressible, independent of different densities between the two mixing streams. At higher Mach numbers, however, the mixing is influenced by compressibility effects, introducing Mach number dependent terms into the Reynolds transport equations - specifically in the pressure-velocity correlation and (possibly) the pressure gradient. Using the shear layer growth as a metric,

Brown and Roshko found that the shear layer growth was reduced for increasing density ratios for both incompressible and compressible shear layers. The convective Mach number, which is the Mach number with respect to a frame of reference traveling with the average large scale structure of the flow (Samimy and Elliott, 1990) is defined as:

$$M_{c1} = \frac{U_1 - u_c}{a_1} \quad \text{and} \quad M_{c2} = \frac{u_c - U_2}{a_2} \tag{1.1}$$

where a is the speed of sound, U the mean velocity and u_c is the eddy convective velocity. Subscripts (1) and (2) stand for the jet core and the co-annular flow. At high convective Mach numbers shear layer growth is strongly reduced compared to the incompressible case, asymptotically reaching about 20% of the incompressible value at high density ratios (Gutmark et al., 1995).

The symmetric value of the convective Mach number is a measure of the overall compressibility of a shear flow:

$$M_{csym} = \frac{U_1 - U_2}{a_1 + a_2} \tag{1.2}$$

For the case of a single air jet into air, the symmetric convective Mach number becomes $M_{csym} = \frac{M_1}{1+a_2/a_1}$ and is only a function of the exit Mach number, the total temperature and ambient temperature.

In order to determine the development of flow structures and associated length scales, Brown and Roshko (1974b) recorded high-speed video in their subsonic testing facility and analyzed the development of discernible structures. As their experiment is based on similarity assumptions, a general increase in length scale (mean size of eddy and mean spacing between eddies) with distance was expected. As each eddy travels at a constant convection speed, this would require a decreasing frequency of occurrence at any given station. From this apparent conflict and their statistical observations, the authors determined the process of vortex pairing, which was first described by Winant and Browand (1974) as the likely phenomenon.

The effect of the convective Mach number — as a measure of the compressibility on the growth and entrainment of compressible shear layers was investigated by Samimy and Elliott (1990). The authors found the scaling factors suitable to collapse both their data and literature values using the shear layer growth rate as well as momentum thickness, both heavily dependent on compressibility effects. Additionally, they noted a decrease in stream-wise and lateral turbulence fluctuations, and a decrease in lateral transport of kinetic energy with increasing convective Mach numbers, suggesting a concurrent decrease in small and large-scale mixing (Samimy and Elliott, 1990). Goebel et al. (1990) applied a laser Doppler velocimeter to a supersonic shear flow in order to measure mean flow properties and turbulence statistics. As the convective Mach numbers in this study were between 0.2 (s = 1.41) and 0.45 (s = 0.64), the compressibility effects observed were only moderate. The authors reported increased shear layer growth of

the high density ratio case, however, based on Brown and Roshko's analysis (1974b), density ratio and compressibility effects likely contributed to these results at similar orders of magnitude.

A very comprehensive review on mixing enhancement in supersonic free shear flows, including a comparison between subsonic and supersonic shear layers, is given by Gutmark et al. (1995). In subsonic shear layers, the fluid entrained by the vortices in the shear layer stays unmixed until vortex pairing. Span-wise instability generates stream-wise vorticies leading to enhancement of the mixing process. This interaction increases the three-dimensionality of the flow (Dimotakis and Brown, 1976), similar to what can be seen in figure 1.3, near the end of the potential core. Similarly, increasing convective Mach numbers leads to increasing 3-dimensionality. Further, supersonic jets often exhibit Mach wave radiation (Ffowcs Williams, 1963) generated from eddies moving at supersonic phase speeds compared to ambient conditions.

1.2. Fundamentals of jet noise and the application of the acoustic analogy

1.2.1. Jet noise

Supersonic jet noise may be composed of several major acoustic phenomena: (1) the screech tone phenomena, (2) broadband shock associated noise and (3) turbulent mixing noise. While the screech tone can be predicted relatively well, difficulties arise on the understanding of the turbulence in the supersonic jet (Tam and Auriault, 1999). The magnitudes of these acoustic phenomena vary strongly with direction.

Screech is primarily present in supersonic cold jets operated at over-expanded conditions. This narrow band noise phenomenon is created by a self-sustaining feedback mechanism within the jet shock train (Camussi, 2013). The screech tone propagates mainly in the upstream direction and has higher harmonics present orthogonal to the stream-wise direction(Tam, 1995). Its intensity decreases with increasing jet temperature (Tam, 1995) and is therefore less of an issue for aircraft noise.

Broadband shock associated noise is jet noise associated with the presence of shocks due to either off-design operation or to nozzle imperfections. It has discrete tones and a broadband component and is strongly directional (Camussi, 2013).

In the current work, the large scale turbulent mixing noise is of primary interest. A large portion of this noise component stems from a phenomenon called Mach wave radiation, which is caused by supersonically convecting eddies. Previous works (Tam and Morris, 1980) have demonstrated that the large scale structures, which may be explained by instability waves from a wavy wall analogy (Tam et al., 1992), radiate directly to the far field.

1.2.2. Acoustic analogy for jet noise prediction

Acoustic analogies for noise prediction have been used since the early 1950's when Lighthill (1952) presented his theory on aerodynamically generated sound. Morris and Farassat (2002) give an excellent definition of the meaning of the acoustic analogy:

> "The definition of an acoustic analogy [...] is an aerodynamic noise theory in which the equations of motion for a compressible fluid are rearranged in a way that separates linear acoustic propagation effects. By definition, this rearrangement results in a set of equivalent sources that are assumed to be non-negligible in a limited region of space".

It is to be noted that these equivalent sources are fictitious and of a mathematical nature (Farassat et al., 2004), which means that they are not based on any physical assumptions but rather stem from the rearrangement of the Navier-Stokes equations. Many models have been developed based on the acoustic analogy as proposed by Lighthill, they deviate mainly by the way how the acoustic sources and the propagation are decomposed. Ffowcs Williams (1963) pioneered the acoustic analogy for jet noise prediction by taking into account the relative movement of the noise sources to the observer (Karabasov, 2010). Many acoustic analogies based on Lighthill and extending the work done by Ffowcs Williams can be found in the literature. Bailly et al. (1997) give an excellent overview of some of the models used for jet noise prediction.

A widely used analogy has been proposed by Ffowcs Williams (1963) and was refined by Ribner (1969), which is described here in brief based on the nomenclature presented by Bailly et al. (1997).

$$\frac{\overline{\rho'(x,t)\rho'(x,t+\tau)}}{\rho a_0^{-3}} = R_a(x,\tau) \tag{1.3}$$

$$R_a(x,\tau) = \frac{1}{16\pi^2 a_0^5 x^2}\frac{\partial^4}{\partial \tau^4}\iiint_V D_{ijkl}R_{ijkl}\left(\mathbf{y},\eta,t\right)\delta\left(t-\tau-\frac{x\cdot\eta}{xa_0}\right)dy\,d\eta\,dt \tag{1.4}$$

where $D_{ijkl} = r_i r_j r_k r_l / r^4$ and $R_{ijkl}\left(y,\eta,\tau+\frac{x\cdot\eta}{xa_0}\right) \approx \overline{T_{ij}[y,t]T_{kl}[y+\eta,t+\tau]}$ and T_{ij} is the Lighthill stress tensor.

$$T_{ij} = \rho u_i u_j + (p - a_0^2\rho)\delta_{ij} - \tau_{ij}$$

In the convective frame this correlation function can be expressed as

$$R_a(x,\tau) = \frac{1}{16\pi^2 a_0^5 x^2}\frac{1}{C^5}\iiint_V D_{ijkl}\frac{\partial^4}{\partial t^4}R_{ijkl}(\mathbf{y},\xi,t)\,\delta\left(t-\frac{\tau}{C}\right)dy\,d\xi\,dt \tag{1.5}$$

where $C = \left[\left(1-M_a\cos\hat{\theta}\right)^2+\alpha^2 M_a^2\right]^{1/2}$*and R_{ijkl} in the convective reference frame is $R_{ijkl}(y,\eta,\tau) = R_{ijkl}(y,\eta,\tau-u_c t y,\tau) = R_{ijkl}(y,\xi,t)$. The noise intensity $I(x)$ can be found by evaluating the correlation function $R_a(x,\tau)$ at $\tau = 0$.

The aim of this section was not to give an extensive overview of the theoretical approaches in the literature, but rather to indicate how the fluid mechanics influences the acoustics. The application of most, if not all, acoustic analogies to jet flows leads to the following ramifications with regards to how the properties of the turbulent flow relate to the observed noise intensity:

- The efficiency and directionality of the noise radiation is directly affected by the convective speed of the correlated turbulent structures.
- The intensity of the density fluctuations is proportional to the volumetric integral of the delay time fourth-order correlations R_{ijkl}.
- The turbulence level feeds into the equivalent source field as part of the Lighthill stress tensor T_{ij}. Similarly the spatial correlation of turbulence influences the power spectral density (which is the Fourier transform of the correlation function) of noise.

*for the purpose of this analogy the acoustic Mach number is defined as $M_a = \frac{u_c}{a_0}$. The acoustic Mach number is also known as convective Mach number, but exact definition may change from author to author.

2. Velocimetry for compressible flows

Various techniques have been developed to experimentally determine velocities and related turbulence statistics in a flow. Generally, most techniques were first proven in the application to subsonic and incompressible flows and then extended to compressible flows. Commonly, the available velocimetry techniques can be divided into intrusive and non-intrusive techniques. A non exhaustive qualitative hierarchy of commonly used techniques for compressible turbulent flows is shown in figure 2.1 . The overview given here focuses on high temperature flow applications.

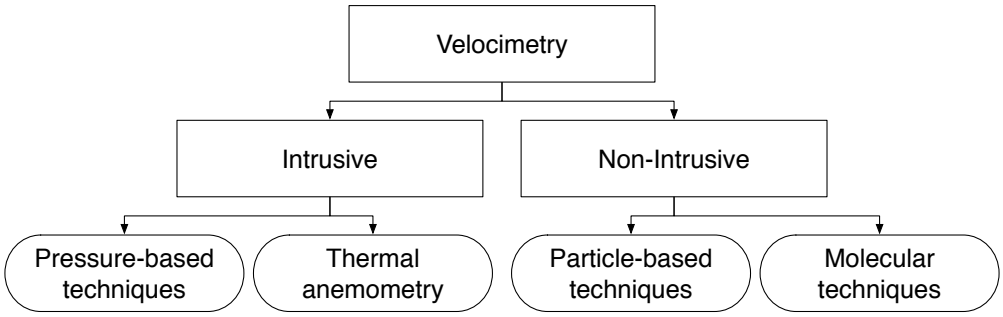

Figure 2.1: Measurement techniques for compressible flows

2.1. Pressure-based techniques

The very first pressure based instruments capable of measuring fluid velocities were developed by French engineer Henri di Pitot around 1732, and systematically refined by Henry Darcy in 1856 (Brown, 2001). This instrument as it was developed is still used today in a large variety of flow applications. Today modern multi-hole probes capable of measuring velocity vectors exist. Due to the intrusive nature of the technique, supersonic flow causes a bow shock around the tip of the probe , which results in sensing the flow properties downstream of the shock instead of the freestream. Similarly, the integral measure of the pressure over the spatial extent of the probe hole may cause non-linear readings with exaggerated velocity magnitudes in flows with large shear gradients (Tropea et al., 2007). An overview of pressure-based aerodynamic probes for time-resolved applications in turbomachinery has been given by Kupferschmied et al. (2000). Current fast-response aerodynamic probes have typical frequency responses up to 50 kHz and find application in moderately hot (T_{max} = 200 $^{\circ}C$) flows. Recent developments have shown special high-temperature probes with application to flows up to 533 K (Lenherr et al., 2011). Applications of pressure-based techniques for velocimetry in supersonic jet flows, with emphasis on turbulence or eddy convective velocities, are not known to this author.

2.2. Thermal anemometry ("Hot-wire" anemometry)

Hot-wire anemometry, a subset of thermal anemometry, has been used for many flow experiments, especially when frequency response and time series data is of interest, and it is still considered a standard for velocimetry (Bowersox, 1996; Johnson and Rose, 1975). Introduced in the early 19th century, hot-wires are capable of measuring mean and fluctuating flow variables (velocity, temperature, mass flux) at a point in up to three dimensions. The key element of the hot-wire instrument is the thin conductive wire held by a system of prongs in the flow under observation. An electric current is applied to the wire element and modified by the flow-induced heat transfer. Three types of hot-wire techniques exist: the constant-temperature anemometer (CTA), constant-voltage anemometer (CVA) and the constant-current anemometer (CCA). Hot-wires have successfully been used in all kinds of flows ranging from subsonic low-speed flows (Vagt, 1979), supersonic boundary layers (Bowersox, 1996), supersonic shear layers (Martens et al., 1996) to hypersonic flows (Maddalon et al., 1970; Spina and McGinley, 1994).

The wire element has a diameter between $0.5 - 5\mu m$ and a length between 0.1 and 2 mm (Lomas, 2011; Tropea et al., 2007). The wire is heated by an electric current to a temperature above the static temperature of the fluid. Hot-wires are typically heated to up to about 300 $^{\circ}C$, and limitations arise due to increasing non-linearity in the heat transfer coefficient with temperature loading (e.g. compare Kovasznay, 1950). The ratio of the hot-wire temperature to the static temperature of the flow is called overheat ratio. Materials used for the wire element include tungsten, platinum, platinum-iridium, platinum-rhodium or even carbon filaments. Material selection is based on mechanical strength (velocity induced shear), maximum temperature (oxidation), as well as sensitivity.

Johnson and Rose (1975) as well as Bowersox (1996) compared the use of a laser velocimeter and a CTA in a supersonic boundary layer and found good agreement between both techniques. Smits et al. (1983) reviewed the practice of hot-wire anemometry in supersonic flow and found the following issues: (1) formation of a detached shock from the prong tips leads to a complicated flow field, and (2) attenuation of small scale contributions due to the length of the hot wire filaments being much larger than the typical Kolgmorov length scales in a supersonic shear layer - therefore leading to a distortion of the high frequency end of the spectrum. In compressible flows, the probe sensitivities due to density, pressure and stagnation temperature are difficult to separate (Smits et al., 1983; Walker et al., 1989). Walker et al. (1989) compared two constant temperature hot-wire probes in supersonic flow for mass flux and temperature measurements. They used a single hot-wire with rapid overheat scanning and a two wire probe with different overheat ratios, and found the two-wire technique prone to error.

In heated flows, additional limitations due to the material of the hot-wire arise. Oxidation of the probe wire might significantly alter the heat transfer properties and lead to incorrect readings. Bare tungsten wire will begin to oxidize above temperatures of 600 K (Smits et al., 1983). Platinum wires wires have a threshold of about 1373 K before

oxidation occurs. Platinum-iridium and platinum-rhodium alloy probes have a lower oxidation temperature of about 1073 K (Lomas, 2011). An overview of some of the typical hot-wire material properties from the literature is given in table 2.1. Previous work (Maddalon et al., 1970) has shown problems with wire failure due to unequal temperature distribution caused by temperature fluctuations on the hot-wire. As Troutt and McLaughlin (1982b) write, "The most reliable turbulence instrument, the hot-wire anemometer, cannot be used in conventional high-speed air jets because the dynamic pressures are too great for the fragile probes." Today almost all features of the hot-wire instrument can be covered by non-intrusive optical instruments, further described in the next sections, as well as in chapter V of this dissertation.

Table 2.1: Hot-wire material properties

Material	Oxidation temperature	Reference
Tungsten	600 K	Smits et al. (1983)
Platinum plated tungsten	∼600 K	Vagt (1979)
Platinum-iridium	1073 K	Lomas (2011)
Platinum-rhodium	1073 K	Lomas (2011)
Platinum	1373 K	Lomas (2011)

2.3. Particle-based techniques

Particle-based techniques measure the velocity of very small tracer particles assumed to follow the local flow. The most commonly encountered techniques are laser Doppler velocimetry (LDV), particle image velocimetry (PIV) and Doppler global velocimetry (DGV). While both LDV and DGV are based on the optical Doppler effect, PIV extracts velocity from the correlation between two consecutive images.

In 1964 the first LDV[†] systems were introduced as a technique for experimental fluid mechanics. Due to its non-intrusive nature LDV quickly became a standard for velocimetry and is still widely used today. Most modern systems are based on the dual beam configuration, which is also known as the fringe technique. The working principle is as follows: Two coherent laser beams are crossed and define a measurement volume. A particle passing through this volume scatters the light, wich is recorded by a sensor. The optical Doppler effect describes the change in the apparent frequency of the light due to a moving emitting source. From the recoded light signal the differential Doppler frequency can be detected. Using the measurement geometry, the particle velocity can be estimated at low uncertainties. using several beam pairs two and three-component velocity measurements are possible. The fundamentals of LDV are described in detail in Tropea et al. (2007); Albrecht et al. (2002). LDV has extensively been used for measurements in cold and hot subsonic and supersonic jets in the past (Lau et al., 1979; Lau, 1980, 1981; Kerhervé et al., 2004a,b,

[†]The LDV technique is also known as laser Doppler anemometry (LDA).

2006; Brooks and Lowe, 2014; Brooks et al., 2014).

DGV is an optical, non-intrusive, particle-scattering-based velocimetry technique which like LDV is based on the Doppler effect. To determine the Doppler shift it uses the absorption characteristics of molecular gas cells. It was first developed in 1990 by Komine (1990) and further refined by Komine et al. (1991); Meyers and Komine (1991); Meyers (1992); Meyers et al. (2001a). DGV is a planar alternative to particle image velocimetry (PIV) and is particularly well suited for high-speed flows due to its absolute uncertainties. As multiple particles may contribute to the Doppler signal, sufficiently high concentrations of very small particles may produce continuous data sets with minimal particle lag. Using multiple cameras and lasersheets enables two and three-component measurements. DGV has been applied to supersonic jets for mean velocity (Cadel et al., 2014a) and instantaneous velocity fields (Smith, 1998), spectra and turbulence statistics (Ecker et al., 2014a) as well as convective velocity measurements (Ecker et al., 2014b; Lowe et al., 2012a; Ecker et al., 2014a; Thurow, 2005; Thurow et al., 2008; Ecker et al., 2014c). Some of these results are contained within this dissertation and can be found in parts III, V and VI. An exhaustive review of the current state-of-the-art of the DGV technique can be found in part III.

Particle image velocimetry (PIV)[‡] was introduced in the 1980s and evolved as a very successful measurement technology, especially after the introduction of digital cameras and new computational processing techniques (Willert and Gharib, 1991). PIV compares two recorded camera frames via a windowed cross-correlation technique in order to determine the frame displacement. From this, the velocity within the interrogation windows can be determined. Commonly PIV is used for two (planar PIV) and three-component (stereoscopic PIV) velocity measurements in a plane, but also small volumetric measurements using holographic and tomographic techniques have been demonstrated (Elsinga et al., 2006; Sheng et al., 2006; Fahringer and Thurow, 2012). While the original digital PIV systems only allowed a datarate (based on camera frame rate) of 30 Hz or lower, new systems known as time-resolved PIV (TR-PIV) allow data rates up to 50 kHz (Wernet, 2007b). An overview of PIV specifically in supersonic flows, including the implications of flow seeding, is given by Scarano (2008a). In previous studies PIV and TR-PIV were applied to cold and hot subsonic, as well as supersonic jets and used to determine turbulence statistics and time correlations (Fleury et al., 2008; André et al., 2014, 2013; Bridges and Wernet, 2011b; Bridges et al., 2011; Pokora and McGuirk, 2012; Alkislar et al., 2000).

The application of optical techniques in supersonic jets is further surveyed in part V. All these techniques rely on particles introduced into the flow, therefore particle lag and frequency response need to be considered. Ultimately the amount of particles seeded into the flow also determines the possible data rates. Seeding for high pressure facilities is never trivial and it accounts largely for the success of an experiment. Each facility and instrumentation has different

[‡]The digital variant of PIV was termed DPIV, but the original term PIV has continued to be used.

requirements; Ecker (2011) gives an overview of current seeding mechanism and discusses in detail the implications of particle lag. Further general information on seeding may be found in Crosswy (1985); DeLapp and Reeder (2006); Kähler et al. (2002); Lepicovsky and Bruckner (1996); Melling (1997); Meyers (1991); Sabroske (1993); Seegmiller (1985). Hot flows have additional requirements that may prevent certain seeding materials from being used. Commonly used polystyrene latex spheres have a melting point of about $80°C$ (SPF, 1995) . Similarly, many oil based seeding methods cannot be used due to danger of combustion and smoking, therefore metallic or ceramic powders are often used in hot and combusting flows. Wernet et al. (1995) demonstrated a stabilized alumina/ethanol technique that prevents conglomeration when seeding high temperature flows.

2.4. Molecular techniques

Molecular based techniques, unlike particle based techniques do not require flow seeding. Instead they rely on photonic excitation (usually by a laser) of the fluid molecules in the flow. Molecular tagging velocimetry and Rayleigh scattering are some of the measurement techniques in this category. Some of these techniques are more suitable to obtain other flow properties, or in some cases velocimetry only in combination with other measurements. A very brief overview is given here.

Rayleigh scattering originates from the oscillation of electrons in the fluid molecule, caused by an electromagnetic field. The Rayleigh scattering is coherent and sensitive to density fluctuations within the flow. More information on Rayleigh scattering can be found in Miles et al. (2001). This technique has been used extensively for determining density fluctuations in supersonic flows (Miles et al., 1992; Smith et al., 1989; Panda and Seasholtz, 2002b; Panda, 2006). Previous works (Stockhausen et al., 2010; Most and Leipertz, 2001) have also demonstrated the combination of DGV or PIV with Rayleigh scattering to obtain planar velocity and temperature maps.

Molecular tagging velocimetry (MTV) works by exciting the molecules in the flow using fluorescence or phosphorescence (Hsu et al., 2009). Using laser grids, one- and two-component measurements can be made by calculating the displacement from camera frames. Seeded and unseeded approaches are used to enable fluorescence. With seeded flows, gaseous additives (e.g. acetone) allow the tagging via certain laser wavelengths. Unseeded flows use the natural capability of the investigated gases to exhibit fluorescence. Time-resolved velocity measurements with molecular techniques are currently still limited to very low velocities (Maynes and Webb, 2002). As the intensity of the scattering used for MTV techniques is much smaller than the Mie-scattering from particles, good measurement signal to noise ratios are challenging to achieve. The main advantage for high-speed flows is that the molecules follow the flow perfectly, avoiding the problem of particle lag near strong velocity gradients alltogether. More information on the various different MTV techniques can be found in Tropea et al. (2007).

2.5. Summary

From this brief overview it may been seen that many ways exist to successfully measure velocities in compressible heated flows. Hot wire anemometry and pressure probes have had many applications in compressible flows, but their intrusive nature and limitations with regards to high temperature flows restrict their use for supersonic hot jet research. While molecular based methods are non-intrusive and offer advantages in flows with shocks, no notable time-resolved technique for high speed flows exists. For the purpose of time-resolved and non-intrusive measurements, particle based methods are the still the best choice. Depending on the application DGV offers some advantages to be exploited:

- The direct measurement of the Doppler effect allows each sensor point to represent one data point (unlike PIV where the cross-correlation processing uses windows)
- The flexibility in seeding requirements allows DGV to have theoretically higher data rates than PIV or LDV. The data rate for LDV is limited by a dead time,which means that only one particle at a time is permitted to be present in the measurement volume. Similarly the particle density for PIV is limited by the spatial resolution and cross-correlation processing. Because DGV directly measures the Doppler effect, there is no limitation on how much seeding may be present within the measurement plane.
- Further, high amounts of seed may be used to improve signal to noise ratios, compensating for lower light collection efficiency in mid- and large-scale facilities.

Nomenclature

$\hat{\theta}$ angle between the local source position y and the observer position x

ρ density

τ_{ij} viscous stress tensor

D_{ijkl} directivity tensor

a speed of sound

a_0 speed of sound in the ambient medium at rest

M Mach number

M_a acoustic Mach number

M_c convective Mach number

NPR nozzle pressure ratio - ratio between total pressure p_0 and ambient pressure p_a

p pressure

p_a ambient pressure

p_e exit pressure

r distance between observer and source position

R_a pressure auto-correlation function

s density ratio - the ratio between the density of the core stream ρ_1, and the density of the co-flow ρ_2

T_0 total temperature

T_a ambient temperature

TTR total temperature ratio - ratio between total temperature T_0 and ambient temperature T_a

U velocity

u_c convective eddy velocity

x observer position

y local source position

References

SFPE handbook of fire protection engineering. Quincy, Mass: National Fire Protection Association., 1995.

H. E. Albrecht, M. Borys, N. Damaschke, and C. Tropea. *Laser Doppler and Phase Doppler Measurement Techniques*. Springer, 1 edition, Dec. 2002.

M. B. Alkislar, L. M. Lourenco, and A. Krothapalli. Stereoscopic PIV measurements of a screeching supersonic jet. *Journal of Visualization*, 3(2):135–143, June 2000. doi: 10.1007/BF03182406.

B. André, T. Castelain, and C. Bailly. Broadband Shock-Associated Noise in Screeching and Non-Screeching Underexpanded Supersonic Jets. *AIAA Journal*, 51(3):665–673, Feb. 2013. doi: 10.2514/1.J052058.

B. André, T. Castelain, and C. Bailly. Experimental exploration of underexpanded supersonic jets. *Shock Waves*, 24 (1):21–32, Jan. 2014. doi: 10.1007/s00193-013-0457-4.

C. Bailly, P. Lafon, Sé, and b. Candel. Subsonic and supersonic jet noise predictions from statistical source models. *AIAA Journal*, 35(11):1688–1696, Nov. 1997. doi: 10.2514/2.33.

R. D. W. Bowersox. Combined laser Doppler velocimetry and cross-wire anemometry analysis for supersonic turbulent flow. *AIAA Journal*, 34(11):2269–2275, Nov. 1996. doi: 10.2514/3.13390.

J. Bridges and M. P. Wernet. The NASA Subsonic Jet Particle Image Velocimetry (PIV) Dataset. Technical Report NASA/TM—2011-216807, NASA, 2011b.

J. Bridges, M. P. Wernet, and F. Frate. PIV measurements of chevrons on F400-series tactical aircraft nozzle model. In *49th AIAA Aerospace Sciences Meeting Including the New Horizons Forum and Aerospace Exposition*, number AIAA 2011-1157, Orlando, FL, Jan. 2011. doi: 10.2514/6.2011-1157.

D. R. Brooks and K. T. Lowe. Fluctuating Flow Acceleration in a Heated Supersonic Jet. In *12th International Symposium on Applications of Laser Techniques to Fluid Mechanics*, Lisbon, Portugal, July 2014.

D. R. Brooks, T. Ecker, K. T. Lowe, and W. F. Ng. Experimental Reynolds Stress Spectra in Hot Supersonic Round Jets. In *AIAA Scitech (52nd Aerospace Sciences Meeting), National Harbor, MD*, number AIAA 2014-1227, National Harbor, MD, July 2014. doi: 10.2514/6.2014-1227.

G. L. Brown and A. Roshko. On density effects and large structure in turbulent mixing layers. *Journal of Fluid Mechanics*, 64(04):775–816, July 1974b. doi: 10.1017/S002211207400190X.

G. O. Brown. Henry Darcy and the Pitot tube. *International Engineering History and Heritage*, pages 360–366, 2001. doi: 10.1061/40594(265)43.

D. R. Cadel, T. Ecker, and K. T. Lowe. Volumetric vector velocity measurements in a hot supersonic jet. In *12th International Symposium on Applications of Laser Techniques to Fluid Mechanics*, Lisbon, Portugal, July 2014a.

R. Camussi. *Noise Sources in Turbulent Shear Flows: Fundamentals and Applications: Fundamentals and Applications*, volume 545. Springer Science & Business Media, 2013. ISBN 978-3-7091-1457-5. doi: 10.1007/978-3-7091-1458-2.

F. L. Crosswy. Particle Size Distribution of several commonly used seeding aerosols. *Wind Tunnel Seeding Systems for Laser Velocimeters, NASA Workshop*, 1985.

C. J. DeLapp and M. F. Reeder. Clean Seeding Material for Particle Image Velocimetry Measurements. In *25th AIAA Aerodynamic Measurement Technology and Ground Testing Conference*, number AIAA 2006-2807, San Francisco, CA, June 2006. doi: 10.2514/6.2006-2807.

P. E. Dimotakis and G. L. Brown. The mixing layer at high Reynolds number: large-structure dynamics and entrainment. *Journal of Fluid Mechanics*, 78(03):535, April 1976. doi: 10.1017/s0022112076002590.

T. Ecker. Experimental Investigation of Particle Lag behind a Shock Wave using a Novel Laser Doppler Accelerometer. Master's thesis, Virginia Tech, Blacksburg, VA, Aug. 2011.

T. Ecker, D. R. Brooks, K. T. Lowe, and W. F. Ng. Development and application of a point Doppler velocimeter featuring two-beam multiplexing for time-resolved measurements of high-speed flow. *Experiments in Fluids*, 55 (9):1–15, Sept. 2014a. doi: 10.1007/s00348-014-1819-0.

T. Ecker, D. R. Brooks, K. T. Lowe, and W. F. Ng. Spectral analysis of over-expanded cold jets via 3-component point Doppler velocimetry. In *AIAA Scitech (52nd Aerospace Sciences Meeting)*, number AIAA 2014-1103, National Harbor, MD, Jan. 2014b. doi: 10.2514/6.2014-1103.

T. Ecker, K. T. Lowe, W. F. Ng, and D. R. Brooks. Fourth-order Spectral Statistics in the Developing Shear Layers of Hot Supersonic Jets. In *AIAA Propulsion and Power (50th AIAA/ASME/SAE/ASEE Joint Propulsion Conference)*, number AIAA 2014-3742, Cleveland, OH, July 2014c. doi: 10.2514/6.2014-3742.

G. Elsinga, F. Scarano, B. Wieneke, and B. van Oudheusden. Tomographic particle image velocimetry. *Experiments in Fluids*, 41(6):933–947, Oct. 2006. ISSN 0723-4864. doi: 10.1007/s00348-006-0212-z.

K. Ennix, F. Burcham Jr, and L. Webb. Flight-determined engine exhaust characteristics of an F404 engine in an F-18 airplane. In *29th Joint Propulsion Conference and Exhibit*, number AIAA 1993-2543, Reston, VA, Aug. 2012. doi: 10.2514/6.1993-2543.

T. W. Fahringer and B. S. Thurow. Tomographic reconstruction of a 3-d flow field using a plenoptic camera. In *42nd AIAA Fluid Dynamics Conference and Exhibit*, volume 2826, New Orleans, LA, June 2012. doi: 10.2514/6.2012-2826.

F. Farassat, M. J. Doty, and C. A. Hunter. The acoustic analogy-a powerful tool in aeroacoustics with emphasis on jet noise prediction. In *10th AIAA/CEAS Aeroacoustics Conference*, number AIAA 2004-2872, Manchester, UK, May 2004. doi: 10.2514/6.2004-2872.

J. E. Ffowcs Williams. The Noise from Turbulence Convected at High Speed. *Proceedings of the Royal Society A: Mathematical, Physical and Engineering Sciences*, 255(1061):469–503, Apr. 1963. doi: 10.1098/rsta.1963.0010.

V. Fleury, C. Bailly, E. Jondeau, M. Michard, and D. Juvé. Space-time correlations in two subsonic jets using dual particle image velocimetry measurements. *AIAA Journal*, 46(10):2498–2509, Oct. 2008. doi: 10.2514/1.35561.

E. Gamble. Nozzle Selection and Design Criteria. In *40th AIAA/ASME/SAE/ASEE Joint Propulsion Conference and Exhibit*, number AIAA 2004-3923, Fort Lauterdale, FL, July 2004. doi: 10.2514/6.2004-3923.

S. G. Goebel, J. C. Dutton, H. Krier, and J. P. Renie. Mean and turbulent velocity measurements of supersonic mixing layers. *Experiments in Fluids*, 8(5):263–272, Feb. 1990. doi: 10.1007/BF00187228.

E. Gutmark, K. C. Schadow, and K. H. Yu. Mixing Enhancement in Supersonic Free Shear Flows. *Annual Review of Fluid Mechanics*, 27(1):375–417, Jan. 1995. doi: 10.1146/annurev.fl.27.010195.002111.

J. K. Holzman, L. D. Webb, and F. W. Burcham Jr. Flight and static exhaust flow properties of an F110-GE-129 engine in an F-16XL airplane during acoustic tests. Technical Report NASA Technical Memorandum 104326, 1996.

A. G. Hsu, R. Srinivasan, R. D. W. Bowersox, and S. W. North. Two-component molecular tagging velocimetry utilizing no fluorescence lifetime and no2 photodissociation techniques in an underexpanded jet flowfield. *Applied Optics*, 48(22):4414–4423, Aug. 2009. doi: 10.1364/AO.48.004414.

D. A. Johnson and W. C. Rose. Laser Velocimeter and Hot-wire Anemometer Comparison in a Supersonic Boundary Layer. *AIAA Journal*, 13(4):512–515, Apr. 1975. doi: 10.2514/3.49739.

C. J. Kähler, B. Sammler, and J. Kompenhans. Generation and control of tracer particles for optical flow investigations in air. *Experiments in Fluids*, 33(6):736–742, Dec. 2002. doi: 10.1007/s00348-002-0492-x.

S. A. Karabasov. Understanding jet noise. *Philosophical Transactions: Mathematical, Physical and Engineering Sciences*, 368(1924):3593–3608, Aug. 2010. doi: 10.1098/rsta.2010.0086.

F. Kerhervé, P. Jordan, Y. Gervais, and P. Braud. Two-point laser Doppler velocimetry measurements in a Mach 1.2 cold supersonic jet for statistical aeroacoustic source model. *Experiments in Fluids*, 37(3):419–437, Sept. 2004a. doi: 10.1007/s00348-004-0815-1.

F. Kerhervé, O. Power, J. Fitzpatrick, and P. Jordan. Determination of Turbulent Scales in Subsonic and Supersonic Jets from LDV Measurements . In *12th International Symposium on Applications of Laser Techniques to Fluid Mechanics*, Lisbon, July 2004b.

F. Kerhervé, J. Fitzpatrick, and P. Jordan. The frequency dependence of jet turbulence for noise source modelling. *Journal of Sound and Vibration*, 296(1-2):209–225, Sept. 2006. doi: 10.1016/j.jsv.2006.02.012.

H. Komine. System for measuring velocity field of fluid flow utilizing a laser-doppler spectral image converter . US Patent Office, 1990.

H. Komine, S. J. Brosnan, A. B. Litton, and E. A. Stappaerts. Real-time, Doppler global velocimetry. In *29th AIAA Aerospace Sciences Meeting*, number AIAA 91-0337, Reno, NV, Jan. 1991. doi: 10.2514/6.1991-337.

L. Kovasznay. The hot-wire anemometer in supersonic flow. *Journal of the Aeronautical Sciences*, 17(9):565–572, Sept. 1950. doi: 10.2514/8.1725.

P. Kupferschmied, P. Köppel, W. Gizzi, C. Roduner, and G. Gyarmathy. Time-resolved flow measurements with fast-response aerodynamic probes in turbomachines. *Measurement Science and Technology*, 11(7):1036–1054, July 2000. doi: 10.1088/0957-0233/11/7/318.

J. C. Lau. Laser velocimeter correlation measurements in subsonic and supersonic jets. *Journal of Sound and Vibration*, 70(1):85–101, May 1980. doi: 10.1016/0022-460X(80)90556-8.

J. C. Lau. Effects of exit Mach number and temperature on mean-flow and turbulence characteristics in round jets. *Journal of Fluid Mechanics*, 105:193–218, Apr. 1981. doi: 10.1017/S0022112081003170.

J. C. Lau, P. J. Morris, and M. J. Fisher. Measurements in subsonic and supersonic free jets using a laser velocimeter. *Journal of Fluid Mechanics*, 93(01):1–27, July 1979. doi: 10.1017/S0022112079001750.

C. Lenherr, A. I. Kalfas, and R. S. Abhari. High Temperature Fast Response Aerodynamic Probe. *Journal of Engineering for Gas Turbines and Power*, 133(1):011603, Jan. 2011. doi: 10.1115/1.4001824.

J. Lepicovsky and R. J. Bruckner. Seeding for Laser Velocimetry in Confined Supersonic Flows With Shocks. Technical Report NASA Technical Memorandum 107265, NASA, 1996.

M. J. Lighthill. On Sound Generated Aerodynamically. I. General Theory. *Proceedings of the Royal Society A: Mathematical, Physical and Engineering Sciences*, 211(1107):564–587, 1952. doi: 10.1098/rspa.1952.0060.

C. G. Lomas. *Fundamentals of Hot Wire Anemometry*. Cambridge University Press, 2011. ISBN 0521283183.

K. T. Lowe, W. F. Ng, and T. Ecker. Early development of time-resolved volumetric doppler velocimetry for new insights in hot supersonic jet noise. In *18th AIAA/CEAS Aeroacoustics Conference (33rd AIAA Aeroacoustics Conference)*, number AIAA 2012-2273, Colorado Springs, CO, June 2012a. doi: 10.2514/6.2012-2273.

E. Mach and P. Salcher. Weitere ballistisch-photographische Versuche. *Sitzungsber Akad Wiss Wein*, 1889a.

E. Mach and P. Salcher. Über die in Pola und Meppen angestellten ballistisch-photographischen Versuche. *Sitzungsber Akad Wiss Wien*, 1889b.

E. Mach and P. Salcher. Optische Untersuchung der Luftstrahlen. *Annalen der Physik und Chemie*, 277(9):144–150, 1890. doi: 10.1002/andp.18902770910.

D. V. Maddalon, R. D. WAGNER JR, and L. M. Weinstein. Influence of measured freestream disturbances on hypersonic boundary-layer transition. *AIAA Journal*, 8(9):1664–1670, Sept. 1970. doi: 10.2514/3.5962.

S. Martens, K. W. Kinzie, and D. K. McLaughlin. Structure of coherent instabilities in a supersonic shear layer. *AIAA Journal*, 34(8):1555–1561, Aug. 1996. doi: 10.2514/3.13271.

D. Maynes and A. R. Webb. Velocity profile characterization in sub-millimeter diameter tubes using molecular tagging velocimetry. *Experiments in Fluids*, 32(1):3–15, Dec. 2002. doi: 10.1007/s003480200001.

A. Melling. Tracer particles and seeding for particle image velocimetry. *Measurement Science and Technology*, 8(12): 1406, Dec. 1997. doi: 10.1088/0957-0233/8/12/005.

J. F. Meyers. Generation of Particles and Seeding. Technical report, 1991.

J. F. Meyers. Doppler Global Velocimetry - the next generation? In *AIAA 17th Aerospace Ground Testing Conference*, number AIAA 1992-3897, Nashville, TN, July 1992. doi: 10.2514/6.1992-3897.

J. F. Meyers and H. Komine. Doppler global velocimetry - a new way to look at velocity. In *ASME Fourth International Conference on Laser Anemometry*, pages 289–296, Cleveland, OH, 1991.

J. F. Meyers, J. W. Lee, and R. J. Schwartz. Characterization of measurement error sources in Doppler global velocimetry. *Measurement Science and Technology*, 12(4):357–368, Apr. 2001a. doi: 10.1088/0957-0233/12/4/301.

R. B. Miles, J. N. Forkey, and W. R. Lempert. Filtered Rayleigh scattering measurements in supersonic/hypersonic facilities. In *AIAA 17th Aerospace Ground Testing Conference*, number AIAA 1992-3894, Nashville, TN, July 1992. doi: 10.2514/6.1992-3894.

R. B. Miles, W. R. Lempert, and J. N. Forkey. Laser rayleigh scattering. *Measurement Science And Technology*, 12 (5):R33–R51, May 2001. doi: 10.1088/0957-0233/12/5/201.

P. J. Morris and F. Farassat. Acoustic Analogy and Alternative Theories for Jet Noise Prediction. *AIAA Journal*, 40 (4):671–680, Apr. 2002. doi: 10.2514/2.1699.

D. Most and A. Leipertz. Simultaneous two-dimensional flow velocity and gas temperature measurements by use of a combined particle image velocimetry and filtered rayleigh scattering technique. *Applied Optics*, 40:5379–5387, Oct. 2001.

J. Panda. Two point space-time correlation of density fluctuations measured in high velocity free jets. In *44th AIAA Aerospace Sciences Meeting and Exhibit*, number AIAA 2006-6, Reston, VA, Aug. 2006. doi: 10.2514/6.2006-6.

J. Panda and R. G. Seasholtz. Experimental investigation of density fluctuations in high-speed jets and correlation with generated noise. *Journal of Fluid Mechanics*, 450:97–130, Jan. 2002b. doi: 10.1017/S002211200100622X.

C. Pokora and J. McGuirk. Spatio-Temporal Turbulence Correlations Using High-Speed PIV in an Axisymmetric Jet. In *14th AIAA/CEAS Aeroacoustics Conference (29th AIAA Aeroacoustics Conference)*, number AIAA 2008-3028, Reston, VA, 2012. doi: 10.2514/6.2008-3028.

H. S. Ribner. Quadrupole correlations governing the pattern of jet noise. *Journal of Fluid Mechanics*, 38(01):1–24, Aug. 1969. doi: 10.1017/S0022112069000012.

K. R. Sabroske. Seeding Materials For Use In Laser Anemometry. In *31st Aerospace Sciences Meeting & Exhibit*, number AIAA 1993-0006, Reno, NV, Jan. 1993. doi: 10.2514/6.1993-6.

M. Samimy and G. S. Elliott. Effects of compressibility on the characteristics of free shear layers. *AIAA Journal*, 28 (3):439–445, 1990. doi: 10.2514/3.10412.

F. Scarano. *Overview of PIV in Supersonic Flows*. Springer, 2008a.

H. L. Seegmiller. Seeding subsonic transonic and supersonic flows with 0.5 micron polystrene spheres. *Wind Tunnel Seeding Systems for Laser Velocimeters, NASA Workshop*, 1985.

J. Sheng, E. Malkiel, and J. Katz. Digital holographic microscope for measuring three-dimensional particle distributions and motions. *Appl. Opt.*, 45(16):3893–3901, Jun 2006. doi: 10.1364/AO.45.003893.

M. Smith, A. Smits, and R. Miles. Compressible boundary-layer density cross sections by UV Rayleigh scattering. *Optics Letters*, 14(17):916–919, Sept. 1989. doi: 10.1364/OL.14.000916.

M. W. Smith. Application of a Planar Doppler Velocimetry System to a High Reynolds Number Compressible Jet . In *AIAA 36th Aerospace Sciences Meeting and Exhibit*, number AIAA 1998-428, Reno, NV, Jan. 1998. doi: 10.2514/6.1998-428.

A. J. Smits, K. Hayakawa, and K. C. Muck. Constant temperature hot-wire anemometer practice in supersonic flows. *Experiments in Fluids*, 1(2):83–92, June 1983. doi: 10.1007/BF00266260.

E. F. Spina and C. B. McGinley. Constant-temperature anemometry in hypersonic flow: critical issues and sample results. *Experiments in Fluids*, 17(6):365–374, Oct. 1994. doi: 10.1007/BF01877036.

G. Stockhausen, U. Doll, T. Strehlau, and C. Willert. Combined filtered Rayleigh and Mie scattering for simultaneous planar temperature and velocity measurements . In *15th Int Symp on Applications of Laser Techniques to Fluid Mechanics*, Lisbon, Portugal, 2010.

C. K. W. Tam. Supersonic jet noise. *Annual Review of Fluid Mechanics*, pages 17–43, Jan 1995. doi: 0.1146/annurev.fl.27.010195.000313.

C. K. W. Tam and L. Auriault. Jet Mixing Noise from Fine-Scale Turbulence. *AIAA Journal*, 37(2):145–153, Feb. 1999. doi: 10.2514/2.691.

C. K. W. Tam and P. J. Morris. The radiation of sound by the instability waves of a compressible plane turbulent shear layer. *Journal of Fluid Mechanics*, 98(02):349–381, May 1980. doi: 10.1017/S0022112080000195.

C. K. W. Tam, P. Chen, and J. M. Seiner. Relationship between the instability waves and noise of high-speed jets. *AIAA Journal*, 30(7):1747–1752, July 1992. doi: 10.2514/3.11132.

B. S. Thurow. *On the convective velocity of large- scale structures in compressible axisymmetric jets.* PhD thesis, The Ohio State University, 2005.

B. S. Thurow, N. Jiang, J.-H. Kim, W. Lempert, and M. Samimy. Issues with measurements of the convective velocity of large-scale structures in the compressible shear layer of a free jet. *Physics of Fluids (1994-present)*, 20(6):066101, June 2008. doi: 10.1063/1.2926757.

C. Tropea, A. Yarin, and J. Foss, editors. *Springer Handbook of Experimental Fluid Mechanic*. Springer Verlag Berlin-Heidelberg, 2007. ISBN 978-3-540-25141-5.

T. R. Troutt and D. K. McLaughlin. Experiments on the Flow and Acoustic Properties of a Moderate-Reynolds-Number Supersonic Jet. *Journal of Fluid Mechanics*, 116:123–156, March 1982b. doi: 10.1017/S0022112082000408.

J. D. Vagt. Hot-wire probes in low speed flow. *Progress in Aerospace Sciences*, 18:271–323, Jan. 1979. doi: 10.1016/0376-0421(77)90010-0.

D. A. Walker, W. F. Ng, and M. D. Walker. Experimental comparison of two hot-wire techniques in supersonic flow. *AIAA Journal*, 27(8):1074–1080, Aug. 1989. doi: 10.2514/3.10223.

M. Wernet, G. Skoch, and J. Wernet. Demonstration of a stabilized alumina/ethanol colloidal dispersion technique for seeding high temperature air flows. In *Instrumentation in Aerospace Simulation Facilities, 1995. ICIASF '95 Record., International Congress on*, July 1995. doi: 10.1109/ICIASF.1995.519125.

M. P. Wernet. Temporally resolved PIV for space–time correlations in both cold and hot jet flows. *Measurement Science and Technology*, 18(5):1387, March 2007b. doi: 10.1088/0957-0233/18/5/027.

C. E. Willert and M. Gharib. Digital particle image velocimetry. *Experiments in Fluids*, 10(4):181–193, Jan. 1991. doi: 10.1007/BF00190388.

C. D. Winant and F. K. Browand. Vortex pairing- The mechanism of turbulent mixing-layer growth at moderate Reynolds number. *Journal of Fluid Mechanics*, 63(2):237–255, March 1974. doi: 10.1017/S0022112074001121.

Part III.

Development and application of a point Doppler velocimeter featuring two-beam multiplexing for time-resolved measurements of high speed flow

The contents of this chapter were published in Experiments in Fluids (Tobias Ecker, Donald R. Brooks, K. Todd Lowe, Wing F. Ng, “Development and application of a point Doppler velocimeter featuring two-beam multiplexing for time-resolved measurements of high speed flow”, Experiments in Fluids (2014) 55:1819, DOI 10.1007/s00348-014-1819-0).

Significant portions were previously presented as “Ecker, Tobias, Donald R. Brooks, K. Todd Lowe, and Wing Ng. "Spectral analysis of over-expanded cold jets via 3-component point Doppler velocimetry." In AIAA Scitech (52nd Aerospace Sciences Meeting). 2014”.

Exp Fluids (2014) 55:1819
DOI 10.1007/s00348-014-1819-0

RESEARCH ARTICLE

Development and application of a point Doppler velocimeter featuring two-beam multiplexing for time-resolved measurements of high-speed flow

Tobias Ecker · Donald R. Brooks · K. Todd Lowe · Wing F. Ng

Received: 2 May 2014 / Revised: 12 August 2014 / Accepted: 28 August 2014

Abstract A novel point Doppler velocimeter (pDV) based upon the Doppler global velocimetry principle is presented, which is capable of three-component velocity vector measurements at 100 kHz mean rates over extended time periods. In this implementation, two laser beams are multiplexed to illuminate the flow over alternating time windows, providing for a reduction in the number of sensors required. The implications of this multiplexing paradigm coupled with the fundamental limits set by the optical absorption filter are examined in detail, and uncertainties are predicted via instrumentation modeling and representative synthetic flow data. The results indicate that the multiplexing pDV instrument provides the required temporal and velocity resolution for turbulent shear flows at velocities of nominally 500 m/s. As a demonstration and validation of this time-resolved technique, statistics of three-velocity component measurements in a cold, supersonic, over-expanded jet at jet exit Mach number $M_j = 1.4$ (design Mach number $M_d = 1.65$) are presented. Time resolution up to 250 kHz and instantaneous velocity uncertainties between 6.6 and 11.1 m/s were obtained. Comparisons of mean pDV data with laser Doppler velocimetry data are consistent with uncertainty predictions for the technique. The ultimate value of the instrument is exhibited in the analysis of Reynolds stress spectra in the screeching jet, exposing the spatial development of motions at the harmonics of the screech tone, variable phase-coordinated shock motions, and growth of turbulent fluctuations in the developing shear layer of the jet. From the data presented, the screech tone phenomenon is suspected to be linked to the production of radial–azimuthal shear stresses in extended regions beyond the potential core.

T. Ecker (✉) · D. R. Brooks · K. T. Lowe
Department of Aerospace and Ocean Engineering, Virginia Tech, Blacksburg, VA 24061, USA
e-mail: ecker@vt.edu

W. F. Ng
Department of Mechanical Engineering, Virginia Tech, Blacksburg, VA 24061, USA

1 Introduction

Particle-based velocimetry techniques have been developed toward time-resolved capabilities over the last decade, shedding insight into the complex physics of unsteady fluid dynamics and turbulent phenomena and their associated timescales.

Doppler global velocimetry (DGV) is an optical, non-intrusive, particle-scattering-based velocimetry technique utilizing the absorption characteristics of molecular gas cells. In its essence, it was developed in 1990 by Komine (1990) and matured by Komine et al. (1991) as well as Meyers and Komine (1991) as a planar alternative to particle image velocimetry (PIV) particularly well suited for high-speed flows due to its absolute uncertainties. Compared to laser Doppler velocimetry (LDV), DGV has the potential of a higher temporal response, as it does not require resolution of signals from single particles. As multiple particles may contribute to the Doppler signal, sufficiently high concentrations of very small particles may produce continuous datasets with minimal particle lag.

In this study, we describe the development of a point Doppler velocimeter (pDV) based on the DGV principle and capable of time-resolved measurement in high-speed flows. A distinctive feature of this development aside from the high data rate is the use of a time-shift multiplexing technique to generate time-resolved three-component

Published online: 13 September 2014

velocity vectors with a reduced number of required sensors. Detailed studies on the errors due to the time-shift multiplexing and its data processing technique are presented along with a study on systematic and random uncertainties. Additionally, the influence of the absorption line width on velocity statistics is used to determine instrument capabilities and limitations. At the end of this study, the real-world applicability of the pDV sensor is demonstrated with measurements in a cold supersonic jet generated by a biconic nozzle with design Mach number (M_d) of 1.65. The acousto-optic beam multiplexing technique enables measurements of velocity vectors at 100 kHz mean rates over extended time windows. Validation measurements performed at different nozzle-pressure ratios (NPR) are compared with measurements from a LDV probe. Measurements in a supersonic jet operated at over-expanded and screeching condition (total temperature ratio, TTR $= T_0/T_a = 1$; T_0, total temperature; T_a, ambient temperature; NPR $= 3.2$; jet exit Mach number, $M_j = 1.4$) are used to generate autocorrelations, auto-spectra, mean velocity as well as normal and shear stress information along the streamwise coordinate. The results indicate fundamental structural differences between over and under-expanded jet screech and a link between screech and shear stress production in downstream regions.

1.1 State of the art

DGV is a particle-scattering technique based on the frequency-dependent absorption characteristics of molecular gas cells resulting in direct measurement of the Doppler effect. Meyers et al. (2001) summarize the efforts to characterize the sources of uncertainty in DGV. The main sources of uncertainty are attributed to the molecular gas cell, laser stability and characteristic performance and configuration of the sensor type.

There have been several notable developments of the DGV technique over the past decade. Advances have been made to address one of three goals: measurement uncertainty reduction, reduction of instrumentation cost and complexity, as well as time resolution. Elliott and Beutner (1999) presented a major contribution to the characterization and reduction of DGV uncertainty for several applications. One of the key developments presented therein was the use of vapor-limited gas absorption cells that reduces the errors incurred due to temperature variations in the cell.

There are several efforts reported in the literature to reduce the cost and complexity of DGV by reducing number of detectors. Charret et al. (2004) introduced the two-frequency DGV (2νDGV) approach to eliminate the reference sensor and its associated uncertainties. In this approach, an acousto-optic modulator (AOM) is used to shift the laser line to a frequency with very little absorption by the molecular gas filter. The signal obtained at this frequency is then used as a reference, enabling one detector per velocity component, further reducing equipment cost and measurement uncertainty due to beam-splitting arrangements and sensor gain. Another technique, frequency-modulated DGV (FM-DGV) first introduced by Mueller et al. (1999) reduces the required number of sensors and associated beam-splitting uncertainties by evaluation of first- and second-order harmonics of the resulting amplitude modulation. Other approaches to sensor reduction is the use of fiberoptic bundles to project several fields of view onto the same sensor (Nobes et al. 2004) or a laser frequency-scanning technique combined with cross-correlation processing as recently applied by Cadel et al. (2014a, b).

The development of time resolution techniques for DGV has included several contributions, from optimization of flow-freezing instantaneous measurements to high repetition rates. The first instantaneous measurements in supersonic flow in which the capability to generate velocity vectors that froze the flow at the smallest timescales were first demonstrated by Smith (1998) and Clancy et al. (1999). The ability to provide high repetition measurements came primarily with the development of detector, laser and data acquisition technologies capable of sampling at these high rates. The pDV technique concentrates the laser energy onto a small measurement volume, therefore improving signal-to-noise ratios in an effort of high accuracy and ideally time-resolved data. First efforts were presented by Kuhlman et al. (2001) on the application to turbulent jet flows and instrument uncertainty characterization. The one-component pDV system presented by Cavone et al. (2006) demonstrates first time-resolved measurements similar to LDV at frequencies up to 20 kHz. The FM-DGV technique already mentioned has been demonstrated at points and with arrays of detectors (Müller et al. 1999; Fischer et al. 2008, 2010). Fischer et al. (2007, 2008) reported the uncertainty of the FM-DGV technique to be as low as 0.02 m/s. Current developments show approaches to time resolution to up to 100 kHz for one velocity component (Fischer et al. 2008) and 20 kHz for 3-component probes (Fischer et al. 2011). Thurow et al. (2005) demonstrated the application of a one-component, high repetition rate DGV system based on a high-speed camera (128 $\times$ 64 pixels) in a rectangular Mach 2.0 jet—to our knowledge, the first application of a high repetition rate DGV technique in a supersonic jet flow. Measurements were performed at 250 kHz frame rates, but image buffer limitations constrained the recording timespan and therefore prevented the observation of flow structure evolution at integral timescales. According to our survey, true time-resolved measurements using DGV, where the time-resolved term refers to the capability of resolving all or

most timescales of interest [as used by Wernet (2007) for time-resolved PIV in jets], has only been demonstrated by the FM-DGV technique (e.g., Fischer et al. 2011) and in the current work.

The article by Thurow et al. (2005) demonstrates the current trade-off between spatially and temporally resolving optical, non-intrusive measurements in high-speed flows that must to be addressed to gain deeper understanding of the physics involved. In a first step to address these trades-off for our application in high-speed jet flows, we here introduce an effort to obtain time-resolved measurements at reduced equipment complexity for a single point with a optically non-distorting configuration that allows extension to multiple points and planes in the future. In continuation of this approach, Ecker et al. (2014a) presented an extension to 32 points using a newly developed photomultiplier (PMT) camera.

1.2 Principle of Doppler global velocimetry

DGV relies on the detection of the Doppler shift of laser light scattered by submicron-sized particles following the local flow. A single-longitudinal-mode laser is tuned such that the Doppler-shifted light scattered by particles lies within a frequency range of high transmission sensitivity for the molecular gas filter. The frequency of the scattered light is therefore transformed to a function of the intensity of light exiting the gas filter. In its classic implementation, DGV techniques utilize the ratio of filtered-to-unfiltered light intensity in a reference design to obtain Doppler shift frequencies, as done in the present work.

The Doppler shift of scattered light depends upon the laser frequency, vector particle velocity and laser propagation and observation directions (Meyers and Komine 1991) (see Fig. 1):

$$f_D = f_0 \frac{\vec{U} \cdot \vec{e}}{c} \tag{1}$$

where f_0 is the incident laser light frequency, c is the speed of light, $\vec{U}$ is the particle velocity vector, $\vec{e} = \hat{o} - \hat{i}$ defines the velocity measurement component direction, wherein the laser propagation direction is the unit vector $\hat{i}$ and the direction of observation is given by $\hat{o}$. With a three-component measurement, the resulting velocity vector in the coordinate system of interest may be reconstructed from the measured components and their base vectors as:

$$\vec{U} = \begin{bmatrix} \vec{e}_1^T \\ \vec{e}_2^T \\ \vec{e}_3^T \end{bmatrix}^{-1} \begin{pmatrix} u_1 \\ u_2 \\ u_3 \end{pmatrix} = \begin{bmatrix} R_{11} & R_{12} & R_{13} \\ R_{21} & R_{22} & R_{23} \\ R_{31} & R_{32} & R_{33} \end{bmatrix} \begin{pmatrix} u_1 \\ u_2 \\ u_3 \end{pmatrix} \tag{2}$$

where $\vec{e}_i$ represents the measurement vectors and u_i the magnitude of the respective directly measured velocity component. Similarly, R represents the geometrical calibration deduced for every instrument configuration.

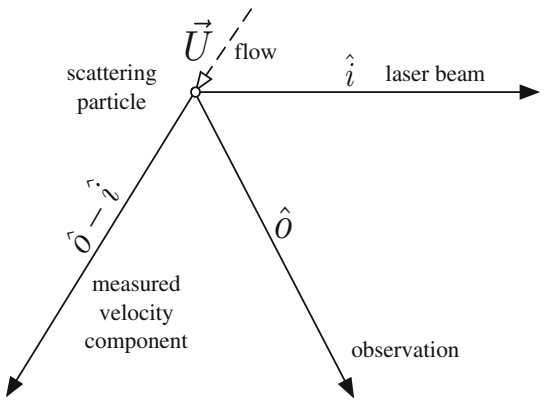

Fig. 1 Vector geometry and nomenclature of the DGV measurement principle

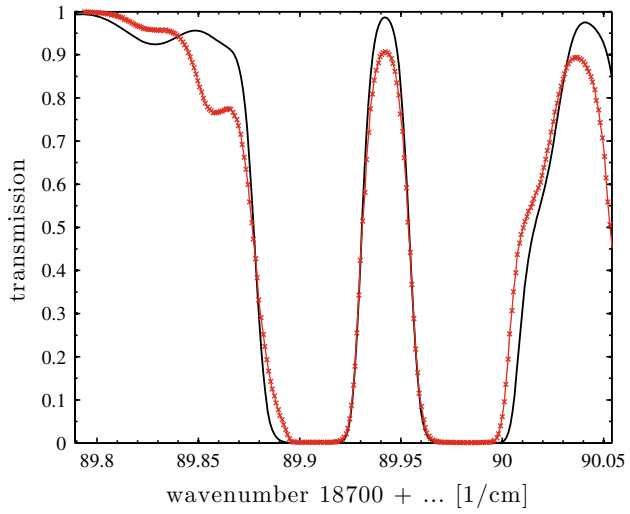

Fig. 2 Measured iodine cell scan (*red*) compared to model using code by Forkey (*black*)

The laser frequency may be tuned in steps to characterize the transmission function of the molecular gas cell as well as to choose the exact reference frequency. The calibration scan can then be converted into usable calibration data by matching the experimental scan to numerical transmission spectra based on a model developed by Forkey (1996) or by comparing it to a known frequency shift, e.g., using a calibration wheel, AOM or measurement of a known flow.

This numerical calibration scheme has been used successfully by Fischer et al. (2000), Meyers and Lee (2010) and other authors (Müller et al. 1999; Jones 2001; Fussell 2003). Figure 2 shows an experimental scan compared to the numerically obtained transmission spectrum, using model and code developed by Forkey et al. (1997). Further

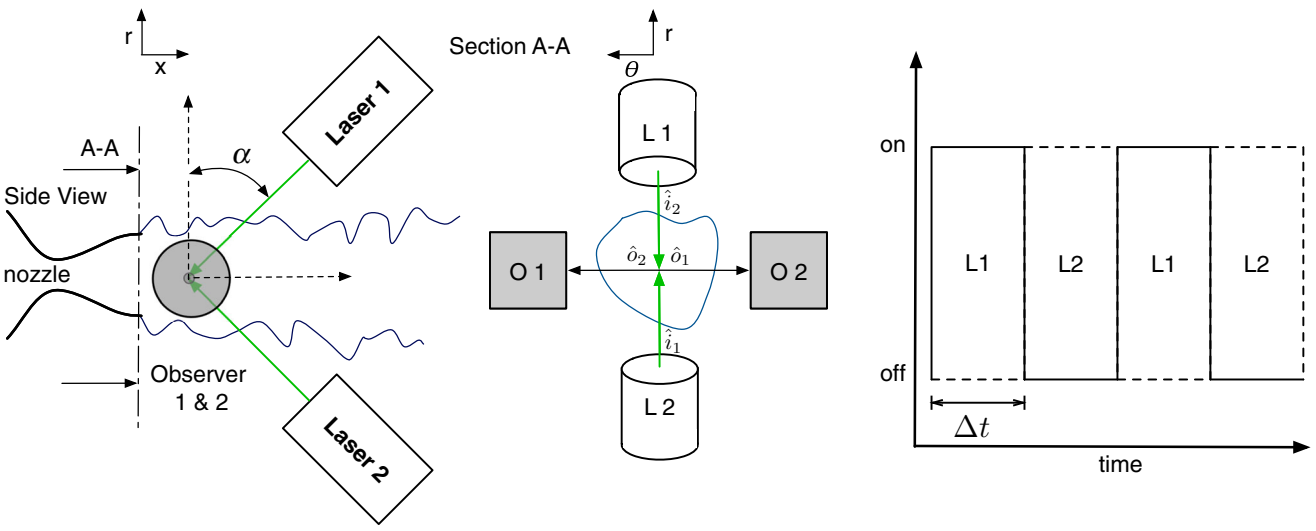

Fig. 3 Schematic of the pDV optical arrangement (*O 1* observer 1, *O 2* observer 2, *L 1* laser 1, *L 2* laser 2) (**a**), section view (**b**) and beam multiplexing (**c**)

requirements and characteristics to the use of iodine-based absorption filters for DGV can be found in detail in Chan et al. (1995).

2 Apparatus and instrumentation

2.1 Probe design

The presented pDV sensor is based on the DGV principle and utilizes two sets of laser sending optics at the top and bottom of the device at an angle to the main flow direction. Two receiving optics assemblies collect the light from the measurement volume. This configuration can be seen in Fig. 3. In order to distinguish multiple velocity components with a two-receiver setup, time-shifted multiplexing (alternate flashing) of the two laser beams is necessary. AOMs allow sub-microsecond time-shift multiplexing while enabling amplitude modulation and frequency shift capabilities.

While using AOMs present an extra effort and limit the smallest resolvable timescale, their application is essential to the further development of the envisioned applications of planar time-resolved measurements and eventual volumetric scanning (e.g., Lowe et al. 2012). This geometric configuration allows using planar arrays of sensors for planar vector velocity measurements with very little perspective distortion. Further, owing to the reduced perspective distortion and depth of field mitigation, the use of large aperture lenses and compatibility with depth-wise laser sheet scanning are both enabled. More details on the application of laser sheet scanning for volumetric imaging are given by Thurow and Lynch (2009).

Therefore, the presented instrument is based on a quasi-instantaneous time-shift technique, providing two velocity components shifted in time allowing reconstruction of a full 3-component velocity vector with a high temporal resolution. The influence of the time-shift multiplexing and beam intersection angle on temporal errors and physical uncertainties will be thoroughly discussed in the following studies. Additionally, the influence of turbulent fluctuations on flow statistics due to the properties of the transmission-frequency transfer function is discussed.

2.2 Signal processing

The signal processing flow is displayed step by step in Fig. 4. First, a peak detection algorithm determines valid photon signals in both unfiltered channels separately. After applying detector calibration values, complete datasets are identified as such with valid signals present in both unfiltered channels. Due to the beam multiplexing two interleaving datasets exist and missing values are completed from the adjacent multiplexing window and the arrival time is defined as the average arrival time of both data points. Doing so results in 4 transmission values for each time sample. The iodine cell transfer function is then applied to the measured and the known reference transmission values to determine the differential Doppler frequency. From the Doppler measurement direction vectors, a rotation matrix R is created and three-component time-resolved velocity vectors in the base coordinate system determined similar to the process described by Charrett et al. (2007).

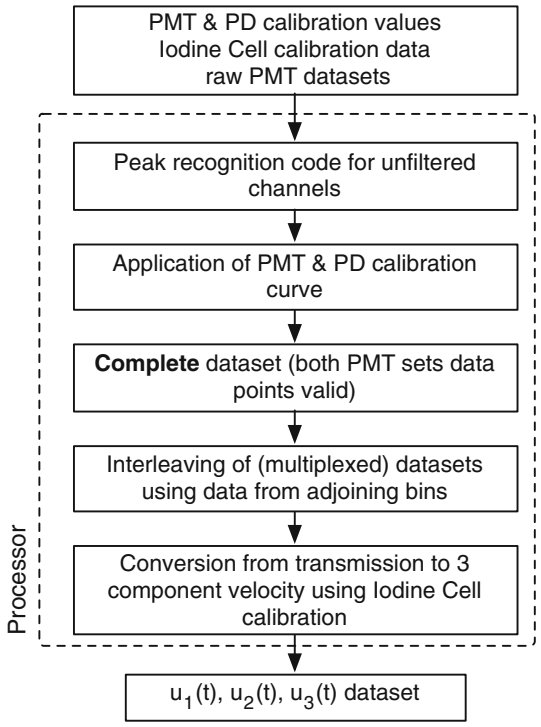

Fig. 4 Flow chart for the multiplexing data processing employed

3 Method verification and performance analysis

3.1 Processing uncertainties

In order to optimize, validate and determine uncertainty of the pDV multiplexing and data processing, a synthetic velocity signal is feed into a model for the instrumentation and particle sampling. The signal is constructed from a one-dimensional model turbulent power spectrum (Pope 2000) and random phase spectrum. The parameters for the model spectrum allow to include integral and Kolmogorov timescales, such that the inverse Fourier transform of the model provides realistic time-series data that may then be scaled and shifted to simulate the desired mean velocity and turbulence intensity. In order to simulate particle arrival statistics, random arrival times are generated using Poisson statistics and the final velocity dataset is obtained at the arrival times from the original oversampled signal.

The velocity and timescales were chosen to be representative of the experiments in supersonic jets. The integral timescales to be resolved for a supersonic jet flow are on the order of the shear layer thickness divided by the eddy convection velocity, which for the flows investigated is about approximately 10–30 μs (Brooks et al. 2014a). The Kolmogorov timescales η in this type of flow are much smaller and can be estimated from the DNS data of Freund et al. (2000) to be on the order of 0.5 μs at the minimum. Quasi-instantaneous techniques like PIV or the here presented time-multiplexed pDV cannot accurately resolve down to the finest scales due to temporal averaging. However, as most relevant and energetic timescales are much larger, this issue loses importance. All reported errors or uncertainties are in relation to measurement of a flow resolved to a smallest timescale of interest of $\tau = 10$ μs. This constraint is realized as a high frequency cutoff at the desired timescale with zero padding up to the Nyquist frequency. Simulation timescales are explained in Table 1. The turbulent kinetic energy (q) values used to generate the model signal are estimated from the prescribed turbulent intensity and the mean velocity of the flow.

Table 1 Simulation timescales and frequencies

Time resolution	Δt
Measurement rate	Particle arrival time (250 kHz)
Sample rate	Not applicable as in practice much higher than particle transit time
Cut off frequency	$1/\tau$

$$q = I^2 U^2 \frac{3}{2}$$

where I is the turbulence intensity and U the mean velocity vector.

The dissipation rate ε is estimated from the Kolmogorov timescale ($\eta = 1$ μs) and the kinematic viscosity for the flow and is about 2.5×10^6 m^2 s^{-3}, resulting in a spectral shape similar to spectra reported by Brooks et al. (2014a).

For the purpose of the numerical uncertainty analysis of the multiplexing portion, the Doppler frequency shift is assumed to be known. When processing the synthetic data, the dataset is first attributed to the two alternating laser beams and then run through the processor. An example of the reconstructed velocity compared to the synthetic velocity data and an example of the reconstructed spectrum is shown in Fig. 5. The spectral information was obtained by using a fuzzy slot correlation processing scheme as introduced by Benedict et al. (2000). All reported quantities are given in a cylindrical coordinate system with streamwise (x), radial (r) and azimuthal (Θ) components, unless otherwise noted.

As will be shown, the main contributor to the random error (the difference between the input and the recovered values) is the multiplexing time interval Δt, which is the time each beam illuminates the measurement volume before it switches to the complementing beam (compare Fig. 3c). This multiplexing time effectively limits the temporal response of the instrument and influences the processing uncertainties due to temporal averaging effects. It is important to note that the processing scheme provided an un-biased mean velocity estimate for all multiplexing time intervals studied in the limit of large sample sets.

Figure 6 shows the instantaneous root-mean-square (RMS) uncertainties of all three components for an example

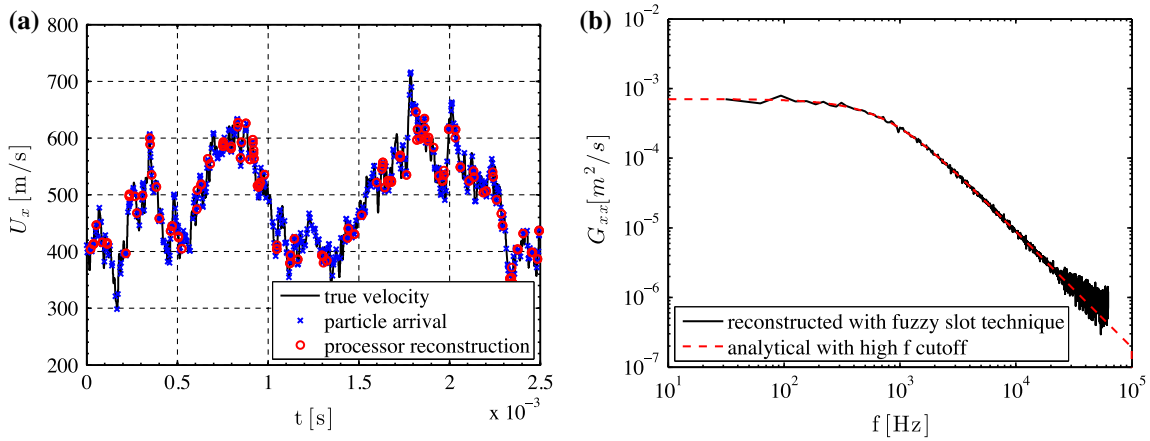

Fig. 5 Streamwise velocity reconstruction (**a**), streamwise velocity spectra (**b**), $\Delta t = 2.0$ µs interval for a 500 m/s, $I = 0.15$ example case, $\eta = 1$ µs

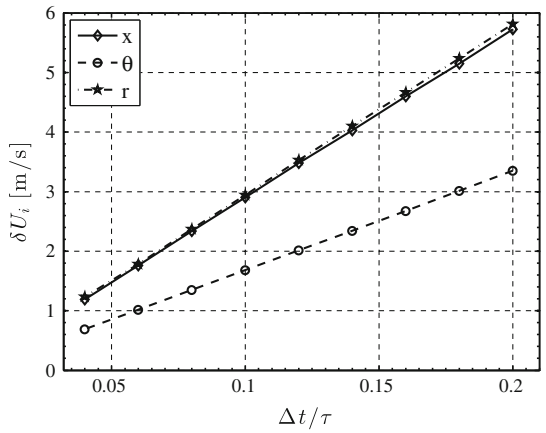

Fig. 6 RMS uncertainty estimate for instantaneous measurement due to temporal averaging

case [$U = (500, 30, 20)$ m/s, $I = 0.15$, $\alpha = 45°$] at different timescale ratios. It can be seen that the error is the largest for the streamwise and radial component, but smaller for the azimuthal component. The differences in the magnitude in the components of these instantaneous velocity errors are caused by the different spatial sensitivities due to the geometric composition of the instrument measurement vectors (compare Eq. 2). This dominantly absolute processing error as such scales with the nature of the flow and its associated timescales to be measured. It may be noted that for heated jets, the uncertainty would increase slightly as temporal scales decrease due to greater convective speeds.

3.2 Physical uncertainties

Each velocity component u_i ($i = 1, 2, 3, 4$) in measurement direction $\left(\widehat{e}_i = \left(\widehat{o} - \widehat{i}\right)_i\right)$ can be described by the Doppler equation.

$$u_i = \left(\frac{f_i}{f_0} - 1\right)c \tag{3}$$

Considering the system as a transfer function $y = F(x_j)$ dependent on $j = 1, 2, \ldots, n$ independent variables, the sensitivity of the system can be described by the sum of linearized Taylor series of the single independent variables.

$$\delta u_i = \sqrt{\left(\frac{\partial u_i}{\partial f_i}\right)^2 (\delta f_i)^2 + \left(\frac{\partial u_i}{\partial f_0}\right)^2 (\delta f_0)^2} \tag{4}$$

where $\dfrac{\partial u_i}{\partial f_i} = \dfrac{c}{f_0}$ and $\dfrac{\partial u_i}{\partial f_0} = -c\dfrac{f_i}{(f_0)^2}$.

The transfer function of the iodine cell can be simplified to a linear function, transducing the transmission T on the flank of a transmission line into frequency f. Subscript i denotes the measured component and subscript 0 refers to the reference state. Therefore, the uncertainty in each measured component is a combination of systematic and random uncertainties, similar to the expression derived by Reinath (1997):

$$\delta u_i = \frac{c}{f_0}\sqrt{\left(\frac{\mathrm{d}f}{\mathrm{d}T}\right)_i^2 (\delta T_i)^2 + T_i^2\left[\delta\left(\frac{\mathrm{d}f}{\mathrm{d}T}\right)_i\right]^2 + \frac{f_i^2}{f_0^2}\left\{\left(\frac{\mathrm{d}f}{\mathrm{d}T}\right)_0^2 (\delta T_0)^2 + T_0^2\left[\delta\left(\frac{\mathrm{d}f}{\mathrm{d}T}\right)_0\right]^2\right\}} \tag{5}$$

Thus, it can be seen that the uncertainty in this reference-based DGV system is dependent on the uncertainty in the slope of the transmission line, the local transmission as well as the frequency of both the shifted and the unshifted signals. These uncertainties are directly related to the respective uncertainties for the iodine cell calibration, in the signal-to-noise ratio and beam splitter transmission ratio. While the transmission uncertainty is mainly random, the uncertainty in the slope of the transmission line is systematic and will represent as bias in the experimental

results. The random errors are most significant for instantaneous time-resolved measurements and the derived higher order moments. The single-component uncertainty and the uncertainty in the measurement vector angles result in the uncertainty for each three-component measurement. The total uncertainty of the measurement including the uncertainty in the geometrical calibration matrix R is represented by:

$$\Delta\vec{U} = \begin{pmatrix} \delta u_x \\ \delta u_\theta \\ \delta u_r \end{pmatrix} = \sqrt{\left(\begin{bmatrix} R_{11} & R_{12} & R_{13} \\ R_{21} & R_{22} & R_{23} \\ R_{31} & R_{32} & R_{33} \end{bmatrix}\right)^2 \begin{pmatrix} \delta u_1 \\ \delta u_2 \\ \delta u_3 \end{pmatrix}^2 + \left(\begin{bmatrix} \delta R_{11} & \delta R_{12} & \delta R_{13} \\ \delta R_{21} & \delta R_{22} & \delta R_{23} \\ \delta R_{31} & \delta R_{32} & \delta R_{33} \end{bmatrix}\right)^2 \begin{pmatrix} u_1 \\ u_2 \\ u_3 \end{pmatrix}^2} \quad (6)$$

3.3 System total uncertainties

The system's uncertainties are a mixture of physical and data processing/time averaging uncertainties and errors. The error in the transmission estimate from the Doppler-shifted photon bursts is estimated by conducting Monte Carlo simulations of a simple Gaussian burst signal model with Gaussian noise superimposed. The Gaussian burst envelope $A(t)$ is modeled as:

$$A(t) = Ke^{-\frac{t^2}{2s^2}} \quad (7)$$

where $s = t_0/6$, t_0 is the particle transit time, K is a constant with units of energy (J). Similar models have been previously used for uncertainty estimates in LDV (Ecker et al. 2012).

Figure 7 depicts the RMS error for each signal-to-noise ratio ($\mathrm{SNR} = 10\log_{10}\left(\frac{P_{\mathrm{signal}}}{P_{\mathrm{noise}}}\right)$; power, P) estimated from a 100,000 bursts Monte Carlo. The SNR is based on the reference and it is assumed that noise is of equal power both for the reference as well as the shifted signal. Therefore, lower transmission values result in higher errors

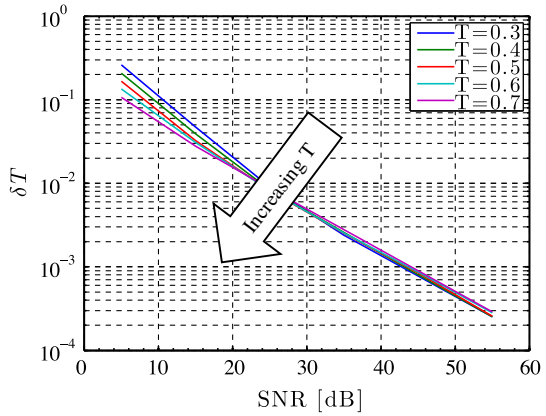

Fig. 7 Transmission error in the burst processing for different SNR

to the transmission estimate. The uncertainty in the reference transmission is assumed to be very low as the SNR can be freely chosen by varying the reference laser power. The parameters used for the following system uncertainty estimates are summarized in Table 2.

Assuming that the sources of errors analyzed here are uncorrelated, all errors may be considered by finding the resulting norm, analogous to applying Eq. 4. Figure 8 gives the total uncertainties due to the DGV sensitivities and data processing errors for an example case [$U = (500, 30, 20)$ m/s, $I = 0.15$, SNR = 20 dB, $\Delta t = 2$ μs]. As the processing error is relative small, the bias and instantaneous uncertainty are dominated by the sensitivities to the uncertainty in transmission and transmission slope as well as the geometric composition of the instrument. While the azimuthal velocity uncertainties are almost constant, the uncertainties in the streamwise and radial component decrease and increase, respectively, with intersection angle. As can be seen from Fig. 8a, b, angles between 30° and 50° offer an ideal balance of uncertainties for this system. The slight linear slope in the bias uncertainty of the azimuthal component is due to changes in transmission with changing intersection angle being dominant.

3.4 Laser stability

According to the Springer handbook of experimental fluid mechanics (Tropea et al. 2007), the laser bandwidth for a successful DGV measurement needs to be smaller than 10 MHz. The Verdi V6 laser used in this study has a line width of about 5 MHz over 20 ms according to Coherent (Coherent Inc. white paper). The line width narrows if observed over smaller timesscales such as implemented with the pDV sensor developed here. The reference photodiodes were sampled at 50 MHz during all measurements, therefore minimizing the influence of laser jitter and laser drift on the measurement.

3.5 Transmission line bandwidth limitations

Another critical component of a successful DGV/pDV measurement is the choice of absorption line. For low flow speed application, the sensitivity to velocity change is the main concern as it directly influences the physical uncertainties. However, for high-speed application with extreme Doppler shifts, the line bandwidth compared with the

Table 2 Parameters used for physical uncertainty estimate

Parameter	Uncertainty
δT_i	0.018
δT_{ref}	0.005
$\delta\left(\frac{\mathrm{df}}{\mathrm{d}T}\right)$	$0.005\overline{\left(\frac{\mathrm{df}}{\mathrm{d}T}\right)}$

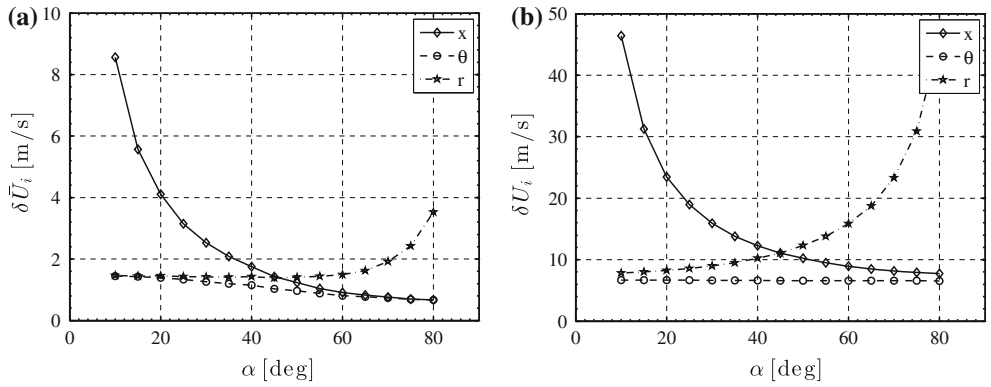

Fig. 8 Bias (**a**) an instantaneous (**b**) velocity uncertainty for example case (α is defined in Fig. 3)

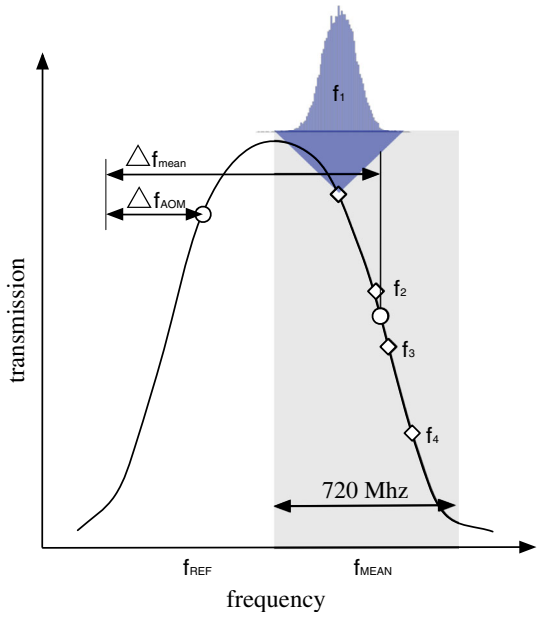

Fig. 9 Transmission line bandwidth limitations for turbulent flows

Doppler bandwidth is most essential. Even when the mean velocity shift is placing the measured transmissions on the center of an absorption line, the turbulent motion of the fluid can cause an extreme standard deviation from the mean shift.

In Fig. 9, an example case with large frequency shifts is displayed. It can be seen from the figure that there are non-unique regions bounding the line bandwidth to about 720 MHz (representative of half bandwidth of line 89.95 1/cm, compare to Fig. 2). In these cases of large Doppler shifts and large standard deviations, this limitation can clip and distort the measured velocity statistics compared to the true values.

The total bandwidth necessary is determined from the difference of the highest and lowest frequency of the frequencies to be measured. As for this particular technique, four possible frequency combinations exist; the lowest possible bandwidth is defined by the lowest bandwidth of one of the possible combinations of f_1, f_2, f_3 and f_4. Measurements that have a lower required bandwidth than the measurement line width can still be subject to bounding as the distribution of frequencies (indicated by a Gaussian histogram in Fig. 9) come close to the bounding sides of the line.

Figure 10 shows the line coverage for synthetic datasets with increasing turbulent intensities ($f_{\mathrm{AOM}} = -80$ MHz, $\alpha = 45°$). For a center frequency (f_{mean}) fixed on the center of the line flank, increasing turbulent intensity leads to clipping—frequencies that are not covered by the bandwidth of the transfer function. Line coverage is here defined as the number of observable data points N_{Line} on a real transmission line divided by the number of observable data points N_{Turb}. on an idealized transmission line. The center of the frequency shift can be shifted relative to the reference frequency f_{REF} by using an AOM, this shift is denoted by f_{AOM} in Fig. 9.

For this example case with relatively high mean velocities and turbulent intensities of 15 %, up to 9 % of the dataset cannot be observed due to bandwidth limitations. Figure 11 shows the absolute error (bias) of the mean velocity for the example case. Individual instantaneous measurements as discussed in the previous section are not affected with a bandwidth-induced error since measurements exceeding the bandwidth are invalid, with no means for estimating velocity. However, statistics and spectral information will obviously be impacted due to bandwidth limits. For measurements of highly turbulent flows with high mean velocities, these physical limitations need to be observed in order to allow accurate measurements of velocity statistics. As the presented results are for a system with 532 nm laser wavelength, the use of a laser with higher wavelength, e.g., 852.3 nm as used by Fischer et al. (2007) would significantly decrease the required Doppler frequency bandwidth and increase the effective dynamic range of the instrument.

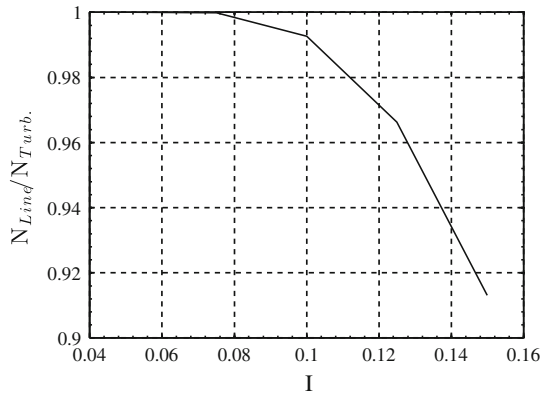

Fig. 10 Line coverage decreasing with increasing turbulent intensity due to clipping, for example case

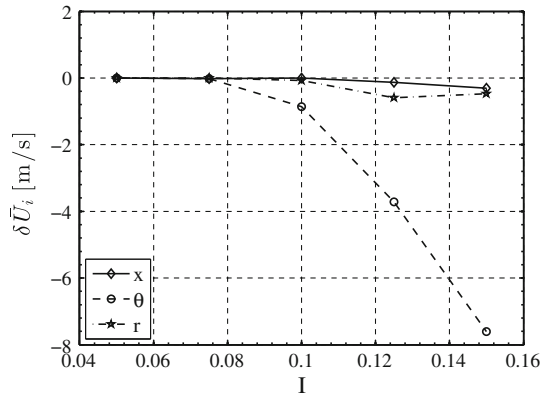

Fig. 11 Mean velocity error due to line bounding at high turbulent intensity, for example case

4 Implementation: apparatus and instrumentation

The interest driving the instrument development is the need to understand the production of noise in supersonic jets. Lighthill (1952) made a first theoretical approach to jet noise in 1952 with his famed acoustic analogy, representing the fluctuations of the local flow by a distribution of quadrupole sources with equivalent energy. This analogy is strongly dependent on the source terms described by the Lighthill stress tensor (Tam 1995), which can be deduced from higher order correlations. To further physical understanding of the noise generation processes and to enable validation of numerical models, time-accurate measurements of supersonic jets are therefore inevitable.

4.1 Facility

The Virginia Tech hot jet facility has been described in past works (Ecker et al. 2014b; Brooks et al. 2014a). This facility provides supersonic flow at TTRs up to 3 at 0.12 kg/s mass flow rate. The air is heated by an electrical 192 kW power inline heater. The biconical nozzle used ($M_d = 1.65$; nozzle diameter, $d = 0.75$ in) was adapted from the geometry studied by Powers and McLaughlin (2012) for military-style nozzles, differing in the present study by being axisymmetric and unfaceted.

For the cold flow studied, flow seeding is performed by introducing di-ethyl-hexyl-sebacat (DEHS) oil droplets generated by a LaVision four-nozzle flow seeder unit. This unit is capable of generating submicron droplet sizes, and particle response time can be estimated for a 1-μm-diameter particle from Stokes drag (Ecker et al. 2012) assuming continuum regime flow, to be about 3.8 μs at a flow static temperature of 200 K.

4.2 Instrument configuration and properties

Figure 12 shows the optical setup for the described pDV system. Essential system parameters are tabulated in Table 3. The setup can be separated into three different zones: (1) instrument, (2) optical conditioning and (3) data acquisition. The instrument here refers to the device that is attached to the facility and generates the measurement volume as well as collects the scattered light. The measurement volume created by the 250 mm focal length sending lens is estimated to be about 60 μm diameter. The two laser heads are consecutively flashing to generate two velocity components at a time. The receiving optics ($f = 200$ mm) focuses the received light into 200 μm telecommunication-grade multimode fiber.

Optical conditioning is performed on a separate optical table in an adjacent room. Multiplexing is enabled by using two 80 MHz AOMs produced by Intraaction Corp. as optical switches, turning on and off the respective beam. A BNC 565 signal delay generator controls the multiplexing time interval, which is the interval each beam consecutively activates. The laser beam is shifted by −80 MHz and then transmitted to the instrument by an 8-μm-core-diameter telecommunication-grade multimode fiber. PMT and photodiode (PD) calibration measurements are performed before every experimental section. As this calibration is performed in situ all errors due to alignment, beam-splitting cubes imperfection and polarization dependencies are taken into account to the greatest extent possible. Two photodiodes (Thorlabs PDA100A) are used to monitor the unshifted laser frequency through the iodine gas cell at all times, reducing the influence of laser frequency drift or fluctuation to a minimum. Four Hamamatsu R4124 PMTs are used for transducing the received Doppler-shifted photons into voltage signals.

The experimental data are acquired by a NI PXIe DAQ system using a 50 mega samples/S (MS/s) Adapter module (NI 5752) on a FlexRIO FPGA (NI PXIe-7965R) unit. All

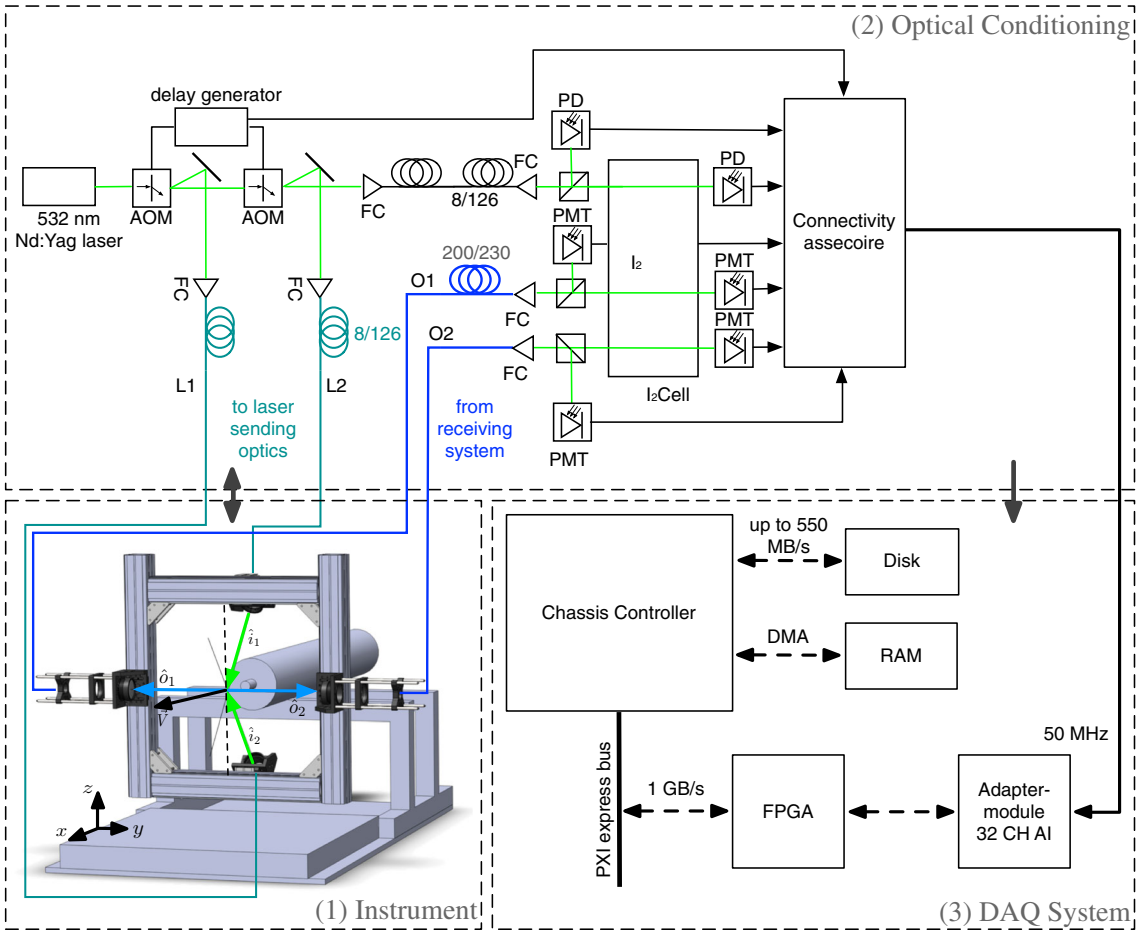

Fig. 12 Optical layout of pDV probe (*FC* beam to fiber coupler, *AOM* acousto-optic modulator, *PD* photodiode, *PMT* photomultiplier tube)

Table 3 Instrument parameters

Parameters	
Measurement volume beam waist diameter	60 μs
Laser power (per beam)	160 mW
Multiplexing time step	2 μs
α	45°
Sampling rate DAQ	50 MS/s
Iodine cell body temperature	60 °C

four PMTs signals, as well as the PD signals and the AOM-switching signals are recorded simultaneously at 50 MS/s. Datasets were typically 50 million samples, which equals to 1 s. in duration. Tuning the cavity length inside the Coherent Verdi V6 CW diode-pumped solid-state laser is performed by controlling a piezoelectric element (PZT) inside the laser, using a 0–72 V BK precision bench-top power supply. This allows choosing the transmission line at which the sensitivity and bandwidth of the transfer function is optimal.

4.3 In situ uncertainties

From the previous analysis, the uncertainty in each measured component can be determined for a 45° angle configuration for an example case [(500, 30, 20) m/s, $I = 0.15$ $\Delta t = 2$ μs, 50,000 samples and SNR 20 dB signal, misalignment of geometry by 0.14°]. Table 4 (top) shows the associated systematic uncertainties. Table 4 (bottom) gives the specific uncertainties for the case of the time-resolved instantaneous measurements. The relative uncertainties are excellent for the streamwise component but somewhat higher for radial and azimuthal components. Different geometrical arrangements and multiplex time steps can be used to decrease the uncertainty in those components. For comparison, Thurow et al. (2005) give a velocity error for their 1-component camera-based system of about 9–33 m/s for measurements in their Mach 2.0 supersonic jet. Fischer et al. (2013) reported a measured uncertainty of about 1 m/s at 100 kHz laser modulation frequency for their laboratory scale experiments.

In the following section, instrument performance is validated with a LDV probe with measurements in a cold

Table 4 Associated uncertainties for example case

	$\delta\bar{U}_x$ (m/s)	$\delta\overline{U}_\theta$ (m/s)	$\delta\overline{U}_r$ (m/s)
Systematic uncertainties			
Processing error	0.042	0.975	0.128
Instrument uncertainty	1.420	1.025	1.362
Geometrical uncertainty	0.597	0.443	0.572
Total uncertainty	1.541	1.482	1.483
	δU_x (m/s)	δU_θ (m/s)	δU_r (m/s)
Instantaneous uncertainties			
Processing error	6.175	1.120	6.195
Instrument uncertainty	9.200	6.508	9.190
Geometrical uncertainty	0.597	0.443	0.572
Total uncertainty	11.10	6.618	11.10

supersonic jet, and an exposition of the instrument time response is provided via measurements of Reynolds stress spectra streamwise development.

5 Results and discussion

In order to evaluate the pDV instrument performance, measurements at different jet NPR at the same location were performed repeatedly. These measurements are then compared to a 2-component LDV measurement at the same location. Details on the LDV probe used can be found in Brooks et al. (2014a, b). The instantaneous uncertainty of the LDV measurements is 0.33 % of the measured velocity, with systematic uncertainty in the fringe spacing of the same order. Uncertainties of the pDV probe are given in Table 4, with approximately the same magnitude for bias errors as the LDV. The horizontal error bars in Fig. 13 are determined from the uncertainties in the NPR value due to uncertainties in the reference pressure and total pressure readings and explain small discrepancies between LDV and pDV measurement over the instrumentation uncertainties themselves. The comparison of the mean velocity data in Fig. 13 shows excellent agreement within positioning, pressure and velocity uncertainties. Measurements were repeatable and consistent over the course of the experiment.

After validation of the pDV probe, measurements along the streamwise axis at a normalized radial coordinate of $r/d = 0.2$ and NPR = 3.2 ($T_0 = 300$ K; isentropic Mach number, $M_j = 1.4$) are performed. At this condition, the jet is highly over-expanded and exhibits the screech phenomenon. The measurement volume moves through several normal and oblique shocks as well as expansion waves before it enters a region where the potential core breaks down and large and small-scale turbulent mixing occurs.

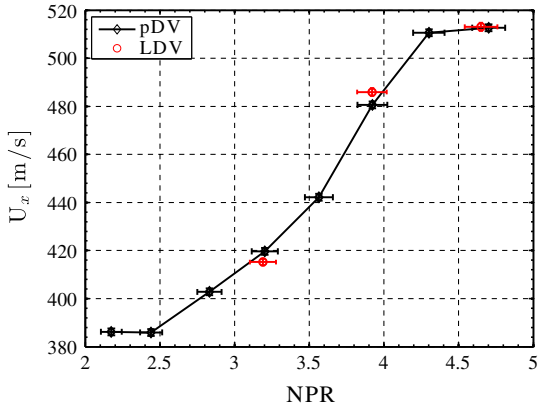

Fig. 13 Mean velocity measurement at a static position in the jet

Mean data rates of up to 100 kHz were reached in the potential core where particle seeding was optimal. Local data rates were up to 250 kHz over periods of time, but could not be sustained due to the Poisson statistics of particle arrival resulting in periods of data dropout.

Mean streamwise, radial and azimuthal velocities along the streamwise coordinate are displayed in Fig. 14. It is to note that the streamwise and radial velocities clearly reflect the shock cell structure in the potential core as well as the breakdown further downstream.

From this measurement, it appears that there are four strong shock cells in the mean at this condition. This is consistent with Schlieren photographs from this region. The azimuthal velocity does not show this behavior. The velocity vectors were rotated using the information at the exit plane to have zero radial and azimuthal velocity. The drift in the mean azimuthal velocity is most likely due to precession of the shock structure; at 7.8 kHz, it would only require a precession radius of 1.3 mm to obtain this effect.

After a distance x/d larger than 4, a strong rise of the Reynolds normal stresses due to shock unsteadiness growth and flow instability can be observed. This trend is displayed for all normal stresses in Fig. 15a. At 5 diameters, the streamwise normal stresses correspond to a turbulence intensity of about 0.12. A similar trend and magnitude was shown by Alkislar et al. (2003) for the streamwise normal and transverse stresses in a rectangular under-expanded supersonic jet, as well as by Lau et al. (1979) and Bridges and Wernet (2008) for normal stresses in axisymmetric fully expanded supersonic jets. Alkislar and Krothapalli's data also showed a peak in the transverse mean Reynolds stress that peaked above the magnitude of the streamwise normal stresses before dropping to lower values, similar to the radial normal stress displayed in Fig. 15a.

A fuzzy slot correlation technique (Benedict et al. 2000) allows to obtain auto and cross-correlation from the non-equally spaced velocity data. The Wiener–Khinchin

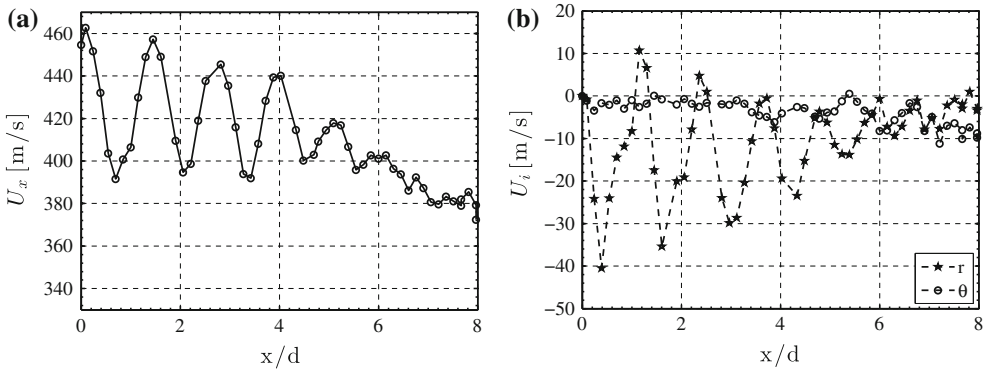

Fig. 14 Mean streamwise (**a**) and radial and azimuthal (**b**) velocities along the streamwise coordinate (NPR = 3.2, $M_j = 1.4$, TTR = 1, $r/d = 0.2$)

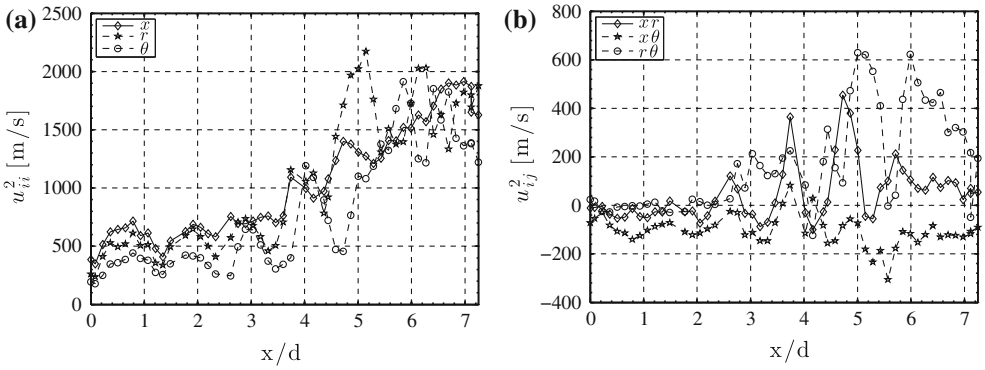

Fig. 15 Normal (**a**) and shear (**b**) stresses along the streamwise coordinate (NPR = 3.2, $M_j = 1.4$, TTR = 1, $r/d = 0.2$)

theorem grants direct conversion of the auto and cross-correlation into auto and cross-spectra.

The behavior of shock unsteadiness, or screech, is examined in the spectral and time-delay domains. As first proposed by Powell (1953), axisymmetric, helical and lateral modes of screech are possible. As verified using Schlieren photography, the jet under study exhibited the helical instability mode. In Fig. 16, the development of the Reynolds shear stress time-delay cross-correlation is exhibited. While the findings from the visualizations of Umeda and Ishii (2001) indicate that the helical mode initiated in the third shock cell for the under-expanded jets they studied, the current results for the over-expanded jet indicate the significant strength of the fundamental screech tone in the shear stress just upstream of the third shock, shifted toward the nozzle exit by ½ a cell compared with the under-expanded jet. The rapid decay of the fundamental tone three shock cells downstream of its appearance is in contrast to the recent results of Edgington-Mitchell et al. (2014) for under-expanded jets, as well. The authors there indicate a strong persistence of the fundamental helical mode signature out to $x/d = 9$. Time-accurate Schlieren videos obtained for the jet currently under study indicated a violent screech mode that likely grew into a nonlinear regime causing its rapid breakdown. Another interesting aspect of the time-delay data is the variable phase shift between the streamwise and radial fluctuation velocities with streamwise distance, particularly visible in the three shock cells with clear fundamental mode content, between 3 and 5 diameters. These shifts occur in the regions of high streamwise velocity gradients, with increasing phase shift magnitude between streamwise and radial velocity fluctuations in shock regions and decreasing phase shift magnitudes in the expansion regions. Again from the Schlieren images, it appears that this variable phase is due to the lag between the helical motion of the jet core and the formation of the shock. The visualization indicates a highly unsteady shock at $x/d = 3$, contributing the mechanism for this phase lag.

Spectral analysis of the Reynolds stresses measured reveals the loci of fundamental and harmonic screech tone dominance (compare Fig. 17). The streamwise normal stress results generally follow the behavior deduced from the time-delay correlation results—the fundamental screech tone is shown to dramatically diminish for $x/d > 6$. However, interestingly, the radial/azimuthal shear stress exhibits significant content from the screech tone throughout the measurement range. It is likely that this difference is explainable due to the appearance of vortical turbulence due to the penetration of the shear layer into the potential core. For the streamwise normal stress, contributions from turbulence produced by axisymmetric shear

are significant and may swamp out the screech signal. However, there are no mechanisms for production of radial–azimuthal shear stress in the axisymmetric jet beyond the screech instability itself. Thus, we would expect that production of that shear stress would be intrinsically linked to the spectral content of the screech mechanism, causing the strong persistence of this signature in the shear stress spectra, as seen in Fig. 17.

6 Conclusions

A new probe making use of the DGV technique has been developed and is presented in the framework of state of the art development of DGV technology. Especially the time-shift multiplexing is a new approach reducing required sensor devices while still enabling the time response capable of high-speed flow applications.

In a study on the data processing and its induced errors, it was found that next to the geometric configuration the flow timescales are of largest impact. Reducing the time-shift period allows reducing associated errors significantly. For timescales relevant to the jet noise application, the instantaneous velocity errors due to processing are about 6.1 m/s for streamwise and radial component and around 1.0 m/s for the azimuthal velocity component for the example case with timescales of interest as low as 10 μs.

The detailed heuristic uncertainty analysis propagates the uncertainties of the linearized DGV transfer function and allows obtaining a reasonable estimate of the measurement uncertainties. Results from the processing analysis were included and the total measurement uncertainty expressed as a root square sum of the uncorrelated contributions of data processing errors and physical uncertainties. The uncertainties for the presented instrument are about 1.5 m/s for mean measurements and between 6.6 and 11.1 m/s for instantaneous measurement of the 3-component velocity vector.

It is shown that using velocity multiplexing is an effective method to reduce instrument cost without sacrificing mean uncertainties. Uncertainties for the instantaneous velocity vectors are mainly characterized by random effects such as signal-to-noise ratio as well as temporal averaging effects. Achieved uncertainties compare favorable to previous work in time-resolved DGV. Implications of the transmission line width for measurement of flows with high mean velocities and high turbulent intensities are discussed and examples for associated uncertainties given. Using a different laser with a higher wavelength could compress the required transfer function bandwidth and increase the dynamic range of the instrument therefore eliminating these physical limitations.

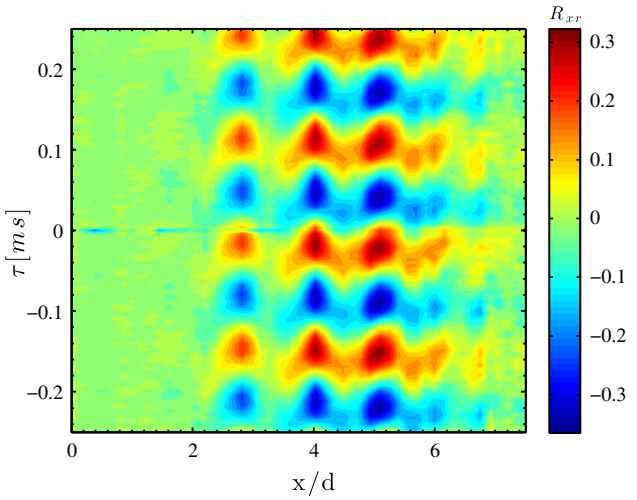

Fig. 16 Cross-correlation of the streamwise and radial velocity along the streamwise coordinate (NPR = 3.2, $M_j = 1.4$, TTR = 1, $r/d = 0.2$)

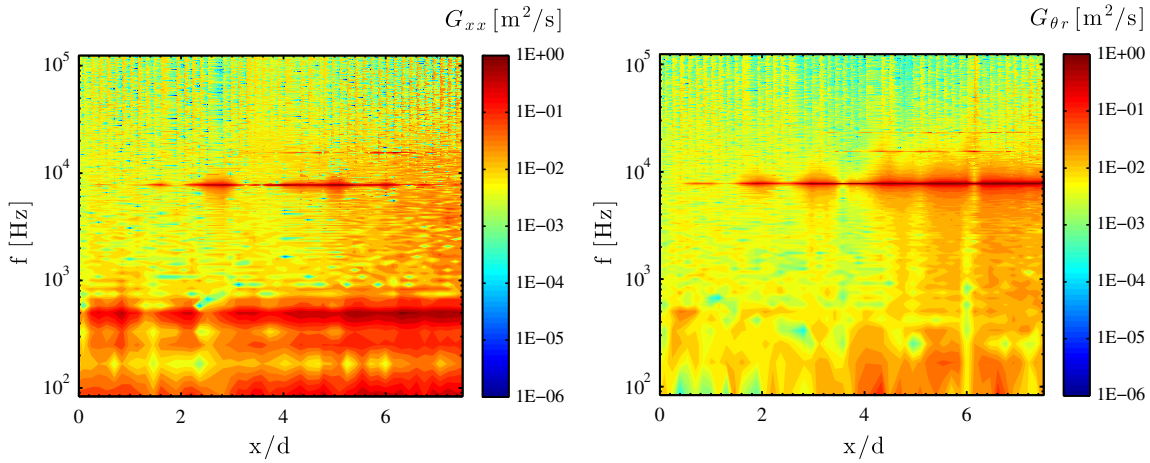

Fig. 17 Streamwise velocity auto (**a**) and radial–azimuthal velocity cross-spectra (**b**) along the streamwise coordinate (NPR = 3.2, $M_j = 1.4$, TTR = 1, $r/d = 0.2$)

First measurements in a supersonic cold over-expanded jet using a pDV instrument have been performed and the temporal capabilities demonstrated. Mean flow velocity measurements at different tunnel operating pressures have been validated by using a LDV and are within the expected uncertainty range for reference-based DGV. By traversing the instrument along the streamwise axis, mean flow and full Reynolds stress tensors were obtained. Global data rates of above 100 kHz with local data rates as high as 250 kHz allowed spectral analysis of the Reynolds stress tensors in the streamwise development.

In combination with time-accurate Schlieren videos, the current study exposes helical screech modes with a spatial extension fundamentally different from the structures at under-expanded conditions found in the literature. Compared to under-expanded conditions, the present study shows rapid breakdown due to shock unsteadiness and vortical nonlinear instability growth The screech tone phenomenon and its higher harmonics present in the potential core and in regions of increased turbulent mixing and is suspected to be linked to the production of radial–azimuthal shear stresses in extended regions beyond the potential core. While the influence of the screech phenomenon onto the normal stresses quickly diminishes at $x/d > 6$, the signature of the screech remains imprinted onto the radial–azimuthal shear stresses beyond the region of investigation.

This measurement provides insight into the usefulness of time-resolved DGV for understanding dominant turbulent structures for noise generation in supersonic jet flow and highlights the need for ongoing development of time-resolved multi-point measurements. This study discusses in detail a geometrical configuration that can be easily extended to allow planar and tomographic operation by using spatially resolving sensors, large aperture lens systems and scanning laser sheets.

Acknowledgments The work described was supported by the Office of Naval Research Hot Jet Noise Reduction Basic Research Challenge and DURIP, Grants N00014-11-1-0754 and N00014-12-1-0803 under program managers Drs. Brenda Henderson and Joseph Doychak.

References

Alkislar MB, Krothapalli A, Lourenco LM (2003) Structure of a screeching rectangular jet: a stereoscopic particle image velocimetry study. J Fluid Mech 489:121–154

Benedict LH, Nobach H, Tropea C (2000) Estimation of turbulent velocity spectra from laser Doppler data. Meas Sci Technol 11(8):1089

Bridges JE, Wernet MP (2008) Turbulence associated with broadband shock noise in hot jets. NASA/TM-2008-215274

Brooks DR, Ecker T, Lowe KT, Ng WF (2014a) Experimental Reynolds stress spectra in hot supersonic round jets. AIAA SciTech (52nd Aerospace sciences meeting)

Brooks DR, Lowe KT (2014b) Fluctuating flow acceleration in a heated supersonic jet. In: Proceedings of the 17th international symposium on applications of laser techniques to fluid mechanics, Lisbon, Portugal, 7–10 July

Cadel DR, Ecker T, Lowe KT (2014a) Time-domain cross-correlation scan DGV (CCS-DGV) for mean-velocity boundary layer measurements. AIAA SciTech (52nd Aerospace sciences meeting)

Cadel DR, Ecker T, Lowe KT (2014b) Volumetric vector velocity measurements in a hot supersonic jet. In: Proceedings of the 17th international symposium on applications of laser techniques to fluid mechanics, Lisbon, Portugal, 7–10 July

Cavone AA, Meyers JF, Lee JW (2006) Development of point Doppler velocimetry for flow field investigations. In: Proceedings of the 13th international symposium on applications of laser techniques to fluid mechanics, Lisbon, Portugal, 26–29 June

Chan VSS, Heyes AL, Robinson DI, Turner JT (1995) Iodine absorption filters for Doppler global velocimetry. Meas Sci Technol 6(6):784–794

Charrett TOH, Ford HD, Nobes DS, Tatam RP (2004) Two-frequency planar Doppler velocimetry (2v-PDV). Rev Sci Instrum 75:4487–4496

Charrett TOH, Nobes DS, Tatam RP (2007) Investigation into the selection of viewing configurations for three-component planar Doppler velocimetry measurements. Appl Opt 46(19):4102–4116

Clancy PS, Samimy M, Erskine WR (1999) Planar Doppler velocimetry: three-component velocimetry in supersonic jets. AIAA J 37(6):700–707

Coherent Inc. white paper, Wavelength control and locking with sub-MHz precision. http://www.coherent.com/download/6823/Wavelength-Control-and-Locking-with-Sub-MHz-Precision.pdf. Accessed 12 Aug 2014

Ecker T, Lowe KT, Simpson RL (2012) Novel laser Doppler acceleration measurements of particle lag through a shock wave. In: 50th AIAA aerospace sciences meeting including the New Horizons forum and aerospace exposition

Ecker T, Lowe KT, Ng WF, Brooks DR (2014a) Fourth-order spectral statistics in the developing shear layers of hot supersonic jets. In: Propulsion and power (50th AIAA/ASME/SAE/ASEE joint propulsion conference)

Ecker T, Brooks DR, Lowe KT, Ng WF (2014b) Spectral analysis of over-expanded cold jets via 3-component point Doppler velocimetry. AIAA Scitech (52nd Aerospace sciences meeting)

Edgington-Mitchell D, Oberleithner K, Honnery DR, Soria J (2014) Coherent structure and sound production in the helical mode of a screeching axisymmetric jet. J Fluid Mech 748:822–847

Elliott GS, Beutner TJ (1999) Molecular filter based planar Doppler velocimetry. Prog Aerosp Sci 35(8):799–845

Fischer M, Heinze J, Matthias K, Röhle I (2000) Doppler global velocimetry in flames using a newly developed, frequency stabilized, tunable, long pulse Nd: YAG laser. In: Proceedings of the 10th international symposium on applications of laser techniques to fluid mechanics, Lisbon, Portugal, 10–13 July

Fischer A, Büttner L, Czarske J, Eggert M, Grosche G, Müller H (2007) Investigation of time-resolved single detector Doppler global velocimetry using sinusoidal laser frequency modulation. Meas Sci Technol 18(8):2529–2545

Fischer A, Büttner L, Czarske J, Eggert M, Müller H (2008) Measurement uncertainty and temporal resolution of Doppler global velocimetry using laser frequency modulation. Appl Opt 47(21):3941–3953

Fischer A, Pfister T, Czarske J (2010) Derivation and comparison of fundamental uncertainty limits for laser-two-focus velocimetry, laser Doppler anemometry and Doppler global velocimetry. Measurement 43:1556–1574

Fischer A, Büttner L, Czarske J (2011) Simultaneous measurements of multiple flow velocity components using frequency modulated lasers and a single molecular absorption cell. Opt Commun 284:3060–3064. doi:10.1016/j.optcom.2011.02.070

Fischer A, König J, Haufe D, Schlüßler R, Büttner L, Czarske J (2013) Optical multi-point measurements of the acoustic particle velocity with frequency modulated Doppler global velocimetry. J Acoust Soc Am 134(2):1102–1111

Forkey JN (1996) Development and demonstration of filtered Rayleigh scattering: a laser based flow diagnostic for planar measurement of velocity, temperature and pressure. PhD Thesis, Princeton University

Forkey JN, Lempert WR, Miles RB (1997) Corrected and calibrated I_2 absorption model at frequency-doubled Nd:YAG laser wavelengths. Appl Opt AO 36:6729–6738

Freund JB, Lele SK, Moin P (2000) Compressibility effects in a turbulent annular mixing layer: part 1. Turbulence and growth rate. J Fluid Mech 421:229–267

Fussell J (2003) Refinement and verification of the Virginia Tech Doppler global velocimeter (DGV). MS Thesis, Virginia Tech

Jones T (2001) Development and testing of the Virginia Tech Doppler global velocimeter (DGV). MS Thesis, Virginia Tech

Komine H (1990) US Patent No. 4,919,536. U.S. Patent and Trademark Office, Washington, DC

Komine H, Brosnan SJ, Litton AB, Stappaerts EA (1991) Real-time, Doppler global velocimetry. In: 29 h AIAA aerospace sciences meeting

Kuhlman J, Collins P, Scarberry T (2001) Two-component point Doppler velocimetry data in circular jets. Meas Sci Technol 12(4):395–408

Lau JC, Morris PJ, Fisher MJ (1979) Measurements in subsonic and supersonic free jets using a laser velocimeter. J Fluid Mech 93:1–27

Lighthill MJ (1952) On sound generated aerodynamically. I. General theory. In: Proceedings of the royal society A: mathematical, physical and engineering sciences, vol 211, pp 564–587

Lowe KT, Ng WF, Ecker T (2012) Early development of time-resolved volumetric Doppler velocimetry for new insights in hot supersonic jet noise. In: 18th AIAA/CEAS aeroacoustics conference (33rd AIAA aeroacoustics conference)

Meyers JF, Komine H (1991) Doppler global velocimetry: a new way to look at velocity. Laser Anemometry 1:289–296

Meyers J, Lee J (2010) Boundary layer measurements in a supersonic wind tunnel using Doppler global velocimetry. In: Proceedings of the 15th international symposium on applications of laser techniques to fluid mechanics, Lisbon, Portugal, 05–08 July

Meyers JF, Lee JW, Schwartz RJ (2001) Characterization of measurement error sources in Doppler global velocimetry. Meas Sci Technol 12:357–368

Müller H, Lehmacher T, Grosche G (1999). Profile sensor based on Doppler global velocimetry. In 8th International conference laser anemometry advances and applications, pp 475–482

Nobes DS, Ford HD, Tatam RP (2004) Instantaneous, three-component planar Doppler velocimetry using imaging fibre bundles. Exp Fluids 36(1):3–10

Pope SB (2000) Turbulent flows. Cambridge University Press, Cambridge

Powell A (1953) On the mechanism of choked jet noise. Proc Phys Soc Lond Sect B 66(12):1039

Powers RW, McLaughlin DK (2012) Acoustic measurements of scale models of military style supersonic beveled nozzle jets with interior corrugations. In: AIAA Paper, 2116, 18th AIAA/CEAS aeroacoustics conference (33rd AIAA aeroacoustics conference)

Reinath MS (1997) Doppler Global velocimeter development for the large wind tunnels at Ames Research Center. NASA TM 112210

Smith MW (1998) Application of a planar Doppler velocimetry system to a high Reynolds number compressible jet. In: Presented at the 36th AIAA aerospace sciences meeting and exhibit, Reno, NV

Tam CK (1995) Supersonic jet noise. Annu Rev Fluid Mech 27(1):17–43

Thurow BS, Lynch KP (2009) Development of a high-speed three-dimensional flow visualization technique. AIAA J 47(12): 2857–2865

Thurow BS, Jiang N, Lempert WR, Samimy M (2005) Development of megahertz-rate planar Doppler velocimetry for high speed flows. AIAA J 43(3):500–511

Tropea C, Yarin AL, Foss JF (eds) (2007) Springer handbook of experimental fluid mechanics, vol 1. Springer, Berlin

Umeda Y, Ishii R (2001) On the sound sources of screech tones radiated from choked circular jets. J Acoust Soc Am 110(4):1845–1858

Wernet MP (2007) Temporally resolved PIV for space–time correlations in both cold and hot jet flows. Meas Sci Technol 18(5):1387

Part IV.

A rapid response 64-channel photomultiplier tube camera for high-speed flow velocimetry

The contents of this chapter were published in Measurement Science and Technology as a technical note (Tobias Ecker, K. Todd Lowe, Wing F. Ng, "A rapid response 64-Channel Photomultiplier tube camera for high-speed flow velocimetry", Meas. Sci. Technol. 26 (2015) 027001 (6pp), DOI: 10.1088/0957-0233/26/2/027001).

IOP Publishing Measurement Science and Technology
Meas. Sci. Technol. **26** (2015) 027001 (6pp) doi:10.1088/0957-0233/26/2/027001

Technical Design Note

A rapid response 64-channel photomultiplier tube camera for high-speed flow velocimetry

Tobias Ecker[1], **K Todd Lowe**[1] **and Wing F Ng**[2]

[1] Department of Aerospace and Ocean Engineering, Virginia Tech, Blacksburg, VA 24061, USA
[2] Department of Mechanical Engineering, Virginia Tech, Blacksburg, VA 24061, USA

E-mail: ecker@vt.edu

Received 6 October 2014, revised 25 November 2014
Accepted for publication 27 November 2014
Published 22 December 2014

Abstract

In this technical design note, the development of a rapid response photomultiplier tube camera, leveraging field-programmable gate arrays (FPGA) for high-speed flow velocimetry at up to 10 MHz is described. Technically relevant flows, for example, supersonic inlets and exhaust jets, have time scales on the order of microseconds, and their experimental study requires resolution of these timescales for fundamental insight. The inherent rapid response time attributes of a 64-channel photomultiplier array were coupled with two-stage amplifiers on each anode, and were acquired using a FPGA-based system. Application of FPGA allows high data acquisition rates with many channels as well as on-the-fly preprocessing techniques. Results are presented for optical velocimetry in supersonic free jet flows, demonstrating the value of the technique in the chosen application example for determining supersonic shear layer velocity correlation maps.

Keywords: optical sensors, photomultiplier, FPGA, velocimetry, high-speed flow

(Some figures may appear in colour only in the online journal)

1. Introduction

The need to better understand physically complex flows is a driving force in pushing the envelope of optical flow instrumentation innovation. Especially in high-speed flows, where the timescales of interest are on the order of microseconds, temporal requirements are of special interest and dictate sensor properties.

For many diagnostic applications, modern high-speed cameras with frame rates up to 1 MHz have filled this need, and enabled time-resolved particle image velocimetry (TR-PIV) (Wernet 2007), high-speed schlieren photography, time-resolved Doppler global velocimetry (TR-DGV) (Thurow *et al* 2005), as well as 3D flow visualization (Thurow *et al* 2013). Limitations of these approaches arise at high Reynolds numbers, high-speed flows, with large ranges of timescales and the frequent need to resolve weak signals requiring low detection thresholds. While photodiode arrays (Dahm *et al* 1991, Fischer *et al* 2009) have been used in the past for laser based flow instrumentation, photomultiplier tube (PMT) arrays with large sensor count (e.g. Hamamatsu H8500C as integrated herein) have only been used in the biomedical (Alva-Sánchez and Martínez-Dávalos 2009), nuclear physics (Pani *et al* 2003) and astrophysics fields.

In this article, we survey the types of data acquisition systems (DAQs) currently in use in fluid dynamics instrumentation and discuss the advantages and applications for field-programmable gate arrays (FPGA) based systems in the evolution of laser based high-speed flow instrumentation. We present the integration of FPGA-based data acquisition into the development of a novel 64-anode PMT array camera system capable of recording flow field data at 10 million samples per second (MS s^{-1}) over the course of several seconds. This camera is used for TR-DGV allowing data rates of 250 kHz, and above, for extended periods of time.

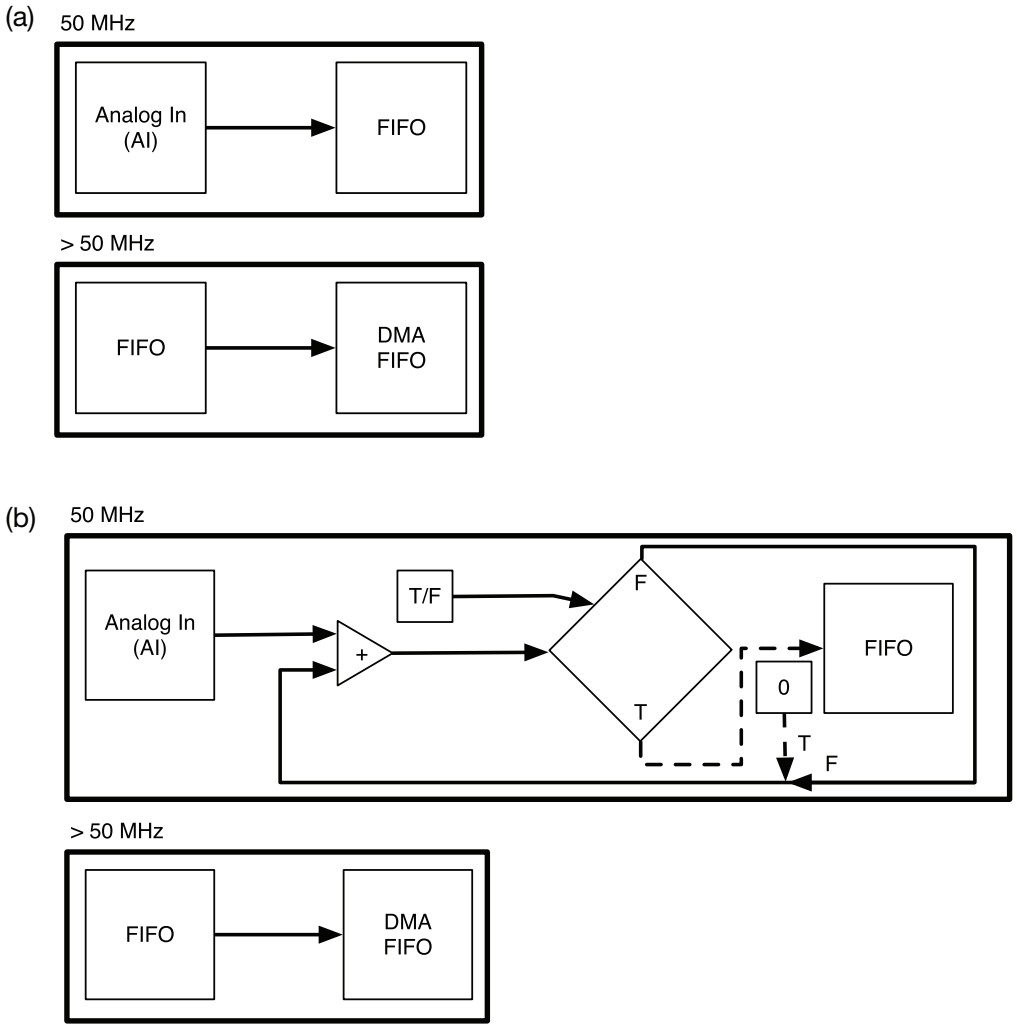

Figure 1. Examples of FPGA-adapter module integration (executed on FPGA hardware).

2. High-speed high-bandwidth data acquisition

A variety of commercial DAQs are used in current experimental fluid mechanics applications, including Ethernet based modular and non-modular DAQ units, USB-based DAQ units, PCIexpress (PCIe) based DAQ cards, and other specialized modular DAQ based on proprietary platforms. While some Ethernet- and USB-based systems offer a large choice of multichannel systems (1–32 channels/board), most systems suffer from interface-related low data rates (up to 2 MS s^{-1}) and high latencies (Starkloff and Bisking 2007, Ullrich 2007). PCIe DAQ cards usually do not offer as many channels but enable unique applications requiring extremely high data acquisition rates as high as 2 GS s^{-1}, e.g., the DAQ used for single-point laser-Doppler velocimetry (Brooks *et al* 2014, Lowe *et al* 2014) in supersonic flow. Chassis systems like the PXI and PXIe systems are a special case as they integrate the PCI/PCIe technology into a modular data acquisition/test system platform (Clark *et al* 2002, Starkloff and Bisking 2007, Nosbusch 2012). While most systems offer FPGA capabilities, current PXIe chassis systems allow the application of multiple FPGA units with ADC modules capable of up to 32 analog input channels (per module) at speeds of 50 MS s^{-1} in addition to high-speed synchronization and trigger capabilities. Thus, current PXIe systems can fulfill the technology requirements for high-speed flow instrumentation.

3. FPGA integration for high-speed data acquisition

FPGAs are logic structures similar to gated arrays with the additional advantage of being reconfigurable for user-specific purposes. While FPGAs perform slower than traditional (fixed) masked arrays by a factor of 3 and have a 10 times lower packing density, their flexible programming makes them optimal for 'rapid product development and prototyping' (Trimberger 1992). Translated to instrument development applications, this means new capabilities in managing and preprocessing high throughput data and data volume in high-speed (>2 MS s^{-1} per channel) measurement applications.

Previously FPGAs have found application in real-time particle image velocimetry (PIV) (Yu *et al* 2006). Direct

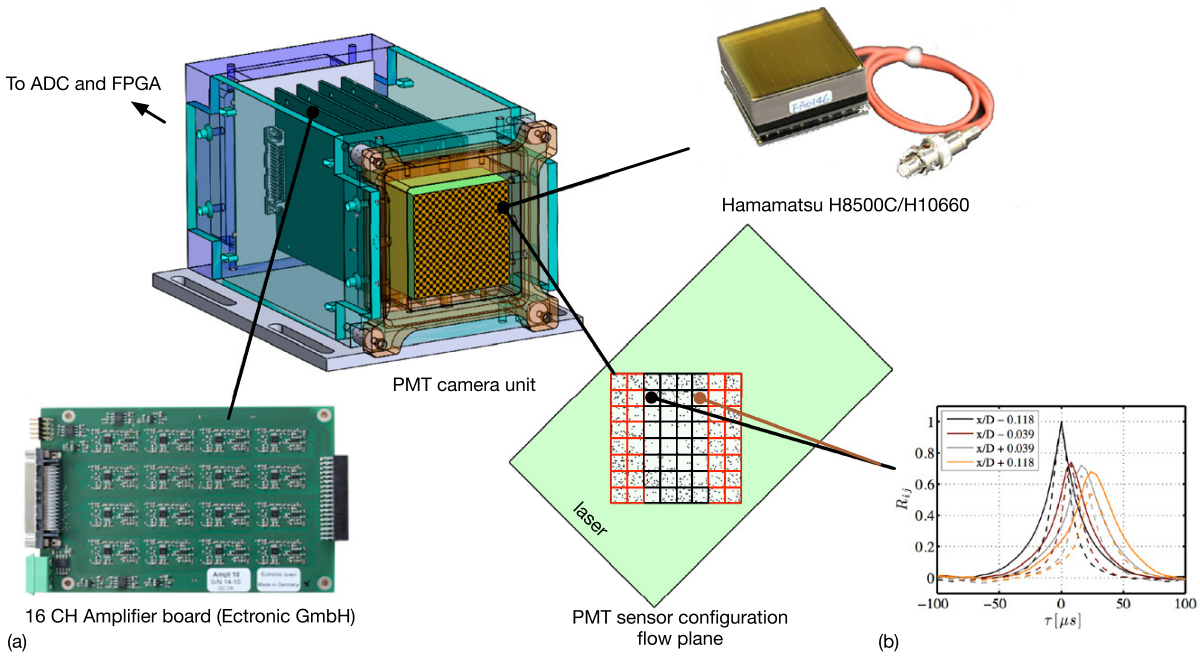

Figure 2. Spatially resolving PMT camera.

processing of a limited amount of camera information using FPGA capability allows for reducing data streams to manageable levels enabling flow control feedback mechanism. Scaling of FPGA-based DAQs for TR-DGV has been demonstrated previously (Ecker *et al* 2014a). Herein further development of a new multi-PMT sensor unit for high-speed flow application is described and demonstrated for an example application.

FPGAs can be reconfigured for user-specific purposes. Before the FPGA code can be run, the FPGA code must be compiled for the specific FPGA unit, which results in a configuration file that specifies how the FPGA unit uses its resources to operate as directed. Once compilation is performed, different codes can be uploaded to the FPGA unit's static memory, allowing rapid reconfiguration of the device logic for different applications.

Depending on application, FPGA programming strategies may vary between two extremes: (1) data streaming (no data processing) and (2) complete processing of the data via FPGA with only fully reduced data being output. The process of data streaming via the FPGA is depicted in a pseudo-flow diagram in figure 1(*a*). While the loop containing the interface to the ADC must run at the prescribed adapter module clock rate, other loops on the FPGA hardware may run on derived clocks. Each loop is executed at its defined clock speed. First-in first-out (FIFO) data streams can be used as buffers to transport information across clock domains, storing data in the FPGA's block RAM and slice memory. Additionally, commercial FPGA software wrappers offer the option to use direct memory access (DMA) FIFO's to stream data directly into the controller's system memory. The code running on the host side can then access these data and process them or write them to disk. Some FPGA units have on-board memory, which can be used to buffer data streams. Because current PXIe FPGA cards are based on first generation PCIe their bandwidth is limited to 1 GB s^{-1} (4 × slot); direct streaming of more than 1 GB s^{-1} is not possible (e.g. 10 channels at 50 MS s^{-1}) without on-board buffering to avoid data stream overflows.

Figure 1(*b*) illustrates inline addition of a set number of samples as a method of data preprocessing and bandwidth reduction. An event trigger is used to gate a true/false loop, either writing the number to the FIFO buffer or returning its value to the next time cycle.

This is an effective approach to reduce the data stream to levels that can be handled by the system's bandwidth. In the simplest variant, this method can be used to integrate a select amount of samples to increase the measurement signal-to-noise ratio (SNR). In a more applied case, the loop could be controlled by an event, e.g., the voltage peak on the output of a PMT induced by photons scattered from particles passing through a laser beam. The integrated value would then simply be a representative measure for the intensity of the elastic Mie scattering. Fast Fourier transform (FFT) based processing techniques like used for laser-Doppler velocimetry could benefit from inline FFT processing, which would allow on-the-fly velocity data at high data rates.

4. PMT camera

For the purpose of time and spatially resolved DGV for high-speed flow application, a PMT camera based on the 64 channel flat panel type Hamamatsu H8500C and H10966 series PMT has been developed. TR-DGV is a velocimetry technique capable of directly sensing the velocity induced Doppler shift. Velocity sensitivity is enabled by using a molecular gas filter, which functions as a transfer function from frequency to intensity. The classic implementation utilizes the ratio between the filtered and unfiltered light to determine the Doppler shift. The

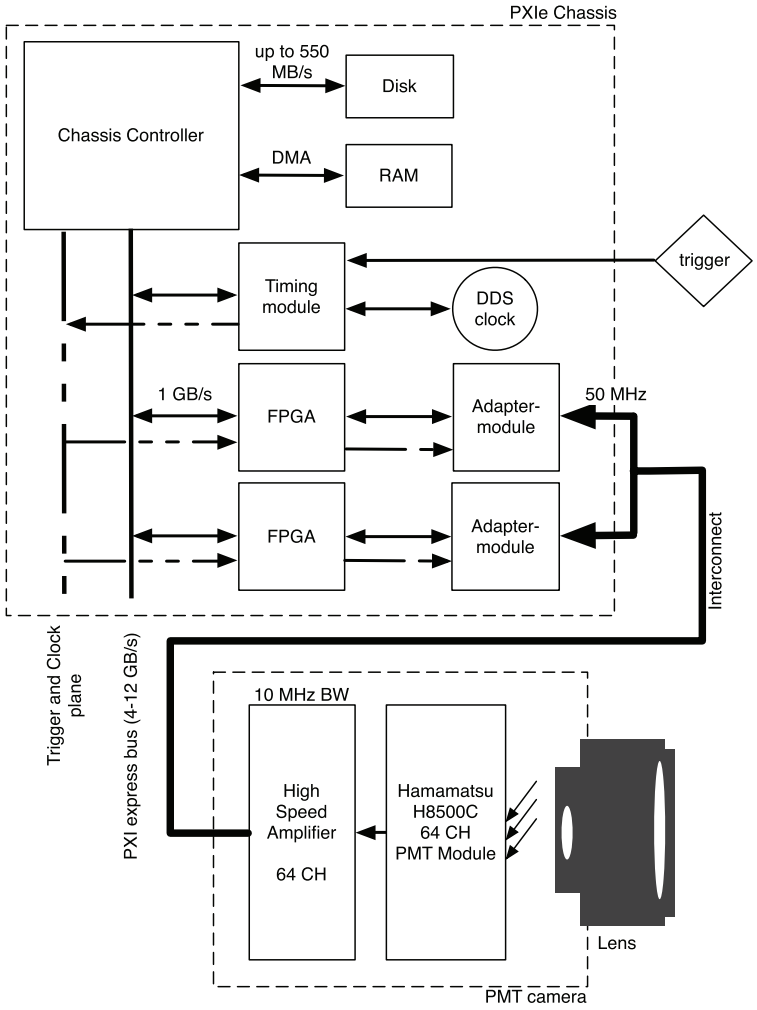

Figure 3. FPGA-based PMT camera system.

examples presented in this report are based on, but not limited to, the application of this classic reference technique for time-resolved velocimetry (Ecker *et al* 2014b). A model of the camera unit with photographs of the amplifier boards (4) and the PMT unit are shown in figure 2(*a*). The PMT configuration imaged onto the flow plane via a camera lens allows correlating all channels at any given time, thereby extracting instantaneous and statistical information on the flow physics. Figure 2(*b*) shows an example of the time delay cross-correlation across four PMTs in a supersonic shear layer.

As multichannel high-speed amplifiers for PMTs are not commercially available, a 16-channel amplifier board (Amp10M) that is directly interfaced with the PMT panel as well as the FPGA-adapter module, was designed and custom built by Ectronic GmbH, Karlsruhe, Germany. This amplifier unit allows amplifying single particle signals on all 64 channels at a bandwidth of 10 MHz (at −3 dB). Each channel of the amplifier unit employs an ac-coupled, two-stage amplification with 200 Ω input and 100 Ω output impedance (50 Ω differential), with an amplification of 100, resulting in maximum output voltages between ± 1V. The board uses an AD8132 differential output driver to enable long (5 m) interconnect distances between amplifier and adapter module.

Figure 3 shows the signal flow integration of both amplifier and PMT unit into the FPGA system. The 64-channel PMT is directly interfaced with the 16-channel high-speed amplifier boards (housed in a custom aluminum case). This camera unit is directly connected to the ADC unit on the 32-channel NI 5752 adapter module via a very-high-density cable interconnect (VHDCI) cable. The adapter module is attached to a NI PXIe-7965R card, which is powered by a Virtex-5 SX95T FPGA chip.

With the current FPGA and PXIe implementation, this setup allows a steady 2 GB s^{-1} data transfer rate per 64-channel camera system. In order to decrease the system's data rate to a manageable amount, the FPGA unit employs inline addition processing as presented in figure 1(*b*). Inline addition of the samples allows reducing the data rate to 1 GB s^{-1} per slot while boosting SNR. The sampling clock rates of the two adapter modules containing the ADC are synchronized by using a direct digital synthesizer (DDS) clock generated by a NI PXIe-6674T timing module and relayed via a timing

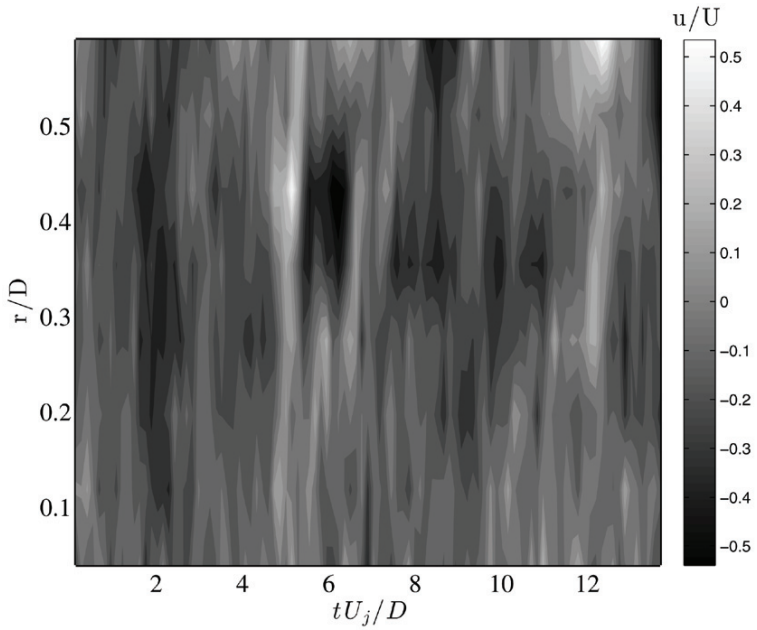

Figure 4. Velocity fluctuation time series in a hot supersonic jet (M=1.65, TTR=1.6, x/D=6).

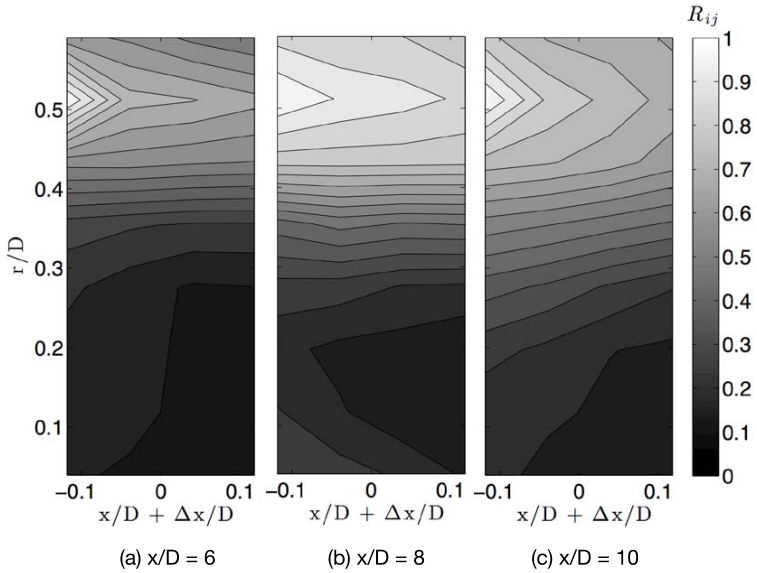

Figure 5. Second-order peak correlation map on the shear layer of a supersonic hot jet (M=1.65, TTR=1.6) using 32 pixels of the PMT camera. Reference at $\Delta x / D = 0$ and r/D=0.52.

bus line. Synchronization of data acquisition is achieved via a global trigger on a different high-speed line network (device to device skew < 500 ps) on the same bus (Ullrich 2007). All data are streamed to the controller memory via DMA and then written to disk. The recording timespan is limited only by the available controller memory, enabling long duration flow observations.

5. Results

Figure 4 shows an application of the PMT camera in a TR-DGV system in a supersonic hot jet (Mach number, M = 1.65; total temperature ratio, TTR = 1.6; nozzle diameter, D = 1.5 inch). The figure shows the velocity fluctuation time series on 8 PMTs arranged along a radial line perpendicular to the streamwise velocity component just downstream of the potential core, revealing strong intermittent velocity fluctuations. All data from the PMT camera were acquired by a NI PXIe DAQ system using 50 MS s^{-1}, consolidated into a 10 MHz signal via on-board processing and down sampled to 250 kHz in post-processing.

Figure 5 shows results from a study conducted by Ecker *et al* (2014b) in the same jet. Using 32 points on the camera system, velocity information was used to generate second and fourth order correlations, peak correlation maps, convective

velocities, as well as integral time scales—leveraging the statistical advantage of the long duration recording capability of the PMT/FPGA system.

6. Conclusions

In this article we briefly discussed commonly available data acquisition systems for flow instrumentation and give a comparison with regards to bandwidth and sampling rate to FPGA-based systems. The working principles of FPGA are summarized and examples on how inline processing can be integrated in a system are given. With the current availability of hardware and software tools, FPGA units give an attractive capability for rapid development of the-state-of-the-art instrumentation.

The integration of a commercial FPGA system with custom high-speed amplifiers and 64-channel PMT arrays into a rapid response 64-channel PMT camera for optical time (up to 10 MHz) and spatially resolved flow velocimetry is described. The applicability of this new camera technique is demonstrated on the example of a TR-DGV system applied to a supersonic, heated jet flow. Based on those experiences, we believe FPGA units to be extremely useful for rapid development of highly complex data acquisition systems, due the flexibility to adapt to quickly changing requirements in high-speed flow velocimetry it provides.

Acknowledgments

The Office of Naval Research Hot Jet Noise Reduction Basic Research Challenge and DURIP, grants N00014-11-1-0754 and N00014-12-1-0803 under program managers Drs Brenda Henderson and Joseph Doychak, supported the work described.

References

Alva-Sánchez H and Martínez-Dávalos A 2009 Initial characterization of a benchtop microPET system based on LYSO crystal arrays and Hamamatsu H8500 PS-PMTs *Nucl. Instrum. Methods Phys. Res.* A **604** 335–8

Brooks D R, Ecker T, Lowe K T and Ng W 2014 Experimental Reynolds stress spectra in hot supersonic round jets *AIAA Scitech, 52nd Aerospace Sciences Meeting* (*National Harbor, MD*) (doi: 10.2514/6.2014-1227)

Clark C, Haddad M, Peck J and Wetzel M 2002 Instrumentation system including a backplane having a switched fabric bus and instrumentation lines *US Patent* 20020080811 A1

Dahm W J, Southerland K B and Buch K A 1991 Direct, high resolution, 4D measurements of the fine scale structure of Sc ≫ 1 molecular mixing in turbulent flows *Phys. Fluids* A **3** 1115–27

Ecker T, Brooks D R, Lowe K T and Ng W F 2014a Development and application of a point Doppler velocimeter featuring two-beam multiplexing for time-resolved measurements of high speed flow *Exp. Fluids* **55** 1819

Ecker T, Lowe K T, Ng W F and Brooks D R 2014b Fourth-order spectral statistics in the developing shear layers of hot supersonic jets *50th AIAA/ASME/SAE/ASEE Joint Propulsion Conf.* (*Cleveland, OH*) (AIAA) (doi: 10.2514/6.2014-3742)

Fischer A, Büttner L, Czarske J, Eggert M and Müller H 2009 Measurements of velocity spectra using time-resolving Doppler global velocimetry with laser frequency modulation and a detector array *Exp. Fluids* **47** 599–611

Lowe K T, Byun G and Simpson R L 2014 The effect of particle lag on supersonic turbulent boundary layer statistics *AIAA Scitech, 52nd Aerospace Sciences Meeting* (*National Harbor, MD*) (doi: 10.2514/6.2014-0233)

Nosbusch D 2012 Architecting high-throughput PXI systems *IEEE AUTOTESTCON, 2012 (Anaheim, CA)* (Piscataway, NJ: IEEE) pp 250–3

Pani R *et al* 2003 A novel compact gamma camera based on flat panel PMT *Nucl. Instrum. Methods Phys. Res.* A **513** 36–41

Starkloff E and Bisking K 2007 New technologies drive synthetic instrumentation *RF Des.* **7**(6) 12–15

Thurow B, Jiang N and Lempert W 2013 Review of ultra-high repetition rate laser diagnostics for fluid dynamic measurements *Meas. Sci. Technol.* **24** 012002

Thurow B S, Jiang N, Lempert W R and Samimy M 2005 Development of megahertz-rate planar Doppler velocimetry for high speed flows *AIAA J.* **43** 500–11

Trimberger S 1992 Guest Editor's introduction: field-programmable gate arrays *IEEE Des. Test Comput.* **9** 3–5

Ullrich A 2007 PXI express for real-time control and high performance acquisition *15th IEEE-NPSS Real-Time Conf.* (*Batavia, IL, April 2007*) (Piscataway, NJ: IEEE) pp 1–5

Wernet M P 2007 Temporally resolved PIV for space–time correlations in both cold and hot jet flows *Meas. Sci. Technol.* **18** 1387

Yu H, Leeser M, Tadmor G and Siegel S 2006 Real-time particle image velocimetry for feedback loops using FPGA implementation *J. Aerospace Comput. Inform. Commun.* **3** 52–62

Part V.

Eddy convection and statistical correlations in the developing shear layers of heated supersonic jets

The contents of this chapter have been submitted for publication, and are currently under review.

Significant portions were previously presented as “Ecker, Tobias, K. Todd Lowe, Wing F. Ng, and Donald R. Brooks. "Fourth-order spectral statistics in the developing shear layers of hot supersonic jets." In Propulsion and power (50th AIAA/ASME/SAE/ASEE joint propulsion conference). 2014”.

Eddy Convection and Statistical Correlations in the Developing Shear Layers of Heated Supersonic Jets

Tobias Ecker[*], K. Todd Lowe[†], Wing F. Ng[‡] and Donald R. Brooks[§]

Virginia Tech, Blacksburg, Virginia 24060

Motivated by the roles eddy convective Mach number and turbulence statistical correlation play in acoustic analogies, a study is presented leveraging non-intrusive measurements in the developing shear layers of hot supersonic jets. A time-resolved Doppler global velocimetry measurement technique with a frequency resolution of 125 kHz is employed to obtain time-resolved measurements and used to determine second- and fourth-order space-time correlations, integral timescales and convection velocities in the shear layer of a heated (total temperature ratios of 1.6 and 2) supersonic, perfectly expanded jet at 1.65 design Mach number. Data obtained in the same facility, using laser Doppler velocimetry are analyzed with respect to fourth-order terms indicating the importance of the fourth-order correlation in the region of immediate interface between the potential core and the shear layer. For these heated jets, streamwise eddy convective velocities on the lip line were between 0.54 - 0.68 of the isentropic jet exit velocity, which is significantly lower than in the cold jet case on the same geometric line. It is shown that the acoustic Mach number for the hotter case is generally greater in the core, but the surface of the sonic convective speed remains surprisingly consistent between both presented cases. Density ratios less than unity are shown to result in significant changes in jet spreading similar to heated subsonic jets.

[*] Graduate Research Assistant, Aerospace and Ocean Engineering.
[†] Assistant Professor, Aerospace and Ocean Engineering.
[‡] Christopher C. Kraft Endowed Professor, Mechanical Engineering.
[§] Graduate Research Assistant, Aerospace and Ocean Engineering.

Nomenclature

a = speed of sound [m/s]

c = speed of light [m/s]

D = nozzle diameter [m]

D_j = perfectely expanded nozzle diameter [m]

d_p = particle diameter [m]

$\vec{e}$ = measurement vector

f = frequency [Hz]

f_0 = characteristic laser light frequency [Hz]

f_D = Doppler frequency [Hz]

$\hat{\imath}$ = laser incidence vector

I = turbulence intensity

μ = dynamic viscosity [Pa s]

M = Mach number

M_a = acoustic Mach number $M_a = u_c/a_a$

M_d = design Mach number

M_j = isentropic Mach number

NPR = nozzle pressure ratio p_0/p_a

$\hat{o}$ = observation vector

p_a = ambient pressure [Pa]

p_0 = total pressure [Pa]

r = radial coordinate [m]

R = correlation coefficient

Δt = laser pulse width [µs]

T = data acquisition period [µs]

T_{ii} = integral time scale [s]

T_0 = total temperature [K]

T_a = ambient temperature [K]

TTR = total temperature ratio T_0/T_a

s = flow variable

Sr = Strouhal number $\left(Sr = fU_j/D_j\right)$

u_c = streamwise eddy convective velocity [m/s]

u = instantaneous velocity [m/s]

$\vec{U}$ = velocity vector in base coordinate system [m/s]

U_j = isentropic jet exit velocity [m/s]

U = mean velocity [m/s]

x = streamwise coordinate [m]

η^* = shear layer similarity coordinate

ρ_p = particle density [kg/m^3]

ρ_j = density after isentropic expansion [kg/m3]

ρ_a = ambient density [kg/m^3]

τ = correlation lag time [s]

τ^* = non dimensional correlation lag time $\left(\tau^* = \tau U_j/D_j\right)$

τ_{St} = Stokes particle lag time [s]

Δx = distance between sensors [m]

I. Introduction

JET noise has been a concern since the introduction of turbojet engines [1] and remains a topic of intense study. In the present article, we leverage new time-resolved flow diagnostics to shed light on some aspects of the turbulent flow field that produces the dominant noise sources in model single stream, heated supersonic jets. The results are interpreted in light of a great deal of experimental, theoretical and computational results presented in the literature. A brief review of pertinent measurement techniques and some of these works on jet aeroacoustics is provided to follow.

In 2012, Lowe et al. [2] have presented a concept for the development of a new instrument based on the Doppler Global Velocimetry (DGV) technique, featuring time resolved measurements at multiple points (from here on referred to as TR-DGV). In a first step, Ecker et al. [3] have demonstrated the fundamental developments for the

TR-DGV technique capable of very high temporal resolution, three-velocity component particle measurements in supersonic jets. This technique is a modification of the classic DGV technique, but with the improvements of using high sensitivity photodetectors, field-programmable gate array (FPGA) based signal processors and a continuous wave laser. The current study advances the presented technique to 32 points in a plane by integrating multi-photomultiplier (PMT) detector units with custom high-speed amplifiers and a FPGA data acquisition backend into a new instrument, capable of bridging the gap between temporal and spatial resolution of current DGV instrumentation.

The structure of this paper is as follows: first a short summary of relevant literature for optical measurements in jet flows and correlations of flow variables is given. In the subsequent parts both the laser Doppler velocimeter (LDV) and the DGV instrument as well as the facility is described. LDV single-point turbulence, fourth-order statistics and DGV multipoint correlation based measurement results are presented. The DGV results include second and fourth-order space time correlations, peak correlation maps and time scales, as well as streamwise convective velocity maps for a perfectly-expanded supersonic jet at total temperature ratios (*TTR*) of 1.6 and 2.0. A brief discussion details the relevance of the presented data and the main achievements of the study.

A. Optical measurement techniques for jet flows

First studies of two-point correlations in supersonic jets were limited to hot wire measurements, which suffered from highly correlated probe noise [4]. Recent progress in laser-based instrumentation has resulted in non-intrusive optical alternatives, some of which are discussed here.

Lau [5] and Kerhervé et al. [6] have applied LDV systems for two-point correlations in supersonic cold jets, presenting valuable data in these flows. Another notable optical instrument used extensively for obtaining space-time correlation information is the optical deflectometer (OD) technique presented by Doty and McLaughlin [7] for air and helium-air jets. This method has provided extensive eddy convection information in cold flow but due to signal-to-noise limitations, has shown limited success in heated or simulated heated flows.

Planar velocimetry techniques, most notably Particle Image Velocimetry (PIV) and DGV, are the current standard for global velocity measurements in low and high-speed flows. The application of PIV and DGV for mean flow velocity measurement in high-speed flows has been discussed by Samimy and Wernet [8] in detail. PIV has been successfully applied to high subsonic and supersonic, cold [9] and hot jets [10], as well as supersonic [11] and

hypersonic windtunnel configurations. Wernet [10], Bridges [12], Ukeily et al. [13] and Fleury et al. [14] have successfully used PIV to compute space-time correlations maps and spectra [12] in hot and cold subsonic jets. Recent developments in high-speed cameras have pushed the envelope towards highly spatially and time-resolved measurement techniques for high-speed flow. Wernet[15] presented a new, truly time-resolved PIV technique (TR-PIV) capable of measurements at rates up to 5 kHz. Time resolution was obtained by coupling a Photron Ultima APX-RS CMOS camera with a Quantronix Infini dual head laser system operated at up to 25 kHz. By using large onboard memory, this TR-PIV system can overcome bandwidth limitations at the cost of dedicating time to transferring the datasets until the experiment is paused or concluded.

DGV has been developed primarily for applications in high-speed flows due to its inherent absolute instrument uncertainty. First introduced by Komine [16] and then further pioneered by Meyers and Komine [17], DGV has proven itself in applications for mean velocity measurements in high-speed flows. Meyers et al. [18] identify that the most common sources of uncertainty in DGV can be attributed to the molecular gas cell, laser stability and characteristic performance of the sensor type. Advances have been made to reduce measurement uncertainty, instrumentation cost, as well as complexity, and to improve time resolution. These advances led to some notable derivative variants of the DGV technique applicable to low speed flows [19]-[21]. Many other applications and developments of the traditional DGV technique, as well as levels of uncertainties, are discussed in detail by Elliot and Beutner [22]. Both PIV and DGV have benefited from the development of high-speed camera systems. Thurow et al. [23] first demonstrated a time-resolved DGV system based on a high-speed camera for use in a rectangular Mach 2.0 jet. This system was capable of measurements at 250 kHz frame rates but was limited in the observable time-scales due to the short measurement duration (28 frames).

The current study presents a DGV instrument capable of providing time-resolved data at multiple points in the flow simultaneously, at constant data rates of 250 kHz for duration of up to two seconds. Measurements in a hot supersonic jet at two heated conditions are performed to demonstrate the instrument's capabilities to deliver higher order space-time correlations and eddy convection information.

B. Correlation measurement of jet flows

Lau [5] presented the first LDV correlation measurements in both subsonic ($M_j = 0.5 - 0.9$) and supersonic ($M_j = 1.37, TTR = 1.0$) heated and unheated jets using two LDV systems and traversing in the flow. He found

the ratio of the streamwise convective velocity to the jet exit velocity u_c/U_j on the lip line to be nearly constant and only slightly varying with jet operating conditions. Heating seemed to cause no significant change in the trend at the lip line for the case of the subsonic jet. For the cold supersonic jet the convection velocity reached about 0.8 of the jet exit velocity. More mean flow and turbulence statistics are presented by Lau et al [24]. It is evident from the data presented, that the profiles of the mean properties scale well with the shear layer similarity coordinate η^*. Brooks and Lowe [25] showed a similar collapse for the mean velocity profiles and additionally presented normal and shear stress information at different streamwise locations for a heated supersonic jet. The similarity coordinate is based on linear spreading of the shear layer and is defined as follows [24]:

$$\eta^* = (r - r_{0.5U_j})/x \qquad (1)$$

where $r_{0.5U_j}$ is the radial location at which the local mean velocity is equal to half the jet exit velocity and *x* represents the streamwise distance from the jet exit plane.

Kerhervé et al. [6] utilized a dual LDV system for two-point correlations in a cold, supersonic ($M_j = 1.2$), screeching jet. They presented mean profiles, stresses, spectra and second- and fourth-order correlations as well as convective velocities. The convective velocity on the shear line ($\eta^* = 0$) was found to be 0.6 of the jet exit velocity. The presented fourth-order correlations show a much steeper fall off in correlation coefficient with streamwise distance. Morris and Zaman [26] showed that the fourth-order cross-correlation coefficient measured in a low speed jet reached only about half the value of the second-order correlation coefficients.

Panda et al. [4] experimentally correlated the data from a Rayleigh scattering based probe, capable of measuring density and velocity fluctuations, with the data from a microphone in the far field of fully expanded unheated high subsonic and supersonic jet plumes. Pressure and momentum fluctuations revealed the highest correlation values just downstream of the potential core on the centerline, identifying it as a strong sound-producing source in the flow. The magnitude of the correlation strongly depended on frequency and observer position, which was varied between 30 and 90 degrees to the jet axis. Above 60 degrees most data was below the noise floor, whereas the shallow 30-degree angle produced the highest correlations. The high correlations values were mostly attributed to the presence of large coherent structures in the frequency range of $0 \leq Sr \leq 1$. On the lip line only the supersonic cases showed significant correlation values, also peaking in the proximity of the potential core breakdown. The maximum values of the correlation measured after the potential core were found to be largely dependent on the jet exit Mach number, with supersonic conditions producing coefficients higher by an order of magnitude or more than subsonic jets due to

the presence of Mach wave radiation. Similarly Papamoschou et al. [27] applied a series of four optical deflectometers in combination with a far field narrow aperture microphone array to a cold, perfectly expanded $M_j = 1.75$ jet. Their experiment yielded increased level of coherence between the OD probe and the microphone array, especially in the jet shear layer, which suggests the relationship of the peak noise with the turbulent structures moving at eddy convective speeds.

Doty and McLaughlin [7] used OD probes to establish two-point space-time correlations in subsonic and supersonic air and helium/air mixture jets. The helium/air mixture served to simulate different TTRs without the need of flow heating capability [28]. For the case of the helium/air jet they found lower correlation values, attributed to problems of the OD technique with density gradients. Comparative measurements using hot wires confirmed this conclusion. Extracted convection velocity ratios ranged from 0.78 ± 0.05 for the air ($TTR = 1$) jet to 0.46 ± 0.1 for the simulated hot case ($TTR = 1.74$) on the lip line, indicative of large-scale structures propagating at subsonic speeds in the shear layer. It is to note, that although the lip line is often used as a geometric line in many investigations, different jet conditions may lead to incorrect comparisons. Petitjean et al. [29] investigated space-time correlations in cold subsonic and supersonic, round and beveled nozzles using an OD instrument. While the bevel had little effect on the convective velocities for the subsonic case, they reported a significant reduction from 0.74 for the supersonic round nozzle to $0.60 - 0.62$ for the beveled nozzle, as well as lower correlation values on the short side of the lip.

Bridges [12] further studied the effect of heat on the space-time correlation in jets using a dual PIV system on subsonic and sonic jets at different temperatures. He showed that the Witze potential core estimate [30] collapses data from different jet conditions relatively well, and demonstrated that the acoustic Mach number appears to have little impact on the convective velocity. More significant effects of the temperature on the convective velocity in the shear layer are evident after the potential core, with heated jets having larger convective velocities than the cold case. Ukeily et al. [31] applied PIV to a high subsonic ($M_j = 0.85$) cold jet, investigating the evolution of two point statistics in all three flow coordinates. Streamwise correlation coefficients were shown to have an increasing trend with streamwise distance, indicating the development of large scale coherent structures propagating downstream similar to what has been reported by earlier investigators (e.g. Mollo-Christianson. [32]).

A study by Bridges and Wernet [33] identifies and summarizes some valuable data sources that could be used for validation of simulation and corroboration of experimental data. The authors noted specifically a lack of turbulence

information for high subsonic and supersonic jets in the current literature. From the review of this non-exhaustive list of literature sources, it becomes clear that information on the time scales, as well as the spatial distribution of flow correlation and convective velocities are sparse for the case of the supersonic heated jet, motivating the present study.

II. Doppler Global Velocimetry

DGV is a velocimetry technique based on the selective absorption characteristics of molecular gas cells and is capable of direct measurement of the Doppler effect. DGV relies on the detection of the Doppler shift frequency of laser light scattered off tracer particles within the flow under study. The frequency of a single-longitudinal-mode laser is set so that the Doppler shifted frequency lies optimally in the absorption spectrum of a molecular gas filter.

In the classic implementation, the DGV technique requires a reference light path to normalize the intensity of the filtered scattering by the intensity of the local scattering based on particle density and laser light amplitude [2].

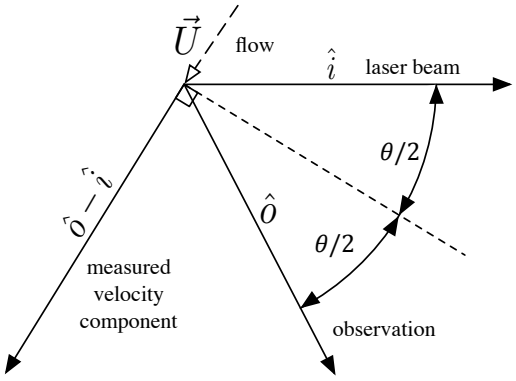

Fig. 1 Vector geometry and nomenclature of the DGV measurement principle.

The Doppler shift f_D of the scattered light depends upon the laser frequency, vector particle velocity, and laser propagation and observation directions and is related by the Doppler equation [17] as:

$$f_D = f_0 \frac{\vec{U}\cdot\vec{e}}{c} \qquad (2)$$

where f_0 is the incident laser light frequency, c is the speed of light, $\vec{U}$ is the particle velocity vector, and $\vec{e} = \hat{o} - \hat{\imath}$ defines the velocity measurement component direction, wherein the laser propagation direction is the unit vector $\hat{\imath}$ and the direction of observation is given by $\hat{o}$. The vector geometry and the associated nomenclature of the Doppler

equation are depicted in Fig.1. With a three-component measurement, the resulting velocity vector in the coordinate system of interest may be reconstructed from the measured components and their base vectors as:

$$\vec{U} = \begin{bmatrix} \vec{e}_1{}^T \\ \vec{e}_2{}^T \\ \vec{e}_3{}^T \end{bmatrix}^{-1} \begin{pmatrix} u_1 \\ u_2 \\ u_3 \end{pmatrix} \qquad (3)$$

where $\vec{e}_i$ represents measurement vectors and u_i the magnitude of the respective directly measured velocity component.

The laser frequency may be tuned in frequency using a piezo element. This scanning procedure allows characterization of the transmission of the molecular gas cell, as well as to the ability to choose the exact reference frequency for each measurement. The transmission is defined as the ratio between light transmitted through the cell to the total amount of light entering the cell.

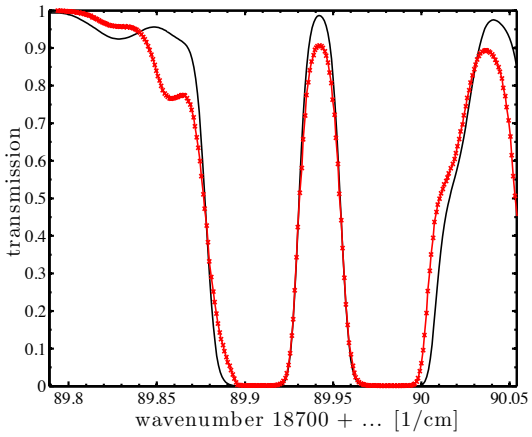

Fig. 2 Experimental Iodine cell scan (red) compared to model spectrum (black) computed by using code by Forkey et al. [34]**.**

This calibration approach has been applied successfully by Fischer et al. [35] and Ecker et al. [3], among others. A comparison of the numerically obtained transmission spectrum using model and code developed by Forkey et al. [34] with an experimental scan can been found in Fig. 2. This spectrum indicates how the molecular gas filter transmits light intensity as a function of its wavelength or equivalently frequency. This calibration scan can be used in conjunction with the model developed by Forkey et al. [34] to determine the frequency characteristics of the iodine gas cell used. The shape of the spectrum requires a careful determination of the reference frequency and the expected Doppler shift in order to accurately determine the exact position of the Doppler shifted signal.

III. Instruments

A. Single-point LDV system

A two-component, single transceiving lens LDV was used to acquire measurements for higher order single point statistics within the heated supersonic jet. The LDV has a measurement volume diameter of 60 μm and a fringe spacing of approximately 2 μm. It utilizes one beam pair of 532 nm laser beams to measure the velocity in stream-wise direction and another beam pair of 514.5 nm laser light to measure the radial component. From a propagation of errors the uncertainty in each velocity component is found to be ±0.3% of the mean velocity component. The LDV is fiber-optically coupled to a laser photonics system. This system uses 4 Coherent Genesis 1 W optically pumped solid-state lasers.

Table. 1 LDV specifications.

	Streamwise Pair	Radial Pair
Wavelength [nm]	532	514.5
Fringe Spacing [μm]	1.78	1.7
Probe Volume Diameter [μm]	60	60
Number of Fringes	34	35
Focal Length [mm]	60	60
Beam Half Angle [deg]	8.5	8.5
Uncertainty [$\delta u/U$]	0.3%	0.3%
Bragg Cell Freq. [MHz]	Unmodulated	120

The raw burst signals were acquired using a National Instruments NI5154 digitizer card, at 500 MHz bandwidth and 1 GS/s acquisition rate. Additional specifications, including single-sample uncertainties are provided in Table 1 and by Brooks and Lowe [25].

B. Multipoint DGV system

Similar to TR-PIV, TR-DGV is a quasi-instantaneous technique, providing measurements at two instances in time allowing reconstruction of the 3-component velocity vector with a high temporal resolution.

For 3-component planar operation, two laser sheets of equal width and thickness illuminate the measurement plane. Acousto-optic modulators (AOM) allow activating each sheet in a consecutive manner. For a receiver system with a measurement plane parallel to the streamwise axis, the maximum sheet width is dictated by the 45-degree angle position, which was also found as the angle with the lowest overall uncertainty by Ecker et al. [2] for this type of sensor geometry.

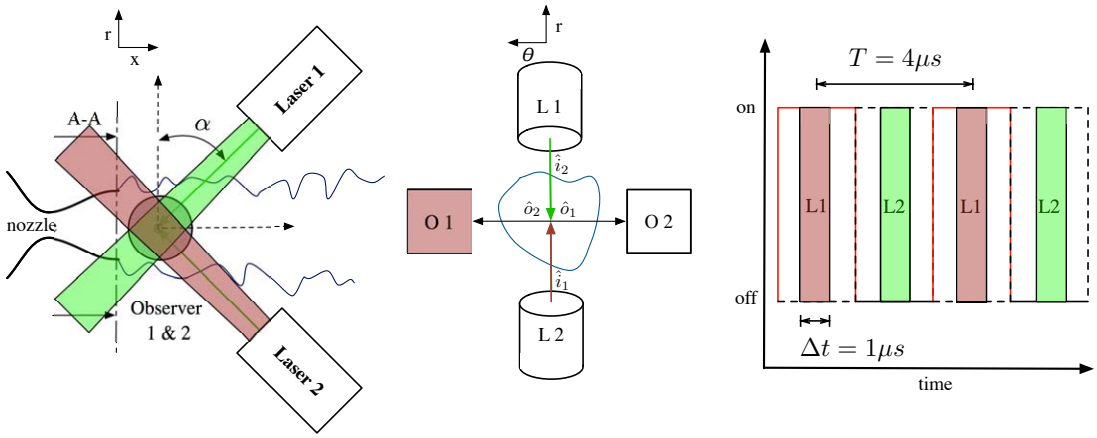

a) Side view b) Section A-A c) Laser sheet multiplexing

Fig. 3 Instrument basic geometry and operation. Red indicates the laser (L) and observer (O) used for this study.

A schematic of this configuration is shown in Fig. 3. The sideview (Fig. 3 a) details the 45-degree position of the two laser sheets and their orientation relative to the nozzle flow direction. The section view (Fig. 3 b) shows the observer units perpendicular to the laser sheets and the jet streamwise axis and all vectors used in the Doppler equation (2). The laser sheet multiplexing is displayed as a schematic in Fig. 3 c, indicating when each sheet is active, as well as the length of the actual laser pulses during the measurement. The period of the laser sheet pulses is 4 µs – equivalent to a data rate of 250 kHz. Each pulse width is 1 µs, avoiding temporal sheet overlap. For the purpose of this study only one sheet (L2) and one camera (O1) unit are used (shown as red in Fig. 3), resulting in a measurement sensitivity vector of $[0.7071, 1.0000, -0.7071]^T$ (compare eq. 3).

Details of the assembled instrument, including receiving light path with iodine cell and PMT camera unit, are presented in Fig. 4. The laser light from the optical table is routed via fiber optics to two laser sheet generating optics. The laser optics are arranged in a 45-degree configuration to the jet centerline and create the measurement plane. On both sides perpendicular to the measurement plane, a receiver unit is placed. Each receiver unit consists of

two PMT cameras, the iodine cell, as well as a beamsplitter and a mirror. The beamsplitter divides the light onto filtered and unfiltered (reference) light paths. The filtered path contains the iodine cell and is sensitive to velocity.

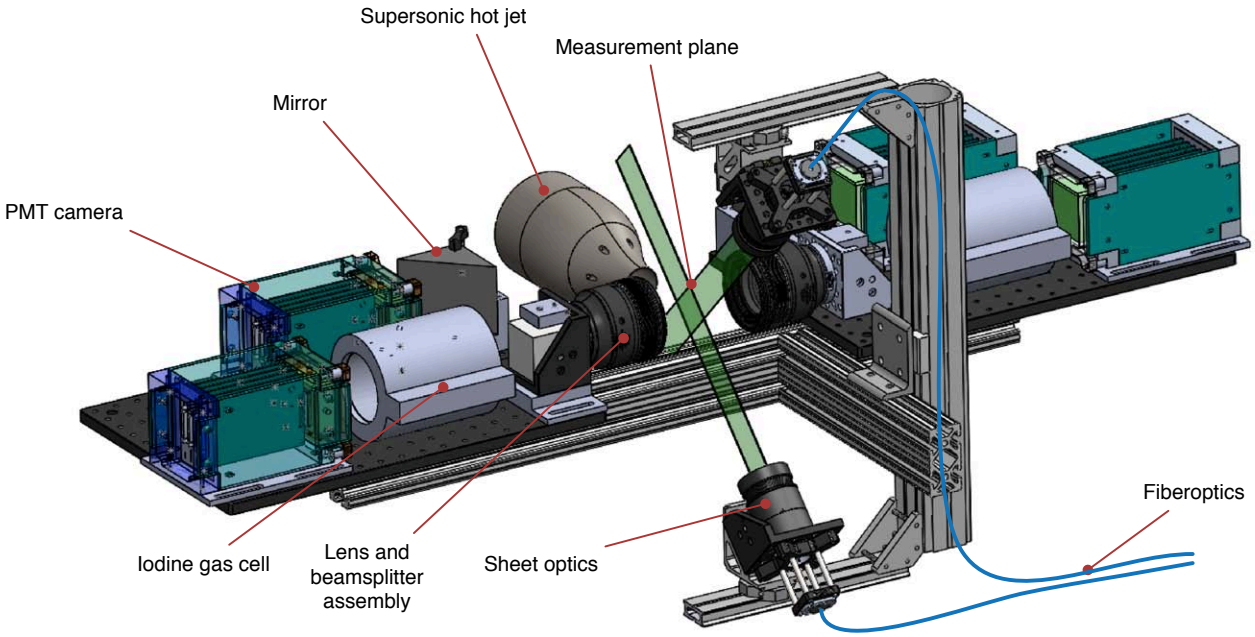

Fig. 4 TR-DGV assembly with components.

Optical conditioning is performed on a separate optical table in an adjacent room, shielded from facility noise. Multiplexing of the two sheets is enabled by two 80 MHz AOMs (Intraaction Corp.) acting as optical switches, turning on and off the respective laser sheet. A BNC 565 signal delay generator is triggered by a digital square wave signal from the DAQ system and controls the multiplexing time interval, which is the interval each beam consecutively flashes. The laser beam is shifted by -80 MHz and then transmitted to the sheet forming optics by an 8 μm core diameter telecommunication grade multimode fiber. Tuning the frequency of the Coherent Verdi V6 CW (532 nm) Diode-Pumped Solid-State Laser is performed by controlling a piezoelectric element (PZT) inside the laser cavity. This is done by applying a voltage between $0 - 72$ V, therefore allowing the user to choose a frequency at which the sensitivity and bandwidth of the transfer function (Fig. 2) is optimized.

Two photodiodes (PD) Thorlabs PDA100A are used to monitor the unshifted laser frequency through the reference iodine gas cell at all times, reducing the influence of laser frequency drift or fluctuation to a minimum. Each of the two measurement cells mounted in the receiver unit is frequency scanned in tandem with the reference

cell in order to generate a calibration data set. All cells are operated at a body temperature of 60 °C and given enough time to equilibrate before calibration or flow measurements are performed.

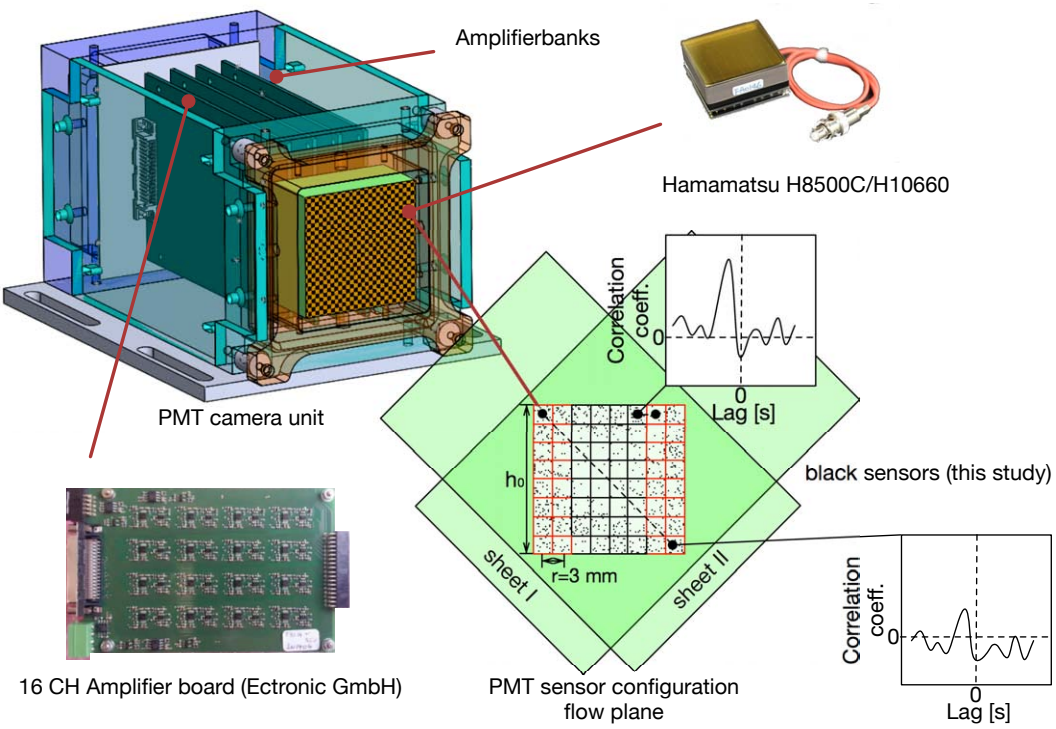

Fig. 5 PMT camera unit.

The PMT camera and its sensor configuration based on a Hamamatsu H8500C PMT module are visualized in Fig. 5. The black squares of the center inset indicate currently used sensors. With the 85 mm focal length camera lens used, the magnification of each sensor represents 3 mm by 3 mm on the measurement plane in the flow. The total coverage area of the 32-sensor PMT is 9 mm by 21 mm. A custom 16-channel (CH) high-speed amplifier from Ectronic GmbH (see Fig. 5) amplifies the signals from the PMT and transmits them to the adapter module of the NI DAQ system via a high-density cable. Each PMT camera currently uses 2 amplifier boards, resulting in 32 useable points. The experimental data are acquired by a NI PXIe DAQ system using 50 MS/s Adapter-modules (NI 5752) with FlexRIO FPGA (NI PXIe-7965R) units. Using on chip FPGA processing and root-mean-square (RMS) post-processing resulted in data sampled at effectively 250 kHz. All datasets recorded contained 2.5×10^5 samples, representing 1 s in flow time. More details about the camera unit can be found in Ecker et al. [36].

C. Definitions and data processing

Multi-point sensors as discussed in section B allow time cross-correlation processing of the experimental data. The time-resolved data *s(x,r,t)* acquired on each sensor pixel were processed and correlated to a reference pixel close to the lip line of the nozzle. The second-order cross-correlation [26] is defined as:

$$R_{ij}(x,r,\varsigma,\xi,\tau) = \overline{s_i(x,r,t)s_j(x+\varsigma,r+\xi,t+\tau)} \qquad (4)$$

The integral time scales are defined in terms of the autocorrelation:

$$T_{ii} = \int_0^{R_{ii}=0} R_{ii}(x,r,\varsigma=x,\xi=r,\tau)\,d\tau \qquad (5)$$

where ς and ξ are the spatial separation and τ the delay timescale from the reference location.

Acoustic analogies [37], [38] indicate that the power spectral density of radiated noise is related to the integrated influence of fourth-order space-time correlations. For the purposes of this study the fourth-order time correlation is defined as:

$$R_{ijkl}(x,r,\varsigma,\xi,\tau) = \overline{s_i s_j(x,r,t)s_k s_l(x+\varsigma,r+\xi,t+\tau)} \qquad (6)$$

For i=j, k=l, the fourth-order space time correlation can be computed from the second-order auto terms[1] as:

$$R_{iijj}(x,r,\varsigma,\xi,\tau) = \overline{s'^2{}_i(x,r,t)s'^2{}_j(x+\varsigma,r+\xi,t+\tau)} \qquad (7)$$

where $s = S(t) - \bar{S}$ and $s'^2 = s^2 - \overline{s^2}$.

The delay time between correlation peaks, which is an integral measure of the time of propagation between 2 sensed locations' correlation in the convective ridge, such that:

$$R(\tau) = R(\varsigma = u_c\tau) \qquad (8)$$

To improve the time estimate of propagation, a model was fitted to the measured data and the lag time at the peak of the fit determined.

The integral convective velocity [39] can be determined from the second-order delay time and the known sensor spacing as:

$$u_c = \frac{\Delta x}{\tau} \quad (9)$$

D. Sensitivity and uncertainty analysis

The uncertainties in the convective velocity estimate stem from the two parameters, the lag time and the physical sensor spacing. Note that the sensor spacing is directly related to the optical magnification of the sensor system.

Propagation of error analysis yields the following uncertainty for convective velocity:

$$\delta u_c = \sqrt{\left(\frac{1}{\tau}\right)^2 (\delta\Delta x)^2 + \left(\frac{\Delta x}{\tau^2}\right)^2 (\delta\tau)^2} \qquad (10)$$

While the uncertainty in the sensor spacing can easily be estimated, the same is not true for the lag time. The estimation of the lag time is convoluted with the uncertainties in the correlation function. Those uncertainties in the velocity fluctuations are absolute uncertainties and are about 6 - 10 m/s [3], but due to second-order nature of the cross correlation their impact is relatively low. A sensitivity study using a Monte-Carlo process was conducted using synthetic flow data with a constant convective velocity in order to determine the inherent processing error. The data are generated by the inverse FFT of a turbulent model spectrum [40] with random phase angles; the process is described more in detail by Ecker et al. [3] as well as de Kat et al. [41]. Different model fits for lag time interpolation were tested; while a six-point Gaussian model gave good results, a simple three-point cubic spline fit proved to be more accurate and more robust when processing measured data.

The Monte-Carlo showed that (simulated) measurement noise has almost no impact on the estimation process – mainly due to the statistical advantage of the long duration velocimetry and the low uncertainty progression. Most electronic noise is contained within the zero lag autocorrelation [42] of the velocity signal which is irrelevant for the lag time estimation. This robustness of the cross-correlation processing can be seen in Fig. 6 for a representative case; at SNR > 0 the uncertainty of the lag time estimate asymptotically reaches values of about 4%.

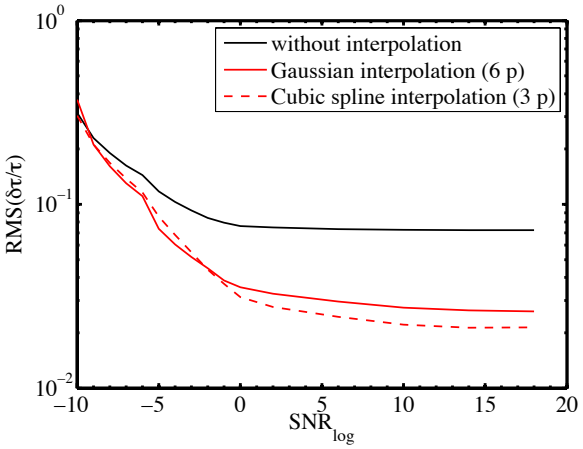

Fig. 6 RMS error of the lag time scaling with signal to noise ratio, $u_c/U_j = 0.8$, $U_j = 650$ m/s, $I = 0.15$ for 200 realizations.

More significant than signal-to-noise ratio is the relationship between the sensor separation, convective velocity and the sampling frequency $u_c/f_s\Delta x$, which is an indicator of the time separation/resolution of the temporal cross-correlation function and is limited by the Nyquist sampling theorem. A systematic study for different velocities and convective velocities was conducted. Once the non-dimensional sampling frequency surpasses 0.5, significant errors due to aliasing arise. Below this threshold the errors are very small and in the range as previously reported for $\mathrm{SNR} > 0$.

IV. Facility

The Virginia Tech hot jet facility has been described in past works [3]. This electrically heated (192 kW) free jet facility provides supersonic flow at total TTRs up to 3 (depending on nozzle diameter) at 0.12 kg/s mass flow rate. The biconic nozzle used ($M_d = 1.65$) was adapted from the geometry studied by Powers and McLaughlin [43] for military-style nozzles, differing in the present study by being axisymmetric. The differences between this type of small scale and midscale industrial facility, as well as real jet engines, have recently been summarized by Harper-Bourne [44]. The present facility addresses conditions with relevance to Mach number and temperature regimes but does not account for forward flight and multi-stream exhaust conditions found in tactical aircraft.

A photograph of the jet facility, including the locations for seeding inlet, and total pressure and temperature measurement location is shown in Fig. 7.

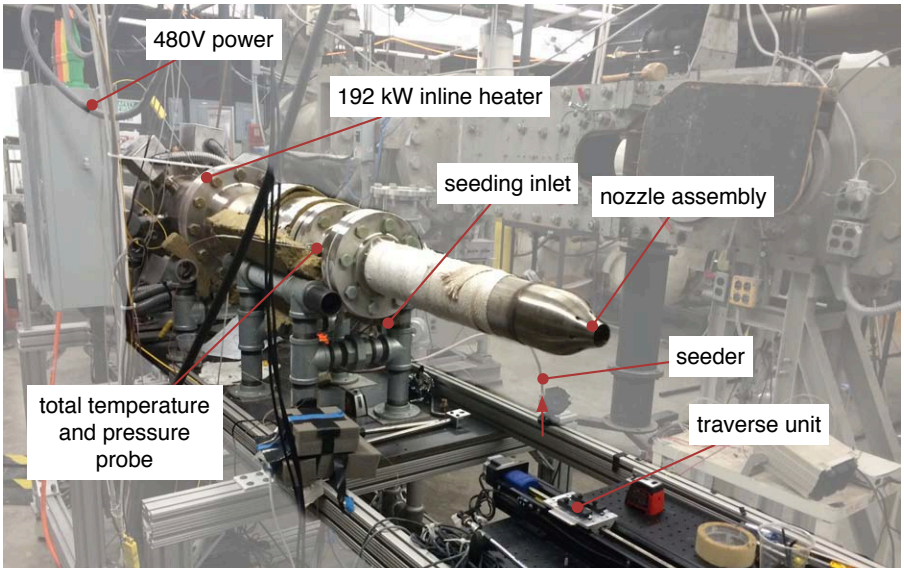

Fig. 7 The Virginia Tech hot supersonic jet facility.

For the cold and hot flow studied, flow seeding is performed by introducing Al_2O_3 particles generated by a cyclone seeder unit. Bias errors in the jet's shear layer due to flow seeding gradients as found by Blohm et al. [45] were minimized by co-flow seeding via entrainment from a smoke generator. The Stokes relaxation time can be estimated as:

$$\tau_{St} = \frac{\rho_p d_p^2}{18\mu} \qquad (4)$$

The approximate Stokes relaxation time for the core and entrainment seeding at the facility are given in Table 2. Shlien and Corrsin [46] have shown Lagrangian integral timescales to be about 30% larger than the Eulerian integral timescales, therefore a mitigated influence of particle lag on the integral statistics is expected.

Table. 2 Approximate Stokes relaxation time.

	Al_2O_3	Mineral Oil
Density ρ_p	3.95 g/cm^3	0.8 g/cm^3
Diameter d_p	300 nm	1 µm
Relaxation time τ_{St}	3.33 µs	2.22 µs
Seeding port	core	entrainment/shear layer

V. Experimental Results

In this part single and two-point correlation results for measurements with a single-point LDV probe and a new multipoint DGV instrument are presented. Measurements at x/D = 4, 6, 8, and 10 were performed with the DGV instrument and are complemented with radial measurements by the LDV instrument at x/D = 4 and 8. Details on the spatial extent of these measurements are shown in Fig. 8. The streamwise coordinate x/D on the centreline is defined as the distance from the nozzle exit plane to the center of the flow plane sensor. The radial coordinate r/D is defined as the distance from the centerline to the center of each sensor pixel. The distance between pixels is 3 mm. The detailed test matrix and information on the jet conditions are contained within Table 3.

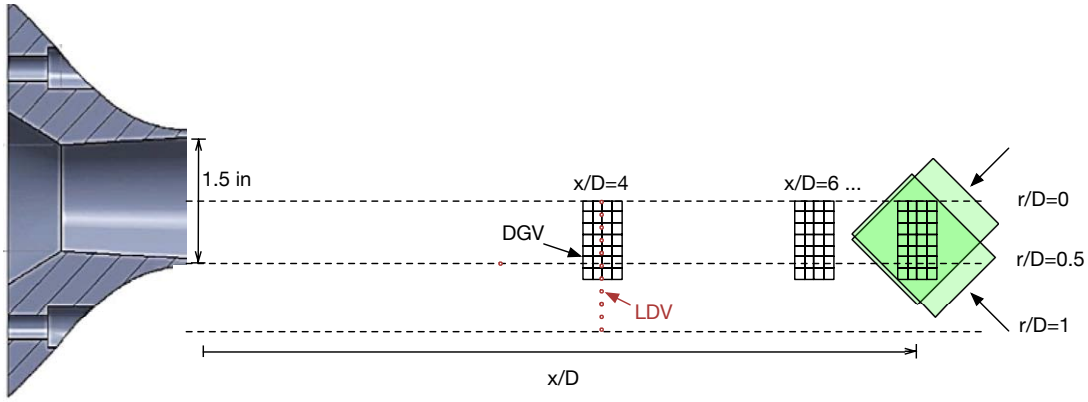

Fig. 8 Measurement setup LDV and DGV.

Higher order single-point statistics computed from LDV data for the jet at $TTR = 2.0$ are discussed in section A. of this part. The subsequent sections present results from the multipoint DGV sensor for integral time scales, second and fourth-order correlations, peak correlations maps, and integral convective velocity distribution, as well as acoustic Mach number distributions for both $TTR = 1.6$ and 2.0 jets.

Table. 3 Test matrix (radial profiles).

NPR	M_d	M_j	$\frac{\rho_j}{\rho_a}$	TTR	Re	$x/D =$ 4	6	8	10
4.80	1.65	1.68	0.96	1.63	1.3M	DGV	DGV	DGV	DGV
4.94	1.65	1.70	0.79	2.0	1.15M	DGV/LDV	DGV	DGV/LDV	DGV

A. Single point statistics

Further analysis of the single-point LDV data set first discussed by Brooks and Lowe [25] yields details of turbulence statistical behavior of the jet. The radial velocity at different streamwise locations, normalized by the exit velocity and with the radial coordinate scaled for shear layer similarity is plotted in Fig. 9. The data at $M_j = 1.65$ collapse onto similarity profiles when compared with cold jet data at $M_j = 1.37$ from Lau et al. [24] and $M_j = 1.2$ from Kerhervé et al. [6].

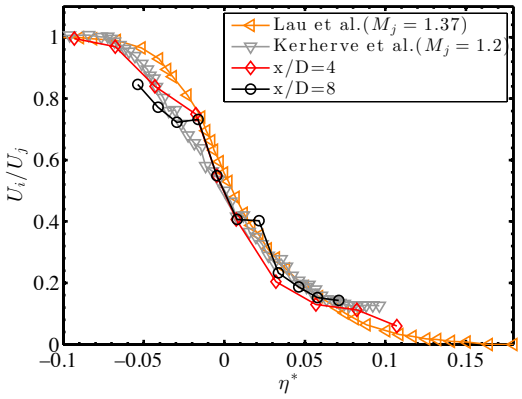

Fig. 9 LDV radial mean velocity profile at $M_j = 1.65$ and $TTR = 2.0$ compared with literature values.

The magnitude of the Reynolds stresses shown for the radial profile in Fig. 10 indicate that the position of peak-turbulence at locations x/D = 4 and 8 corresponds closely to the shear line defined by similarity scaling (see eq. 1). Again their comparison with previous cold supersonic data [24] and hot high subsonic data [47] showed good agreement at x/D = 4. At x/D = 8 the agreement is less, indicating lower Reynolds stresses for the comparison cases at this location. Lau's study [47] indicated a slower fall of the peak turbulence values for higher Mach numbers – likely attributable to differences in shear layer growth rate.

Both the fourth-order auto- and cross-terms of the velocity fluctuations and the kurtosis of the data at the two streamwise locations x/D = 4 and 8 are presented in Fig. 11 - 13. The fourth-order normal terms are nearly constant around peak values at both x/D positions, and drop abruptly on the radial edge of the potential core (see Fig. 11). This drop corresponds to a drop in the normal stresses outside of the high gradient region in the shear layer. As expected, the radial fourth-order auto terms are much lower in magnitude, by nearly an order of magnitude at the peak region.

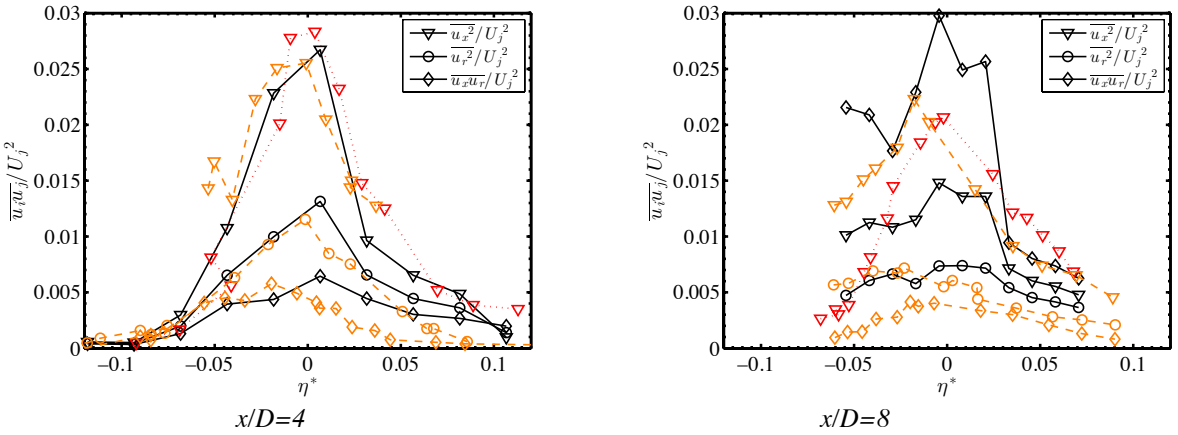

Fig. 10 Normalized Reynolds stresses at $TTR = 2.0$ compared with literature values. Solid (black) line – current study, dotted (red) line – Lau et al. [24] ($M_j = 1.37$, $TTR = 1.0$), dashed (orange) line – Lau [47] **($M_j = 0.9$, $TTR = 2.32$).**

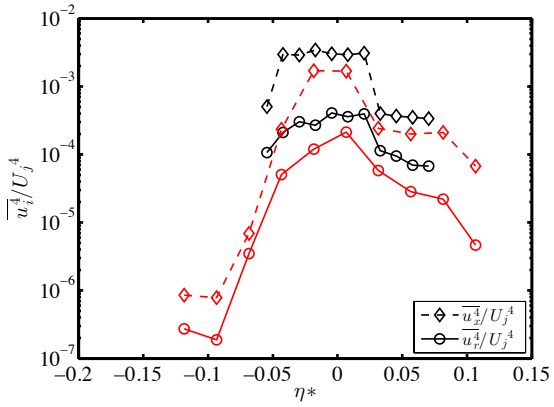

Fig. 11 Scaled fourth-order auto terms at $x/D = 4$ (red) and $x/D = 8$ (black) at $TTR = 2.0$.

The fourth-order cross terms are presented in Fig. 12. The streamwise turbulent diffusion in the radial direction $\overline{u_x u_r^3}$ peaks at the outer edge (low speed side) of the shear layer at $x/D = 4$ and then increases substantially by a factor of two once the potential core starts breaking down ($x/D = 8$). All fourth-order cross terms are found to be only significant in the regions of non-zero shear stress – mainly in the shear layer between $-0.05 < \eta^* < 0.05$. These terms appear directly in acoustic analogies (e.g., Ffowcs Williams [37], eq. 1.11); however, in the axisymmetric flow studied, the difference in value, by more than an order of magnitude, would indicate that these terms do not contribute significantly to the equivalent noise source field.

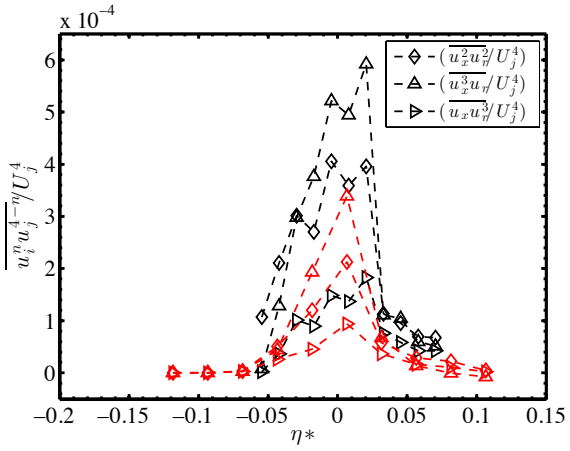

Fig. 12 Scaled fourth-order cross terms at $x/D = 4$ (red) and $x/D = 8$ (black) at $TTR = 2.0$.

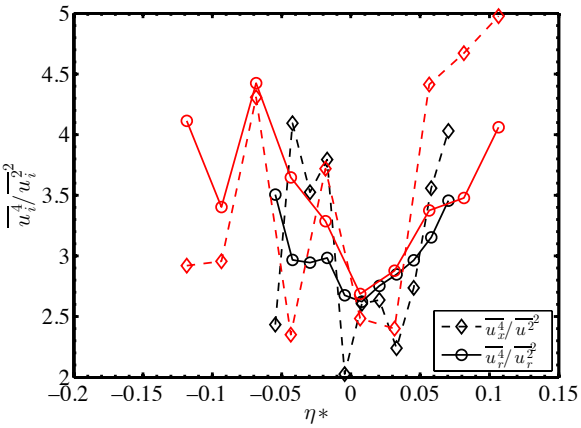

Fig. 13 Kurtosis of axial and radial velocity fluctuations at $x/D = 4$ (red) and $x/D = 8$ (black) at $TTR = 2.0$.

The fourth-order statistics indicate several features that were observed in the histograms of velocity fluctuations. Around $\eta^* = 0$, the histograms exhibit contributions from all regions of the shear layer - from ambient flow to potential core. The result is a very 'flat' histogram with probability balanced on both sides of the shear layer. The kurtosis, a ratio of the fourth-order moment to the square of the second-order moment, (1) is small for flat histogram (2) for histograms with a large peak in probability and (3) takes a value of precisely three for Gaussian histogram. The kurtosis results presented in Fig. 13 provide confirmation of this argument. In contrast to the $\eta^* = 0$ region, the shear layer edges, both outer and inner, have kurtosis values greater than the Gaussian value. This was also observed

in a PIV study conducted in a screeching round jet by Edgington-Mitchell et al. [48]. The authors suggested that this might indicate regions of higher intermittency in the outer shear layer. Juve et al. [49] investigated the role of intermittency in the noise emission of cold subsonic jets and found it to have a great impact at the end of the potential core. Their results indicate that 10% of the time contributed to about 50% of the produced noise.

The current results indicate that the flat histogram of the lip line, high gradient region results in lower values of the fourth-order correlation than would occur for Gaussian statistics. Further, the long tails of the distribution near the shear layer edges result in increased importance of the fourth-order correlation.

B. Integral time scales

The integral time scales for both TTR cases on the geometric lip line are shown in Fig.. The linear fit (red solid line) from LDV data recorded at $x/D = 1 - 4$ by Brooks et al.[50] gives good agreement with the current DGV measurement. A linear fit through the data at $TTR = 1.6$ (black solid line) was similarly obtained but shows higher scatter and respectively lower R^2 values. The R^2 values for the presented data ($TTR = 2.0$) with the fit given by Brooks et al. is 0.75, the R^2 value for the linear fit with the $TTR = 1.6$ data is 0.58. Interesting to note is that a scaling by the ratio of the density, nearly collapses the data for both TTR (the black dashed line in Fig. 14), an effect that was exhibited by Brown and Rothko [51] for integral scale spreading rates. The sensitivity to density ratio is highest for density ratios less than 1, which is the regime currently examined.

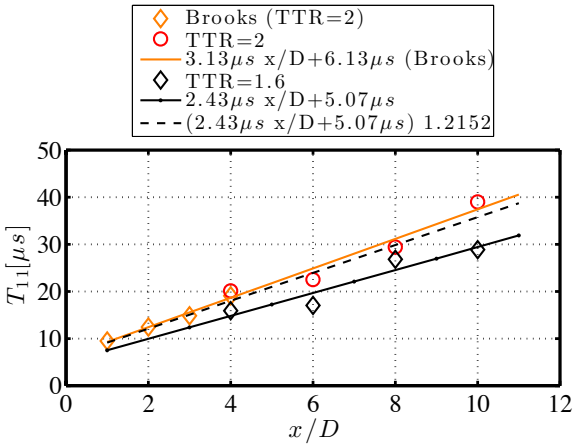

Fig. 14 Integral time scale second-order correlation.

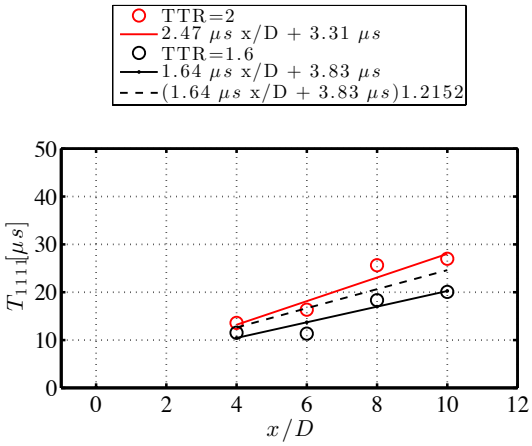

Fig. 15 Integral time scale fourth-order correlation.

Two trends are apparent, (1) supersonic heated jets exhibit a linearly increasing integral time scale (similar to previously reported for supersonic cold jets [6]), (2) the integral time scales of the high Reynolds number $TTR = 2$ hot supersonic jet presented here are larger than the integral time scales of the $TTR = 1.6$ supersonic jet. This means even though the convective velocities of the $TTR = 2.0$ jet are higher, the time scale of the predominant eddies rises due to increased jet spreading.

The respective integral timescales of the fourth-order autocorrelation, a measure for the dominant time scales of the Reynolds stresses [6] are presented in Fig. 15. It can be seen that the fourth-order correlation time scale is considerably shorter than the second-order time scale but follows a similar linear trend. The fits presented have R^2 values of 0.71 and 0.63 for $TTR = 2.0$ and $TTR = 1.6$, respectively.

C. Second- and fourth-order space-time correlation

The second- and fourth-order correlations at several locations on the lip line at $TTR = 1.6$ are shown in Fig. 16. The reference sensor is located at $\Delta x/D$ = -0.118. The respective correlations for $TTR = 2.0$ (not shown) are similar in shape but exhibit wider lobes due to a longer integral time scale (see Fig. 14). Similar shapes, especially with the slight dip into negative correlation coefficients in the cross-correlations, were observed by Doty and McLaughlin [7], in a space-time correlation study on cold air and helium-air mixture jets, and by Morris and Zaman [26], in a

study on a subsonic cold jet. The fourth-order correlation coefficients have a significantly steeper fall off than the second-order correlation coefficients at the same location indicative of a more compact correlation field [6]. Table 4 indicates the fitting parameters for the exponential fit of the form $R(\tau^*) = a \exp(b\tau^*)$ used for estimating the envelope of each cross-correlation series on the lip line for both second and fourth-order correlations.

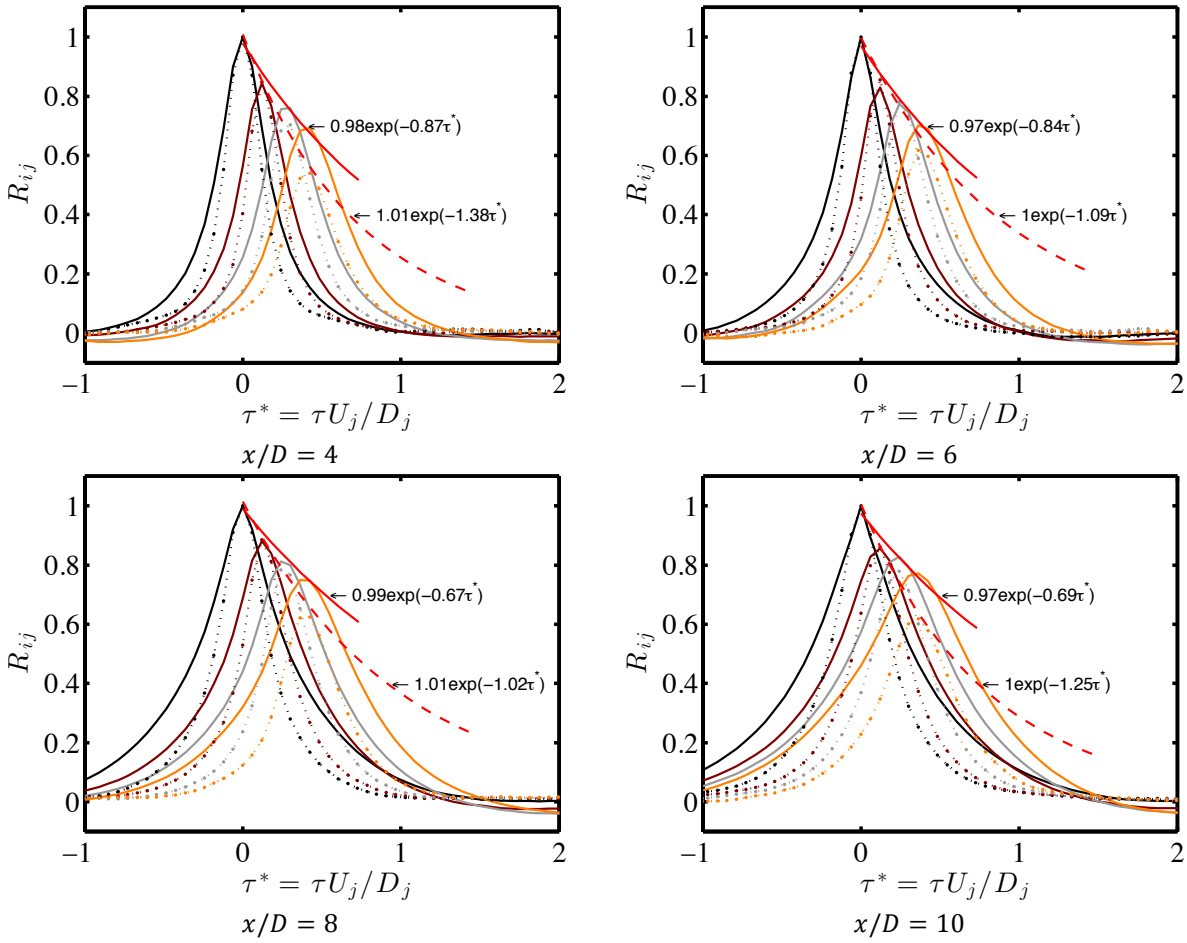

Fig. 16 second- and fourth-order cross-correlation centered at $r/D = 0.51$ at different streamwise locations at TTR=1.6, full line: second-order correlation, dotted line: fourth-order correlation. Separations from left to right $\Delta x/D$ = -0.118, -0.039, 0.039, 0.118. Solid red line: second-order envelope, dashed red line: fourth-order envelope.

Values for the envelope of the peak correlation found in literature are wide spread. Figure 17 displays the exponential envelope fits at $x/D = 4$ for $TTR = 1.6$ and $TTR = 2.0$. The comparison with time correlation envelopes reported by Panda [52] for density fluctuation, data by Doty and McLaughlin [7] as well as data by Kuo et al. [53] for OD, shows reasonable agreement within the spread of literature values. It may be noted that the

envelopes found with the DGV instrument are based on 4 values between the non dimensional lag times 0 and 0.5 only, defined by the physical sensor spacing of the multipoint instrument.

Table. 4 Second-order and fourth-order correlation envelope parameters.

	Second-order			
	$TTR = 1.6$		$TTR = 2.0$	
x/D	*a*	*b*	*a*	*b*
4	0.98	-0.87	0.99	-0.72
6	0.97	-0.84	0.98	-1.04
8	0.99	-0.67	0.99	-0.76
10	0.97	-0.69	1.02	-0.99
	Fourth-order			
4	1.01	-1.38	1.01	-1.21
6	1.00	-1.09	1.08	-2.14
8	1.01	-1.02	0.99	-1.63
10	1.00	-1.25	1.03	-1.55

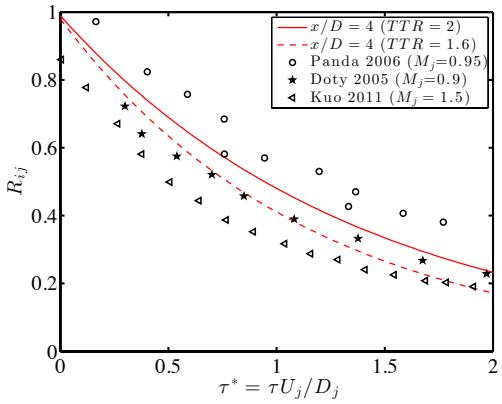

Fig. 17 Comparison of experimentally fitted envelopes with literature values.

The space-time correlation plot can be used to determine how correlated a time signal is throughout a measurement region with respect to a reference location. The peak correlation value of the second-order space-time correlation over the sensor for $TTR = 1.6$ and $TTR = 2.0$ conditions are plotted in Fig. 18. The cross-correlations of the time-resolved signal at several points in the shear layer with reference to a point on the lip line indicate highly correlated structures that penetrate into the core region of the jet. With increasing distance from the nozzle exit those structures expand further down in the core region as well outward into the ambient medium. The correlation values at both temperatures show a similar trend. The differences between the two temperatures are to be explained by the

difference in shear layer growth driven by the density differences. At $x/D = 10$ correlation values at both TTR have a decreasing trend with streamwise direction, indicating the end of the potential core, where correlation values are expected to be the highest [4].

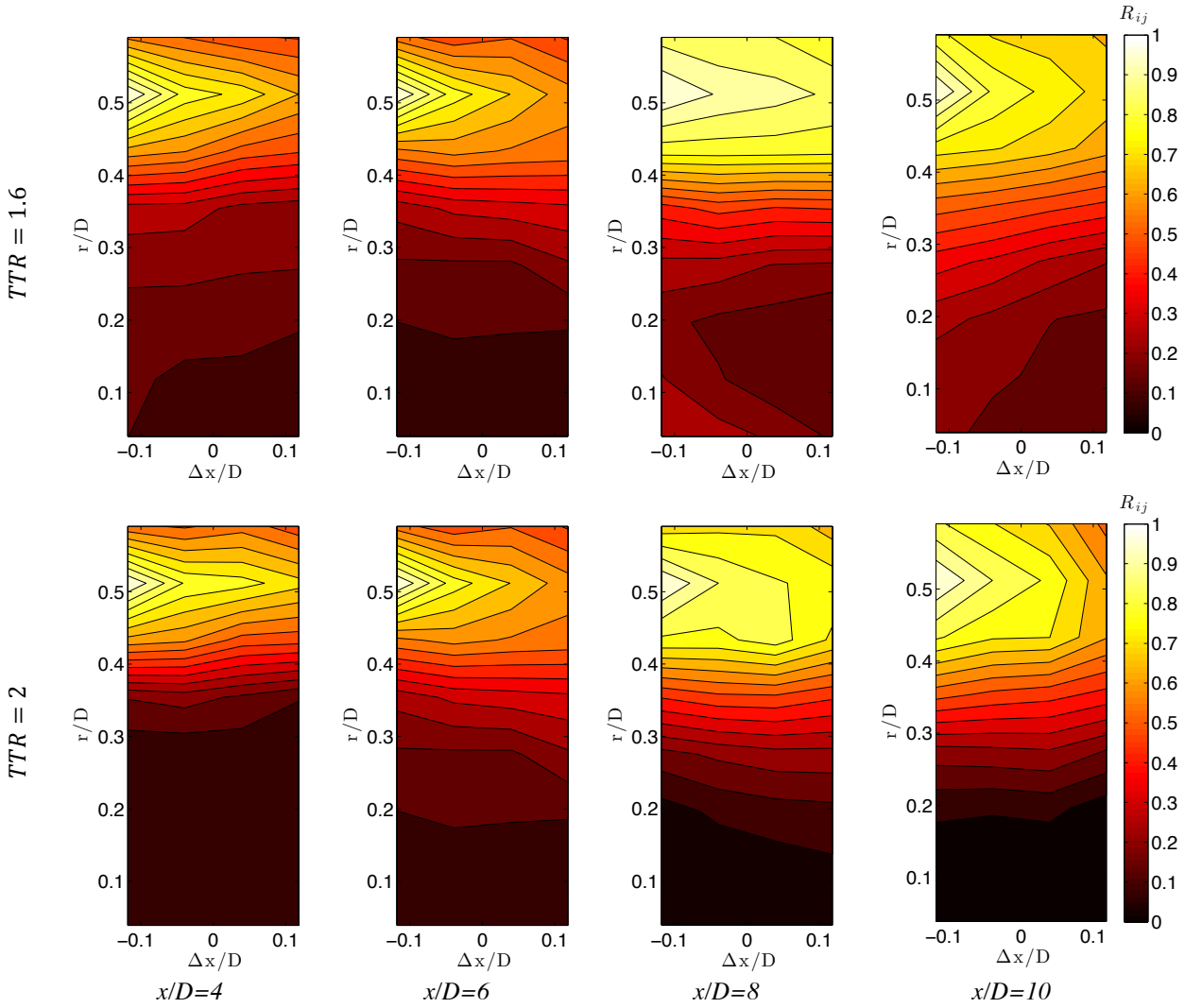

Fig. 18 Second-order space-time peak correlation maps for $TTR = 1.6$ and $TTR = 2.0$. Reference location is at $\Delta x/D = -0.118$ and $r/D = 0.51$.

D. Convective velocities

By determining the time delay for maximum cross correlation for all sensor pixels, it is possible to determine integral convection velocities for the turbulence (see eq. 9). In order to determine the convective velocity, a linear

least squares fit is created of the delay time values of the cross correlation convective ridge at all (2-4) sensor points that obeyed the estimated Nyquist criterion at a radial location.

The ratio of the convective velocity to the jet exit velocity on the lip line is shown for both cases in Fig. 19. The convective velocity exhibits a slight rise for the $TTR = 1.6$ case while remaining almost constant for $TTR = 2.0$. The resulting ratio of about $0.54 - 0.68\ U_j$ is consistent with reported values for heated jets in the literature. The differences along the lip line are best understood in light of the convective velocity distribution through the jet, Fig. 20. The jet spreading differences result in a significantly different convective velocity shear line.

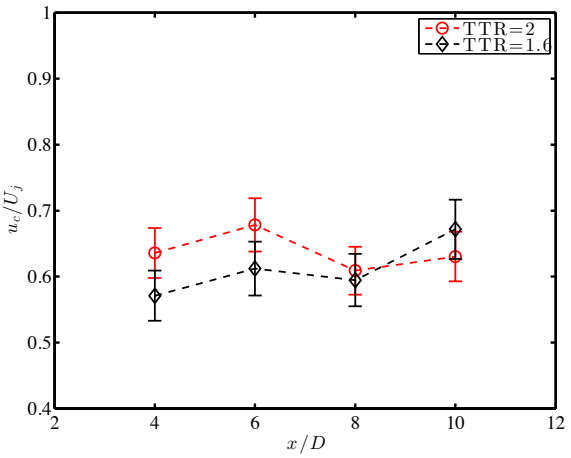

Fig. 19 Convective velocity at r/D=0.51.

A mapping of the convective velocities in the core and developing shear layer is shown in Fig. 20. Near the nozzle exit the core region exhibits values close to the jet exit velocity for both cases. While the core boundary region convective velocities significantly decay for the $TTR = 2.0$ case, a decrease and increase in the $TTR = 1.6$ case is observed. Bridges [12] showed the convective velocities on the lip line to significantly increase and then decrease after the potential core ended. This is mainly due to the use of the lip line as a geometric line, which does not coincide with the shear line accounting for the linear shear layer thickness growth. Similar trends in convective velocity ratios on the lip line have been shown by Papamoschou et al. [54] in a large eddy simulation (LES) of a M=0.9 jet. It is to note that while the $TTR = 2.0$ case shows a generally broader distribution of very high convective velocities, the $TTR = 1.6$ case shows increased convective velocities further downstream. A possible explanation could be the presence of shock and expansion wave in the longer potential core. As heating shortens the

potential core because of increased mixing and the entrainment of cold ambient air, this effect may be less observable in the $TTR = 2.0$ case.

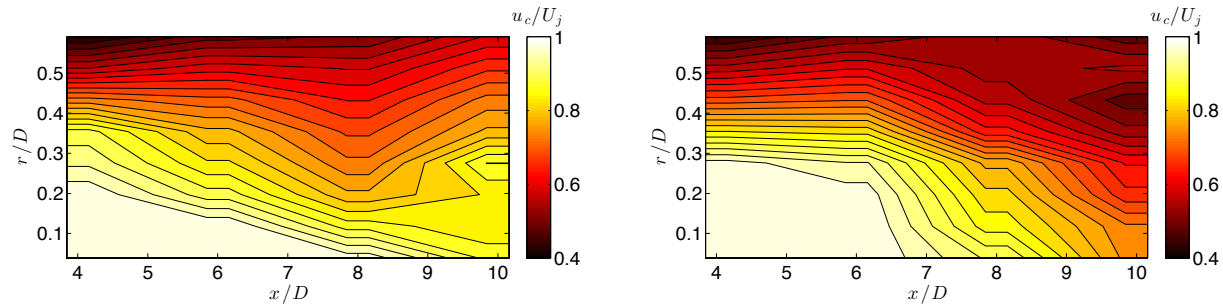

$TTR = 1.6$ $TTR = 2.0$

Fig. 20 Convective velocities in the core region and developing shear layer for $TTR = 1.6$ and $TTR = 2.0$.

Uncertainty in convective velocities

As shown in part III section c, the uncertainty of the convective velocity estimate stems from the uncertainty in the lag time estimate and the physical sensor spacing.

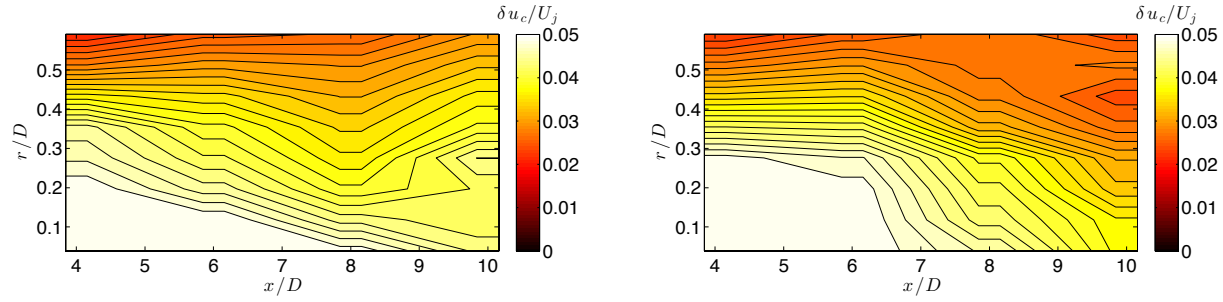

$TTR = 1.6$ $TTR = 2$

Fig. 21 Uncertainty of convective velocities in the core region and developing shear layer for $TTR = 1.6$ and $TTR = 2.0$.

From the sensitivity analysis it was determined that lag times can be estimated by ±4% using cubic spline interpolation and the uncertainty in the magnification of the lens system is estimated to be up to ±2.5%. Since the lag times are found using a multipoint linear interpolation over several sensor stations the lag time uncertainty estimate is likely conservative. Figure 21 shows the estimated convective velocity uncertainty for both cases. The uncertainties are highest close to the potential core as convective velocity is the highest and the lag times are at the

smallest values in this region. For the given velocity contours the highest uncertainties close to the core are between 4 and 6 % and as low as 3% of the jet exit velocity in the outer region of the shear layer. Within the potential core additional uncertainties may arise due to the presence of shock waves.

VI. Discussion

The results presented above hold implications for the fundamental understanding of supersonic annular shear layer dynamics that result in noise production. First, the flows studied contribute to the currently limited database of heated supersonic jet kinematics. The results herein, as well as flow visualization results previously presented [55], indicate that the effect of temperature change in flow development is significant. Specifically, for the same nozzle pressure ratio, the density ratio, $\frac{\rho_j}{\rho_a}$, varies as the total temperature. For the NPR studied, the $TTR = 1.6$ density ratio was nearly unity, while the $TTR = 2.0$ case resulted in a value of 0.79. As shown by Brown and Roshko [51], controlling for effects of compressibility, the enhancement of spreading is greatest for density ratios less than 1. In our study, even for the relatively small change in static density, the effect is clear - the increased spreading diffuses convective speeds more quickly in the hotter jet. The relationship of these findings to large eddy noise production via Mach wave radiation is evident in Fig. 22 for acoustic Mach number distributions.

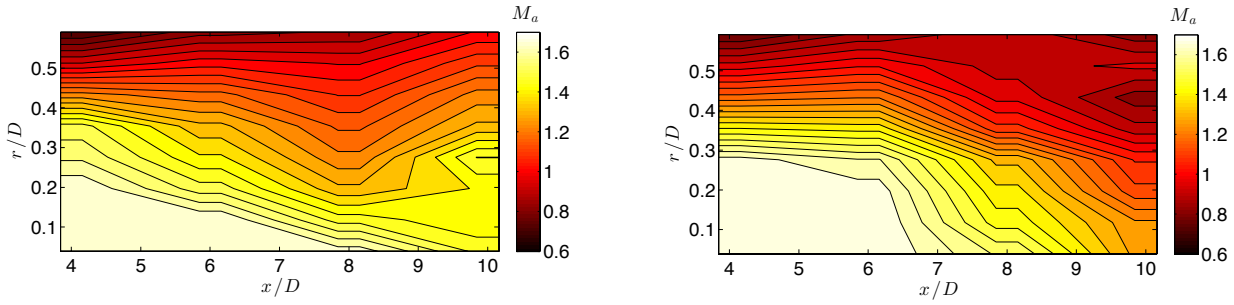

$TTR = 1.6$ $TTR = 2.0$

Fig. 22 Acoustic Mach numbers in the core region and developing shear layer for $TTR = 1.6$ and $TTR = 2.0$.

The higher jet temperature results in faster eddies relative to the ambient sound speed. As noted by Papamoschou et al. [37], among others, the radiation efficiency of these supersonic eddies is much greater than subsonic eddies. Another interpretation originated by Tam et al. [56] is based upon instability waves – known as the wavy wall

analogy – and indicates increased noise radiation efficiency when supersonic phase speeds are reached. However, the increased mixing partially mitigates the effect of heating as entrainment of cold, dense ambient fluid causes a more rapid deceleration, first of the outer shear layer and then progressively toward the core. The acoustic Mach number for the hotter case is generally greater in the core, but the sonic convective wavespeed surface has a similar resemblance for both presented cases, especially at lower diameters. Acoustic analogies like the one by Ffowcs Williams and Maidanik [57], which primarily addresses Mach wave radiation, has its source volume defined by the locations where the acoustic Mach number reaches unity, therefore directly influencing the prediction of the noise intensity in the far field. Based upon the sensitivity observed to temperature/density changes, we assert that the kinematics of supersonic jets $\left(\frac{U_j}{a_j} > 1\right)$ in this regime with aspects relevant to tactical aircraft plumes appear to behave similarly to compressible but subsonic jets $\left(\frac{U_j}{a_j} < 1\right)$ once density ratio effects are accounted.

VII. Conclusions

In this study fourth-order statistics as well as second-order and fourth-order space-time correlations for a hot ($TTR = 1.6$ and $TTR = 2$) supersonic jet at perfectly expanded conditions are presented. A new instrument capable of time-resolved measurement at 250 kHz and based on the DGV technique is presented. A custom 32-pixel PMT camera connected to a FPGA data acquisition system enables long duration velocimetry at very low statistical errors in cross-correlation processing LDV data were presented and analyzed with respect to fourth-order statistics.

The kurtosis of the streamwise term indicated deviations from Gaussian statistics at the lip line as well as the edges of the shear layer, as expected. The increase in kurtosis in the region of immediate interface between the potential core and the shear layer is due to long negatively skewed skirts of the fluctuation histogram. The streamwise turbulent diffusion in the radial direction - a key indicator of turbulent mixing dynamics - peaks at the lip line of the developing shear layer and increases substantially once the potential core starts breaking down.

The multipoint DGV instrument was used for time resolved measurements in the 4 to 10 *x/D* region. The acquired data were used to detect the development of the cross-correlation of turbulent velocity signals on the lip line. It was shown that the correlation between signals increases significantly with downstream location, indicating the breakdown of the potential core and the emergence of very large eddy structures from the rapidly broadening shear layer. Using space-time correlation maps for both heated cases, the development of correlated structure along

the lip line was quantitatively analyzed. Data for both second and fourth-order cross correlation were presented and used to determine integral correlations time scales for streamwise velocity and Reynolds stress fields. Specifically for the $TTR = 2.0$ case good agreement with a previous experiment in the same facility using an LDV instrument was reached for integral time scale estimates.

The time delay of the cross correlation was used to calculate the streamwise eddy convective velocity on the lip line, producing values between $0.54 - 0.58\ U_j$. This is significantly lower than the convective speed in an unheated supersonic jet, owing primarily to the increased divergence of the shear line for heated jets. The same technique was applied to generate convective velocity maps showing similar axial distribution when compared to recent LES calculations [54], for cold subsonic jets.

Acknowledgements

The Office of Naval Research Hot Jet Noise Reduction Basic Research Challenge and DURIP, grants N00014-11-1-0754 and N00014-12-1-0803 under program managers Drs. Brenda Henderson and Joseph Doychak, supported the work described.

References

[1] Lilley, G. M., "The Radiated Noise From Isotropic Turbulence With Applications To The Theory Of Jet Noise," *Journal of Sound and Vibration*, Vol. 190, No. 3, 1996, pp. 463–476.

[2] Lowe, K. T., Ng, W. F., and Ecker, T., "Early Development of Time-Resolved Volumetric Doppler Velocimetry for New Insights in Hot Supersonic Jet Noise," AIAA Paper 2012-2273, June 2012.

[3] Ecker, T., Brooks, D. R., Lowe, K. T., and Ng, W. F., "Development and application of a point Doppler velocimeter featuring two-beam multiplexing for time-resolved measurements of high-speed flow," *Experiments in Fluids*, Vol. 55, No. 9, 2014, pp. 1–15.

[4] Panda, J., Seasholtz, R. G., and Elam, K. A., "Investigation of noise sources in high-speed jets via correlation measurements," *Journal of Fluid Mechanics*, Vol. 537, 2005, pp. 349–385.

[5] Lau, J. C., "Laser velocimeter correlation measurements in subsonic and supersonic jets," *Journal of Sound and Vibration,* Vol. 70, No. 1, 1980, pp. 85–101.

[6] Kerhervé, F., Jordan, P., Gervais, Y., and Valiere, J. C., "Two-point laser Doppler velocimetry

measurements in a Mach 1.2 cold supersonic jet for statistical aeroacoustic source model," *Experiments in Fluids*, Vol. 37, No. 3, 2004, pp. 419–437.

[7] Doty, M. J., and McLaughlin, D. K., "Space–time correlation measurements of high-speed axisymmetric jets using optical deflectometry," *Experiments in Fluids*, Vol. 38, No. 4, 2005, pp. 415–425.

[8] Samimy, M., and M. P. Wernet. "Review of planar multiple-component velocimetry in high-speed flows," *AIAA Journal*, Vol. 38, No. 4, 2000, pp. 553–574.

[9] Alkislar, Mehmet B., Anjaneyulu Krothapalli, and Luiz M. Lourenco. "Structure of a screeching rectangular jet: a stereoscopic particle image velocimetry study," *Journal of Fluid Mechanics,* Vol. 489, 2003, pp. 121–154.

[10] Wernet, M. P., "Time-Resolved PIV for Space-Time Correlations in Hot Jets," 22nd International Congress on Instrumentation in Aerospace Simulation Facilities, IEEE, 2007.

[11] Scarano, F., "Overview of PIV in Supersonic Flows," Springer, 2008.

[12] Bridges, J., AIAA 2006-2534, "Effect of heat on space-time correlations in jets," AIAA Paper 2006-2534, May 2006.

[13] Ukeiley, L., Tinney, C., Mann, R., & Glauser, M., "Spatial correlations in a transonic jet," *AIAA Journal*, Vol. 45, No. 6, 2007, pp. 1357–1369.

[14] Fleury, Vincent, Christophe Bailly, Emmanuel Jondeau, Marc Michard, and Daniel Juvé. "Space-time correlations in two subsonic jets using dual particle image velocimetry measurements," *AIAA Journal*, Vol. 46, No. 10, 2008, pp. 2498–2509.

[15] Wernet, M. P., "Temporally resolved PIV for space–time correlations in both cold and hot jet flows," *Measurement Science and Technology*, Vol. 18, No. 5, 2007, pp. 1387.

[16] Komine, H., Brosnan, S. J., Litton, A. B., and Stappaerts, E. A., "Real-time, Doppler global velocimetry," 29th AIAA Aerospace Sciences Meeting, Jan. 1991.

[17] Meyers, J. F., and Komine, H., "Doppler global velocimetry - A new way to look at velocity," ASME Fourth International Conference on Laser Anemometry, 1991, pp. 289–296.

[18] Meyers, J. F., Lee, J. W., and Schwartz, R. J., "Characterization of measurement error sources in Doppler global velocimetry," *Measurement Science and Technology*, Vol. 12, No. 4, 2001, pp. 357–368.

[19] Fischer, A., Büttner, L., and Czarske, J., "Doppler global velocimetry with laser frequency modulation for

the analysis of complex turbulent flows," 15th Int Symp on Applications of Laser Techniques to Fluid Mechanics, Lisbon, Portugal, July 2010.

[20] Charrett, T. O. H., Ford, H. D., Nobes, D. S., and Tatam, R. P., "Two-frequency planar Doppler velocimetry," *Review of Scientific Instruments*, Vol. 75, 2004, pp. 4487–4496.

[21] Cadel, D.R., Ecker, T., and Lowe, K. T., "Time-Domain Cross-Correlation Scan DGV (CCS-DGV) for Mean-Velocity Boundary Layer Measurements," AIAA Paper 2014-1104, Jan. 2014.

[22] Elliott, G. S., and Beutner, T. J., "Molecular filter based planar Doppler velocimetry," *Progress in Aerospace Sciences*, Vol. 35, No. 8, 1999, pp. 799–845.

[23] Thurow, B., JIANG, N., Lempert, W., and Mo, S., "Development of megahertz-rate planar doppler velocimetry for high-speed flows," *AIAA Journal*, Vol. 43, No. 3, 2005, pp. 500–511.

[24] Lau, J. C., Morris, P. J., and Fisher, M. J., "Measurements in subsonic and supersonic free jets using a laser velocimeter," *Journal of Fluid Mechanics*, Vol. 93, pp. 1–27, 1979.

[25] Brooks, D. R., and Lowe, K.T., "Fluctuating Flow Acceleration in a Heated Supersonic Jet," 17th Int Symp on Applications of Laser Techniques to Fluid Mechanics, Lisbon, Portugal, July 2014

[26] Morris, Philip J., and Zaman, Khairul B.M.Q. "Velocity measurements in jets with application to noise source modeling." *Journal of Sound and Vibration*, Vol. 329, No. 4, 2010, pp. 394–414.

[27] Papamoschou, D., Morris, P. J., and McLaughlin, D. K., "Beamformed flow-acoustic correlations in a supersonic jet," *AIAA Journal*, Vol. 48, No. 10, 2010, pp. 2445–2453.

[28] Kinzie, K. W., & McLaughlin, D. K., "Measurements of supersonic helium/air mixture jets," *AIAA Journal*, Vol. 37, No. 11, 1999, pp. 1363–1369.

[29] Petitjean, B. P., Viswanathan, K., and McLaughlin, D. K., "Space-time correlation measurements in subsonic and supersonic jets using optical deflectometry," AIAA Paper 2007-3613, May 2007.

[30] Witze, P.O., "Centerline Velocity Decay of Compressible Free Jets," *AIAA Journal*, Vol. 12, No. 4, 1974, pp. 417–418.

[31] Ukeiley, L., Tinney, C., Mann, R., and Glauser, M., "Spatial correlations in a transonic jet," *AIAA Journal,* Vol. 45, No.6, 2007, pp. 1357–1369.

[32] Mollo-Christensen, E., "Measurements of Near Field Pressures of Subsonic Jets." NASA report 19630008377, April 1963.

[33] Bridges, J., & Wernet, M. P., "Validating Large-Eddy Simulation for Jet Aeroacoustics," *Journal of Propulsion and Power*, Vol. 28, No. 2, 2012, pp. 226–235.

[34] Forkey, J. N., Lempert, W. R., and Miles, R. B., "Corrected and calibrated I_2 absorption model at frequency-doubled Nd:YAG laser wavelengths," *Applied Optics*, Vol. 36, No. 27, 1997, pp. 6729–6738.

[35] Fischer, M., Heinze, J., Matthias, K., and Roehle, I., "Doppler Global Velocimetry in flames using a newly developed, frequency stabilized, tunable, long pulse Nd: YAG laser," 10th Int Symp on Applications of Laser Techniques to Fluid Mechanics, Lisbon, Portugal, July 2000.

[36] Ecker, T., Lowe, K. T., and Ng, W. F., "A rapid response 64-channel photomultiplier tube camera for high-speed flow velocimetry," *Measurement Science and Technology*, Vol. 26, No. 2, 2015, p. 027001.

[37] Ffowcs Williams, J. E. , "The Noise from Turbulence Convected at High Speed," *Philosophical Transactions for the Royal Society of London. Series A, Mathematical and Physical Sciences,* Vol. 255, No. 1061, 1963, pp. 469–503.

[38] Goldstein, M. E., "A generalized acoustic analogy," *Journal of Fluid Mechanics*, Vol. 488, 2003, pp. 315–333.

[39] Fisher, M. J., and Davies, P. O. A. L., "Correlation measurements in a non-frozen pattern of turbulence," *Journal of Fluid Mechanics*, Vol. 18, 1964, pp. 97–116.

[40] Pope, S. B., "Turbulent Flows", Cambridge, 2000.

[41] de Kat, R., Gan, L., Dawson, J. R., and Ganapathisubramani, B., "Limitations of estimating turbulent convection velocities from PIV," *arXiv*, *physics.flu-dyn*, 2013.

[42] Lau, J. C., "Laser velocimeter correlation measurements in subsonic and supersonic jets," *Journal of Sound and Vibration,* Vol. 70, No. 1, 1980, pp. 85–101.

[43] Powers, R. W., and McLaughlin, D. K., "Acoustic measurements of scale models of military style supersonic beveled nozzle jets with interior corrugations," AIAA Paper 2012-2116, June 2012.

[44] Harper-Bourne, M., "Jet noise measurements: past and present," *International Journal of Aeroacoustics*, Vol. 9, No. 4, 2010, pp. 559–588.

[45] Blohm, M., Lempert, W., Samimy, M., and Thurow, B., "A Study of Convective Velocity in Supersonic Jets Using MHz Rate Imaging," AIAA Paper 2006-45, Jan. 2006.

[46] Shlien, D. J., and Corrsin, S., "A measurement of Lagrangian velocity autocorrelation in approximately

isotropic turbulence," *Journal of Fluid Mechanics*, Vol. 62**,** No. 2, 1974, pp. 255–271.

[47] Lau, J. C., "Effects of exit Mach number and temperature on mean-flow and turbulence characteristics in round jets," *Journal of Fluid Mechanics*, Vol. 105, 1981, pp. 193–218.

[48] Edgington-Mitchell, D., Oberleithner, K., Honnery, D. R., and Soria, J., "Coherent structure and sound production in the helical mode of a screeching axisymmetric jet," *Journal of Fluid Mechanics*, Vol. 748, 2014, pp. 822–847.

[49] Juvé, D., Sunyach, M., & Comte-Bellot, G., "Intermittency of the noise emission in subsonic cold jets," *Journal of Sound and Vibration*, Vol. 71, No. 3, 1980, pp. 319–332.

[50] Brooks D. R. , Ecker T., Lowe K.T. and Wing Ng, "Experimental Reynolds Stress Spectra in Hot Supersonic Round Jets", AIAA Paper 2014-1227, Jan. 2014.

[51] Brown, Garry L., and Anatol Roshko. "On density effects and large structure in turbulent mixing layers," *Journal of Fluid Mechanics*, Vol. 64, No. 4, 1974, pp. 775–816.

[52] Panda, J., 2006, "Two point space-time correlation of density fluctuations measured in high velocity free jets." AIAA Paper 2006-0006, Jan. 2006.

[53] Kuo, C. W., Powers, R., and McLaughlin, D. K., "Space-time correlation of flow and acoustic field measurements in supersonic helium-air mixture jets using optical deflectometry." AIAA Paper 2011-2789, June 2011.

[54] Papamoschou, D., Xiong, J., and Liu, F., "Reduction of Radiation Efficiency in High-Speed Jets." AIAA Paper 2014-2619, June 2014.

[55] Ecker, T., Brooks, D. R., Lowe, K. T., and Ng, W. F., "Quantitative image processing of high-speed Schlieren of a hot supersonic jet," *Bulletin of the American Physical Society*, Vol. 58, No. 18, 2013.

[56] Tam, C. K., Chen, P., and Seiner, J. M., "Relationship between the instability waves and noise of high-speed jets," *AIAA Journal*, Vol. 30, No. 7, 1992, pp. 1747–1752.

[57] Ffowcs Williams, J. E., and G. Maidanik. "The Mach wave field radiated by supersonic turbulent shear flows." *Journal of Fluid Mechanics*, Vol. 21, No. 04, 1965, pp. 641-657.

Part VI.

On the distribution and scaling of convective wavespeeds in the shear layers of heated supersonic jets

The contents of this chapter are to be submitted for publication. (Tobias Ecker, K. Todd Lowe, Wing F. Ng, ”On the distribution and scaling of convective wavespeeds in the shear layers of heated supersonic jets”) .

On the Distribution and Scaling of Convective Wavespeeds in the Shear Layers of Heated Supersonic Jets

Tobias Ecker*, K. Todd Lowe†, Wing F. Ng‡

Virginia Tech, Blacksburg, Virginia 24060

The noise generated by supersonic plumes is of growing concern given the enormous peak noise intensity radiated by tactical aircraft engines as well as the recently revived interest in supersonic transport concepts. Unfortunately, very little data exist for understanding the behavior of eddy convection in high Reynolds number, supersonic plumes, particularly for heated jets, limiting our current ability to develop fundamental concepts that alter compressible eddy convective speeds. Herein, is studied experimentally the scaling of eddy wave-speeds in the developing shear layers of supersonic heated jets. Both radial, and frequency scaling of the eddy convective wavespeeds are presented. It is shown that the radial profiles of the convective velocity successfully collapse with previous data at different conditions when accounting for density ratio and symmetric convective Mach number. The scaling of the convective velocity with frequency at several locations in the shear layer and near the centerline demonstrates the process of high momentum, high velocity large-scale eddies convecting into regions of locally reduced mean velocities. Near the end of the potential core, a zone identified which is dominated by large-scale turbulent structures interacting with the increased mean velocity-spreading rate. This phenomenon results in increased noise efficiency and may be a key driver of noise emission observed in heated supersonic jets.

* Graduate Research Assistant, Aerospace and Ocean Engineering.
† Assistant Professor, Aerospace and Ocean Engineering.
‡ Christopher C. Kraft Endowed Professor.

INTRODUCTION

Despite substantial progress on the topic of noise reduction in subsonic jets, e.g., via the use of chevrons and high bypass engines, the noise generated by supersonic exhaust plumes from engines used in the field has actually increased with time. The relative inefficacy of chevrons — due to compressibility limits to small scale mixing turbulent effectiveness — and the lower bypass required for such engines makes the problem of noise reduction fundamentally more challenging for supersonic engines.

Recent theoretical and computational work (Papamoschou et al., 2014) has built further upon concepts developed earlier (Papamoschou, 1997) on the ability to reduce peak noise radiation by altering the convective Mach number of eddies in the shear layer of such plumes. A version of the new acoustic analogy that was presented indicates that acoustic emissions in plumes have two components — a scaling of the source provided by turbulent fluctuation amplitudes and a radiation efficiency contribution shown to be a function of the acoustic eddy convective Mach number, $M_a = U_c/a$, where the speed of sound a is that of the surrounding ambient medium. While reducing the large-scale eddy turbulence in plumes is possible, considerable effort on the topic has, to date, yielded limited success. Further, the noise produced scales linearly with turbulence intensity. As such, a 50% reduction in large-scale eddy turbulence intensity equating to 3 dB of noise reduction would be considered a major breakthrough when addressing turbulence intensity alone. In contrast, the radiation efficiency — the amount of turbulent kinetic energy that will be converted to acoustic energy — is highly nonlinear with eddy convective Mach number and offers considerably more latitude for noise reduction by fundamentally changing the way that the shear turbulence layer interacts across core and ambient or secondary streams.

To address the lack of information in relevant flows, the authors have developed and validated a very high repetition rate, multi-point velocimetry instrument based upon the time-resolved Doppler global velocimetry (TR-DGV) technique (Ecker et al., 2014a; 2014b; Lowe et al., 2012). The instrument used in this study has been applied to date in the developing shear layer downstream of a supersonic plume operated at diameter Reynolds numbers of approximately 1 million.

In previous work, two-point correlations have been used to obtain integral scale convective velocities by least-squares fit to the time-space loci of peak correlation. It was found that the shear layer turbulence is affected to first order by the density ratio of the core stream to the surrounding medium and the compressibility of the turbulence. Numerous authors have shown that as eddy convective Mach number increases (as is done when heating), shear

layer growth is suppressed, while decreasing the core stream density relative to the ambient density (as is done when heating) has the universal effect of increasing shear layer growth. The data indicates that as the jet is heated, spreading increases and the integral scale convective velocity of the flow is diffused at a greater rate than the cold jet, indicating that the density ratio effect is greater than the compressibility effect for these conditions. Once scaled to account for shear layer growth, the convective values are consistent between the presented conditions as well as with past data (e.g., Kerhervé et al. 2004a).

CONVECTION VELOCITIES IN TURBULENT SHEAR FLOWS

The convection of turbulent fluctuations in shear flows is directly related to the process of noise generation and propagation. Several theories based on acoustic analogies derived from Lighthill (1952) directly relate the pressure fluctuations and the noise intensity to fourth-order correlations and the eddy convective velocity. Bailly et al. (1997) summarize the relevant aspects with regards to the convective amplification factor (Plumblee, 1974) for models by Ribner (1969), Goldstein-Howes, as well as Ffowcs Williams and Maidanik (1965). In all models the convective Mach number, based on the eddy convective velocity can be identified as a driver of the produced noise intensity and similarly the radiation efficiency (Papamoschou et al., 2014).

The convective Mach number based on the eddy convective velocity is defined as the ratio of the convective velocity to the sound speed as shown in equation 1. For co annular jet flows or multi-stream shear layers this core convective Mach number often carries the subscript (1), where as the co-flow is notated as (2).

$$M_c = \frac{U_j - u_c}{a_j} \qquad (1)$$

The theoretical (symmetric) convective Mach number (Papamoschou, 1997) can be estimated from the jet and co-flow properties.

$$M_{c\,sym} = \frac{U_1 a_1 + U_2 a_2}{a_1 + a_2} \qquad (2)$$

For a single stream jet at perfectly expanded condition and same gas properties as the ambient gas a relationship between the isentropic jet Mach M_j number and the symmetric convective Mach number can be easily derived, revealing a simple dependence on the jet density ratio.

$$M_{c\,sym} = \frac{M_j}{\left(1+\sqrt{\frac{\rho_a}{\rho_j}}\right)} \qquad (3)$$

The definition of the convection velocity must be considered in order to arrive at the correct conclusion of its physical significance (Wills, 1964). Originally the definition is based upon the peaks of the space-time correlation and the associated time or space separations of the signal under consideration. This convection velocity is an integral parameter as it is an average representation of all eddies convicting within the turbulent field.

In an alternative approach (Wills, 1964), the frequency (wave-number) dependent convective velocity due to the existence of differently sized eddies moving at different convective velocities within the turbulent field is considered. This perspective implies that both, eddies moving at high velocity and small wave-number components may contribute to the power spectral density, indicating a detachment between turbulent spectrum and turbulent scales due to a non constant convective wave speed. A thorough review of the application of space time correlation in turbulent flow has been given by Wallace (Wallace, 2014).

Fisher and Davies (1964) studied the validity of Taylor's frozen turbulence concept in shear flows via two-point cross-correlation using hot wire anemometry. The frozen turbulence assumption describes an approach to estimate the spatial correlations from the temporal correlations (Pope, 2000). It implies that a turbulent field is advected by the mean flow, from which a constant convective velocity equal to the mean flow velocity would follow. Fisher and Davies (1964), as well as successive studies have proven this to be incorrect for free shear flow, showing a clear frequency dependence of the convective velocity from their experimental results.

Davis et al. (1964) studied the turbulence characteristics in the mixing region of a subsonic round jet. They found two conditions; near the center a fast moving core with small fluctuations is superimposed with flares of strong fluctuations moving at velocities below the mean value. In the outer part of the jet the opposite observation is made. Smaller fluctuations moving at a lower speed are superimposed by stronger fluctuations at higher velocities. Naturally the larger scale fluctuations, containing higher kinetic energy will bias integral measures of the convective velocity towards the velocity at which they are convecting.

Morris and Zaman (2010) studied correlation based measurements in a subsonic jet, focusing on application to noise source modeling. They presented both radial distribution of convective velocities and Strouhal (*Sr*) number dependent convective velocity in the jet shear layer. Their interpretation of the distribution of axial length scales

suggests low St number length scales to scale with the jet width and high St number disturbances to have a universal behavior independent of jet location.

Figure 1 shows conceptually the experimentally established distribution of mean and convective velocities within a jet shear layer. This observed distribution lends hand to an intuitive separation of the jet shear layer into two regions, a region (I) with larger eddies slower than the mean flow and a region (II) with some larger scale eddies being faster than the mean flow.

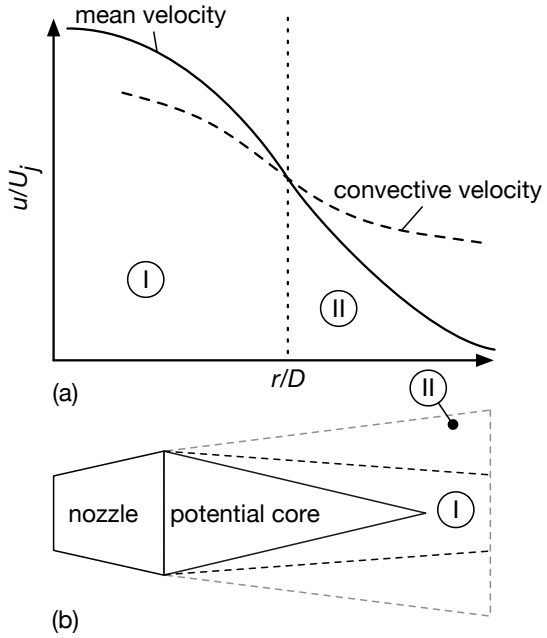

Figure 1. (a) Mean and convective velocity distribution over the jet radius. (b) Indication of the two different convective velocity regions trough the jet domain.

Integral convection velocity

In order to determine the integral convective velocity, the cross-correlation of a signal at two locations must be found. The second order cross-correlation is defined as follows (Morris and Zaman, 2010):

$$R_{ij}(x,r,\varsigma,\xi,\tau) = \frac{}{s_i(x,r,t)s_j(x+\varsigma,r+\xi,t+\tau)} \quad (4)$$

where *s(x,r,t)* is the time-resolved data at a location with coordinate x and r, ς and ξ are the spatial separation and τ the delay timescale from the reference location.

The condition describing the integral convection velocity is then as follows (Davis, 1964):

$$R(\tau) = R(x = \widehat{U}_c\tau) \qquad (5)$$

Wave-number dependent convection velocity

Previous studies (de Kat et al., 2013) have shown limitations in determining wave-number dependent convective velocities due to the effect of low pass filtering of PIV on the power spectra. Restrictions due to the characteristics of the phase spectrum are analyzed and general limiting conditions for experimental parameters (e.g 2π limit) not only limited to PIV are summarized.

Kerhervé et al. (2004b) demonstrated the frequency dependency of the turbulence scales in sub and supersonic jet flows from their non-equally sampled laser Doppler velocimeter (LDV) data. Both the slot correlation technique and the sample-and-hold technique are used to find the cross-correlations and cross-spectra. While both techniques resulted in very similar outcomes, limitations due to noise and data-rate appear to influence the spectra and the derived phase angles presented.

To determine the frequency (*f*) dependent convective wave speed, the cross correlation between the signal at two stations need to be found:

$$(x, r, \varsigma, \xi, f) = \int_{-\infty}^{\infty} R_{ij}\,(x, r, \varsigma, \xi, \tau) e^{-i2\pi f\tau} d\tau \qquad (6)$$

The phase angle can be found from the co- and quadrature-components of the cross spectrum:

$$\phi(f) = tan^{-1} \frac{Im\left[G_{ij}\,(x, r, \varsigma, \xi, f)\right]}{Real\left[G_{ij}\,(x, r, \varsigma, \xi, f)\right]} \qquad (7)$$

which can directly be converted into wave speed:

$$u_c(f) = \frac{2\pi f \Delta x}{\phi(f)} \qquad (8)$$

where Δx is the sensor separation.

Due to aliasing the fraction of frequency dependent wave speeds that can be extracted is limited to approximately:

$$St_{high} \leq \frac{u_c}{U_j}\frac{D}{2\Delta x} \qquad (9)$$

where the non-dimensional frequency, the Strouhal number is defined as $Sr = fD/U_j$, D is the nozzle diameter and U_j is the isentropic exit velocity.

Alternatively a narrow band-pass filter can be used in conjunction with the time delay cross-correlation technique discussed previously. This technique has found widespread application in earlier works, e.g., Goldschmidt (1981) , as well as Fisher and Davies (1964).

DATA PROCESSING

In order to determine the sensitivity of the data processing techniques to different input parameters a Monte-Carlo using synthetic data was performed. The signal is constructed from a one-dimensional model turbulent power spectrum (Pope, 2000) with random phase spectrum. The mean velocity and the turbulent intensity of the dataset are 650 m/s and 0.10 respectively.

The phase of this dataset is then evolved based on the separation between four flow sensors using an empirical fit given by Morris and Zaman (2010), thus creating a non-linear phase angle between the real and imaginary parts of the cross-spectrum between stations. The separation distances were the same as the actual physical sensor spacing used in this study.

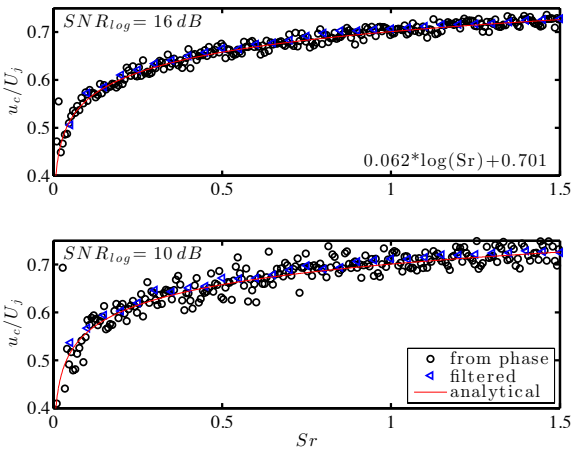

Figure 2. Reconstructed convective velocity for both phase method and band-pass filtered method.

The parameters for the model spectrum allow to include integral and Kolmogorov timescales, such that the inverse Fourier transform of the model provides realistic time-series data which is then is scaled and shifted to simulate the mean velocity and turbulence intensity found in a turbulent shear layer. Two processing techniques were considered: (1) reconstruction based on the phase angle, (2) digital band-pass filtering in combination with time delay cross-correlation processing. Figure 2 shows the reconstructed convective velocity profile using the phase method and the band-pass filter method for two signal to noise ratios.

Phase reconstruction method

From the cross-spectrum, which is found via matlab's CPSD function, the phase spectrum and convective wave speeds respectively are determined.

The input parameters investigated are: (1) ratio of averaged sets length S to dataset length *N* and (2) ratio of window length *W* (at 50% overlap) to set length *S* at a fixed dataset length ($N = 100k$ samples). Further (3) the signal to noise ratio SNR_{log}, (4) the type of window (Square, Hanning, Hamming) and the (5) magnitude of the convective wave speed u_c. Table 1 presents all the cases considered in this sensitivity analysis.

The influence of set and window length on the RMS error of the convective velocity estimate are shown in figure 3. The set length represents the number of samples the processing is performed on and the computed cross-spectrum is averaged before the phase-spectrum is determined. It is shown that a small set length and a small window size leads to lowest RMS errors. At low *SNR*, the RMS error is strongly impacted by the sensitivity of the phase spectrum to noise and uncertainties in the phase unwrapping process – especially at higher *W*/*S* and *S*/*N* ratios. Only a minimal sensitivity to the mean convective velocity, which imposes a time shift between the signals at the two stations, has been noted. Errors tend to be slightly higher for higher convective velocities as the phase angles are shallower and therefore more sensitive to noise.

Convective velocities at low frequencies were found to be inherently uncertain due to the small phase angle and the small statistical basis of those scales imposed by recording length. Those frequencies were excluded from the datasets by a lower cut-off frequency chosen as $f_{low} \geq 0.1 \frac{U_j}{2\Delta x}$.

Table 1. Monte Carlo parameters phase method.

Case	Window	*S/N*	*W/S*	SNR_{log}	u_c/U_j
HN1	Hanning	0.2	0.2	-5 - 20	profile
SQ1	Square	0.2	0.2	-5 - 20	profile
HM1	Hamming	0.2	0.2	-5 - 20	profile
HN2	Hanning	0.2-1	0.2-1	20	profile
HN3	Hanning	0.2	0.2	20	0.3-0.9

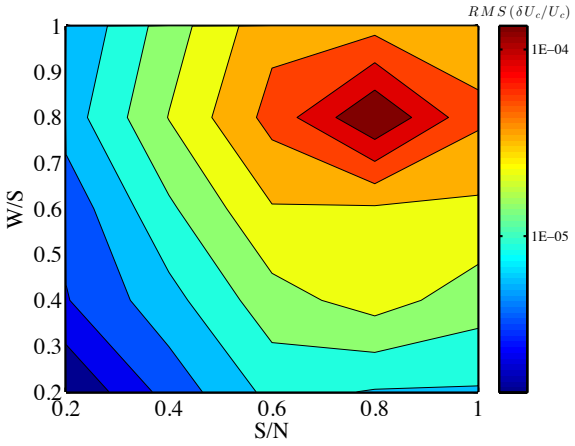

Figure 3. RMS error of the convective velocity estimate dependent on the window- and set-length (for a synthetic dataset (case HN2).

Digital band-pass filter method

The filter method was implemented by applying a narrow band-pas filter to the data set before performing a time delay cross-correlation processing. The digital band-pass filter used is based on a fast Fourier transform (FFT) method. The cases considered in the analysis of the performance of the filter method are summarized in table 2.

Table 2. Monte Carlo parameters filter method.

Case	Window	*S/N*	SNR_{log}	u_c/U
FHN	Hanning	0.2	-5 - 20	profile
FSQ	Square	0.2	-5 - 20	profile

Overall processing uncertainty

The dependence of the average root-mean-square (RMS) error on SNR_{log} and window type is shown in figure 4. The SNR_{log} in this case is defined as – and represents – the influence of measurement noise and loss of coherence between the signals at both stations. Comparing both processing techniques, explicit differences in SNR_{log} requirements arise; the phase method requires very high SNR_{log}, whereas the filter method is very robust even at SNR_{log} as low as 5 dB. Above 12.5 dB the error due to the processing is about $\mp 1\%$ of the u_c/U_j for the filter technique. Due to the robustness at low SNR_{log} the filter method is used to obtain all results presented within this study.

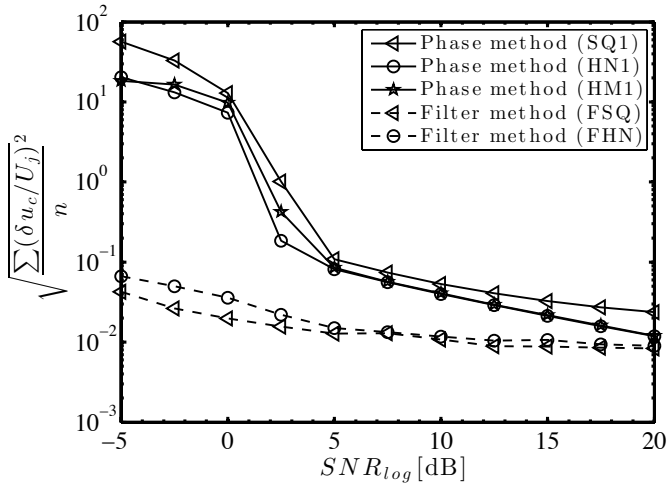

Figure 4. RMS error of the convective velocity dependent on the signal to noise ratio and the window type used (cases HN1, SQ1, HM1, FSQ, FHN).

EXPERIMENTAL APPARATUS AND FACILITY

DGV instrument

The laser-based time-resolved DGV (TR-DGV) concept has frequency response to 125 kHz and three-velocity-component capability at 32 simultaneous points in the flow and a contiguous acquisition time of greater than one second.

The development and application of the TR-DGV instrument and the PMT sensor system used, are documented in Ecker et al. (2014b, 2015).

The approach of using high repetition rate, long record and low spatial resolution offers a few key advantages. First, millions of velocity samples are used in statistical calculations, enabling the measurement of high order statistics such as fourth-order correlations at low standard error of the mean. Second, when measuring eddy convection, techniques based upon particle image velocimetry (PIV) have relied upon measurement of the structure function over long spatial distances but at much lower time resolution. In this, the fundamental measurement of eddy convective velocity suffers from the fact that the mean flow changes substantially over the 1 stream-wise distance considered, introducing some ambiguity of interpretation to the results. By measuring very high time response over a short stream-wise distance for correlation, the constant eddy convective concept is valid, providing ready interpretation.

Hot jet facility

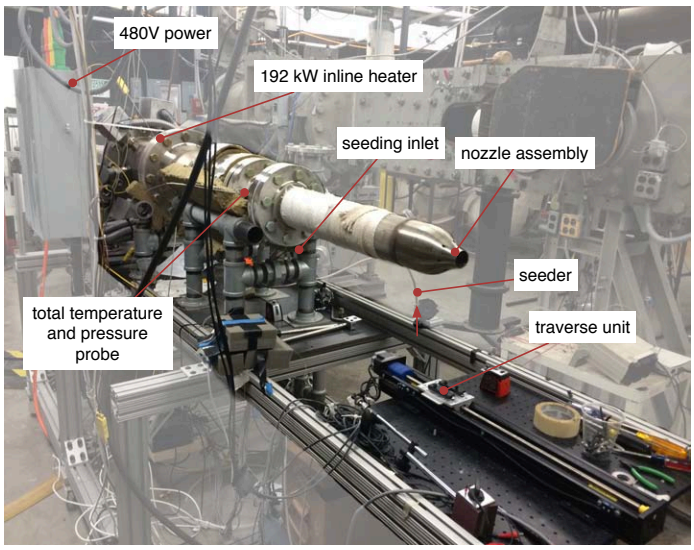

Figure 5. The Virginia Tech hot supersonic jet facility.

The Virginia Tech hot jet facility has been described in past works (Ecker et al., 2014a). This electrically heated (192 kW) free jet facility provides supersonic flow at total temperatures ratios, T_0/T_a up to 3 (depending on nozzle diameter) at 0.12 kg/s mass flow rate. The biconic nozzle used ($M_d = 1.65$) was adapted from the geometry studied by Powers and McLaughlin (2012) for military-style nozzles, differing in the present study by being axisymmetric. The diameter D of the nozzle is 1.5 in.

A photograph of the jet facility, including the locations for seeding inlet and total pressure and temperature measurement location is shown in figure 5. For improved mixing of the seed an extension of 2 ft has been appended to the nozzle assembly. For the hot flow studied, flow seeding is performed by introducing Al_2O_3 particles generated by a cyclone seeder unit. Bias errors in the jet's shear layer due to flow seeding gradients are minimized by co-flow seeding via entrainment from a smoke generator.

Test matrix and geometry

For this study two cases (A and B) at two different total temperature ratio (TTR) conditions at 4 different streamwise locations (x/D = 4, 6, 8 and 10) were experimentally investigated.

The parameters of the two cases are presented in table 3. Recording time length was 1 s with an effective data rate of 250 kHz.

Table 3. Hot jet cases.

Case	*Re*	M_j	ρ_j/ρ_a	*TTR*
A	1.3M	1.68	0.96	1.63
B	1.15M	1.70	0.79	2.0

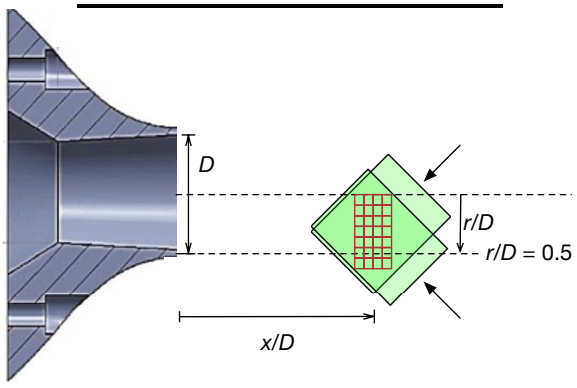

Figure 6. Nozzle and sensor configuration and nomenclature.

A drawing of the nozzle and the flow plane sensor configuration are displayed in figure 6. The streamwise coordinate *x/D* on the centerline is defined as the distance from the nozzle exit plane to the center of the flow plane sensor (red). The radial coordinate *r/D* is defined as the distance from the centerline to the each sensor pixel. The distance between pixels is 3 mm.

RESULTS

Mean flow statistics

The mean velocity and turbulence statistics have previously been investigated by Brooks and Lowe (2014). As shown in previous studies (Lau, 1980), the mean velocity as well as normal and shear stresses can be collapsed radially with a similarity scaling based on the radial location of 50% of the jet exit velocity and linear shear layer growth.

$$\eta^* = (r - r_{0.5U_j})/x \qquad (10)$$

The results for the mean velocity distribution of this jet, compared with results from studies by Kerhervé et al. (2004a) and Lau et al. (1979) are shown in figure 7. Generally the data by Brooks and Lowe show more scatter, in particular close to $\eta^* = 0$, which is assumed to be generated by the shock-cell structure present in the supersonic jet generated from the biconic nozzle. The data by Kerhervé et al. and Lau were measured in jet emerging from a contoured nozzle which at perfectly-expanded condition does not contain a shock-cell structure.

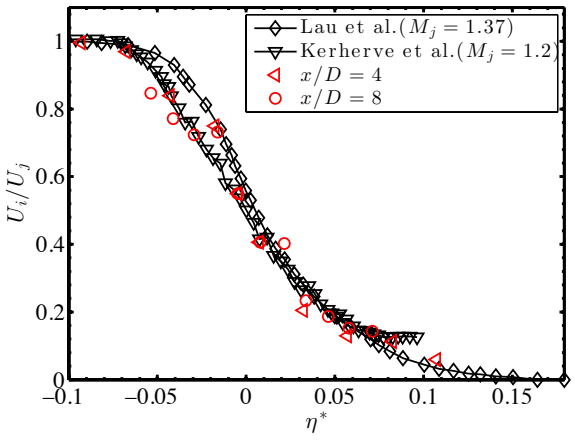

Figure 7. Similarity profiles for the streamwise mean velocity for case B at *x/D* = 4 and 8 compared to other studies.

Integral convective velocity distribution and scaling

Few studies of the radial distribution of the integral convective velocity in round incompressible and compressible jets exist. Applying the same similarity scaling, which successfully collapses the mean velocity, has only led to partial collapse for the case of the convective velocity.

We here propose a similarity scaling based on the symmetric convective Mach number and the density ratio. Simplified for perfectly expanded jets with equal gas properties for jet and ambient this leads to the following similarity coordinate.

$$\eta_c = (r - r_{0.5M_{c\,sym}})/x\,K^2 \qquad (11)$$

where[§]

$$K = \left(\frac{\rho_j}{\rho_a} + \frac{\gamma - 1}{2} M_{c\,sym}^2 \left[1 + \sqrt{\frac{\rho_j}{\rho_a}}\right]^2\right) \qquad (12)$$

This proposed similarity scaling is solely based on flow parameters and contains no empirical constant. For plane shear layers a factor of $\pi/4$ may need to be applied. K represents a simplified expression equivalent to an adjusted total temperature ratio.

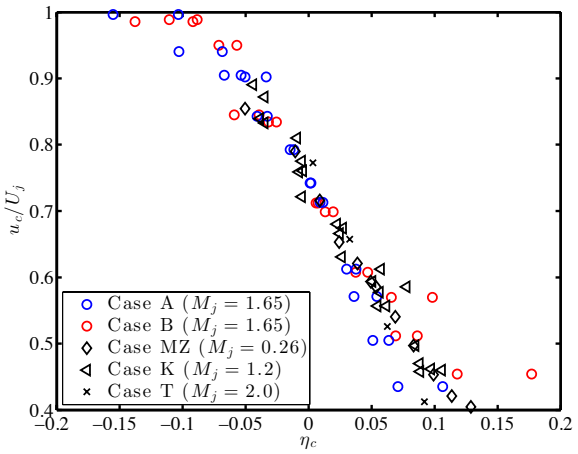

Figure 8. Similarity profiles for the streamwise integral convective velocity for case A and B (see table 3), as well as different literature cases (see table 4).

[§] For the case of a single stream jet exhausting into still air.

Figure 8 shows the successful collapse of convective velocity data from various Mach numbers and density ratios at different streamwise locations. The literature case parameters are summarized in table 4. The slightly higher scatter in the convective velocity distribution in this study may be explained due to the interaction of the convecting eddies with the shock-cell structure.

A polynomial fit of this data could be used to allow prediction of the distribution of the convective velocity within the shear layers of noise-producing high-speed jets.

Table 4. Literature cases.

Case	Reference	*Re*	M_j	ρ_j/ρ_a	*TTR*
MZ	Morris and Zaman 2010	0.24M	0.26	0.98	1.0
K	Kerhervé et al. 2004b	1.1M	1.2	0.77	1.0
T	Thurow 2005	2.6M	2.0	0.55	1.0

Convective velocity scaling with frequency

The scaling of the convective velocity with frequency has been investigated more in depth at four locations in the flow for case B. The convective velocity in the shear layer at a position before (*x/D = 8*) and close to the mean flow potential core length (*x/D = 10*) is shown in figure 9. At the position before the potential core length (see figure 9, top) a velocity distribution similar to previously reported data, e.g. by Morris and Zaman (2010), Kuo et al. (2011) or Goldschmidt et al. (1981) is observed. This distribution shows a strong increase of convective velocity up to $Sr = 0.5$, followed by a more gradual increase after. For the investigated frequencies, which are limited by temporal and spatial aliasing no convergence to the mean velocity value is observed. The distribution of the convective velocities further downstream presents very differently (figure 9, bottom); at low Sr numbers the convective velocity rises rapidly and reaches a distinctive peak close to the integral convective velocity value near $Sr = 0.45$. Following this the convective velocity decreases again to a plateau with a slightly increasing trend.

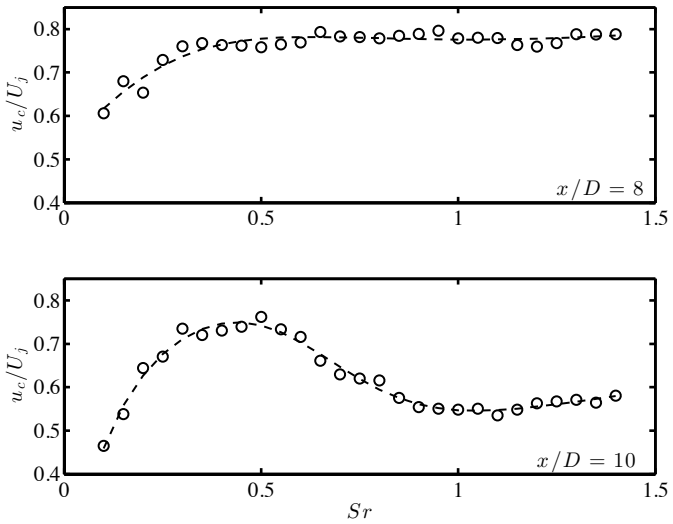

Figure 9. Convective velocity scaling with frequency at $r/D = 0.276$ at $x/D = 8$ (top) and $x/D = 10$ (bottom) for case B, circles are measured data, dashed line for visualization purposes.

The convective velocity data near the centerline is shown in figure 10. The velocity distribution shows similar features as before, but is less pronounced due to the vicinity of the potential core, which is not broken down completely.

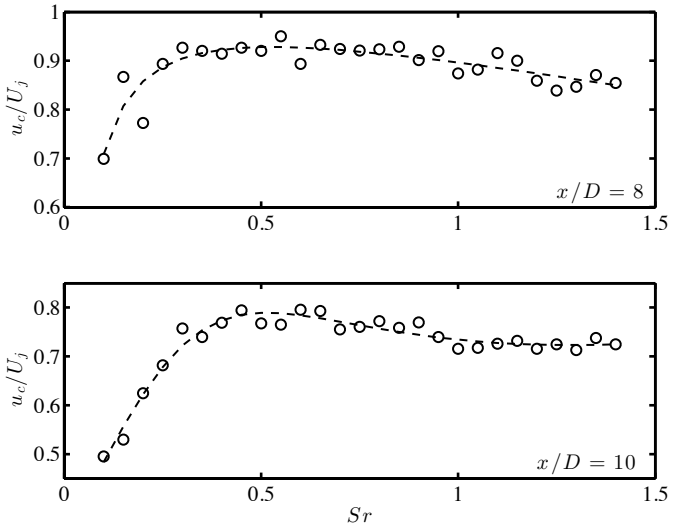

Figure 10. Convective velocity scaling with frequency at $r/D = 0.039$ at $x/D = 8$ (top) and $x/D = 10$ (bottom) for case B; circles are measured data, dashed line for visualization purposes.

DISCUSSION

The results presented above lay the basis to conceptually explain the high noise emissivity present in heated supersonic jets. Large scale turbulent eddies, energized from the mean flow potential core convect into regions of low mean velocity and create a region of eddies with high local convective Mach numbers. These high local convective Mach numbers directly impact the noise radiation efficiency causing high convective amplification factors pertinent to currently used acoustic analogies.

This conceptual relationship between of the eddy convection and radiation efficiency is displayed in figure 11. Highly energized eddies moving from region (I) into region (II) transport high momentum remnants of irrotational fluid from the potential core and create a zone with highest convective amplification values. This zone is located after and surrounding the mean flow potential core. These irrotaional fluid packets are then exposed to the shear layer mean velocity gradient, leading to the formation of ring vortex-like eddies.

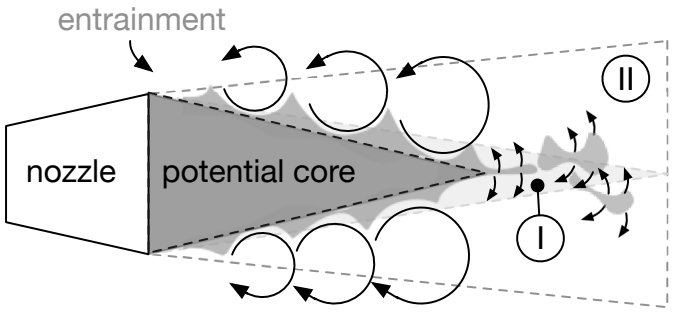

Figure 11. Conceptual relationship between the mean and convective velocity creating regions of high radiation efficiency.

This region, just beyond the potential core, has previously been identified as a strong sound-producing zone by Hileman and Samimy (2006). Similarly Mora et al. (2014) found significant growth of pressure fluctuation skewness values in the shear layer surrounding the potential core region. Results from a direct numerical simulation of a slightly heated $M_j = 1.92$ supersonic jet, coupled with a linear wave equation model for the far field indicate increased pressure fluctuations consistent with Mach wave radiation emanating from the end of the potential core (Freund et al., 2000). A qualitative interpretation of the dilatation contours indicates an increase in noise emission towards the location of the mean velocity potential core breakdown. Presented overall sound pressure levels corroborate this observation. Further, instantaneous velocity snapshots from recent large-eddy simulations (Khalighi

et al., 2010) for a jet with similar Mach number, Reynolds number and total temperature ratio show the presence of non continuous regions with high velocity, right at the end of the potential core, corroborating the present findings.

The present study indicates that the increased diffusion of the mean velocity field due to the heating leads to a pronounced effect of the radiation efficiency caused by eddy convective velocity overhead. This coupled with Mach wave radiation from supersonic phase speeds gives rise to strongly intensified noise emission by hot supersonic jets compared to their cold counterparts. Additionally the local static temperature distribution may influence the local acoustic Mach number, affecting the phase speed relative to ambient conditions.

It is also evident from the presented experimental convective velocity distributions and the observations made in past studies, that intermittency effects must play a key role and are strongly coupled with the process of fast convecting eddies entering the regions of locally low mean velocities. Core intermittency may also further contribute to the dynamics of the noise generation process at the end of the mean velocity potential core.

CONCLUSIONS

A heated supersonic jet at two different density ratios was experimentally investigated for the scaling of the eddy convective velocities. Radial profiles of the convective velocity were presented and successfully collapsed with previous data at different conditions by accounting for density ratio and symmetric convective Mach number. The difference in diffusion of the mean velocity field and the integral eddy convective velocity indicates regions of locally high convective Mach numbers and increased radiation efficiency. The investigation of the scaling of the convective velocity with frequency at several locations in the shear layer and near the centerline demonstrated the intrusion of high momentum, high velocity large-scale eddies into regions of locally reduced mean velocities. The region right after the potential core is identified as the main zone of this phenomenon. It is hypothesized that this large-scale turbulence intermittency effect, interacting with the increased spreading rate and the emergence of Mach wave radiation is one of the key drivers of noise emission observed in heated supersonic jets.

ACKNOWLEDGEMENTS

The Office of Naval Research Hot Jet Noise Reduction Basic Research Challenge and DURIP, grants N00014-11-1-0754 and N00014-12-1-0803 under program managers Drs. Brenda Henderson and Joseph Doychak, supported the work described.

REFERENCES

Bailly, C., Lafon, P., Sé, and Candel, B., 1997, "Subsonic and supersonic jet noise predictions from statistical source models", *AIAA Journal,* Vol. 35, No.11, pp. 1688-1696.

Brooks, D. R., & Lowe, K. T., 2014, "Fluctuating Flow Acceleration in a Heated Supersonic Jet", Presented at the 12th International Symposium on Applications of Laser Techniques to Fluid Mechanics, Lisbon.

de Kat, R., Gan, L., Dawson, J. R., and Ganapathisubramani, B., 2013, "Limitations of estimating turbulent convection velocities from PIV", *arXiv.org*.

Ecker, T., Brooks, D. R., Lowe, K. T., and Ng, W. F., 2014a, "Development and application of a point Doppler velocimeter featuring two-beam multiplexing for time-resolved measurements of high-speed flow", *Experiments in Fluids*, Vol. 55 No. 9, pp. 1–15.

Ecker, T., Lowe, K. T., and Ng, W. F., 2015, "A rapid response 64-channel photomultiplier tube camera for high-speed flow velocimetry", *Measurement Science and Technology*, Vol. 26, No. 2, 027001.

Ecker, T., Lowe, K. T., Ng, W. F., and Brooks, D. R., 2014b, "Fourth-order Spectral Statistics in the Developing Shear Layers of Hot Supersonic Jets", *Presented at the AIAA Propulsion and Power (50th AIAA/ASME/SAE/ASEE Joint Propulsion Conference), Cleveland, OH*.

Ffowcs Williams, J. E., and G. Maidanik, 1965, "The Mach wave field radiated by supersonic turbulent shear flows" ,Journal of Fluid Mechanics, Vol. 21, No. 04, pp. 641-657.

Fisher, M. J., and Davies, P. O. A. L., 1964, "Correlation measurements in a non-frozen pattern of turbulence", *Journal of Fluid Mechanics*, Vol. 18, pp. 97–116.

Freund, J. B., Lele, S. K., and Moin, P., 2000, "Numerical Simulation of a Mach 1.92 Turbulent Jet and Its Sound Field", *AIAA Journal,* Vol. 38, No. 11, pp. 2023-2031.

Goldschmidt, V. W., Young, M. F., and Ott, E. S., 1981, "Turbulent convective velocities (broadband and wavenumber dependent) in a plane jet", *Journal of Fluid Mechanics*, Vol. 105, pp. 327–345.

Hileman, J. I., and Samimy, M., 2006, "Mach Number Effects on Jet Noise Sources and Radiation to Shallow Angles", *AIAA Journal*, Vol. 44, No. 8, pp. 1915–1918.

Mora, P., Heeb, N., Kastner, J., Gutmark, E. J., and Kailasanath, K., 2014, "Impact of Heat on the Pressure Skewness and Kurtosis in Supersonic Jets", *AIAA Journal,* Vol. 52, No. 4, pp. 777–787.

Morris, P. J., and Zaman, K. B. M. Q., 2010, "Velocity measurements in jets with application to noise source

modeling", J*ournal of Sound and Vibration*, Vol. 329, No. 4, pp. 394–414.

Khalighi, Yaser, Frank Ham, Parviz Moin, Sanjiva K. Lele, Tim Colonius, Robert H. Schlinker, Ramons A. Reba, and John Simonich, 2010, "Unstructured large eddy simulation technology for prediction and control of jet noise", *In ASME Turbo Expo 2010: Power for Land, Sea, and Air*, pp. 57-70.

Kerhervé, F., Jordan, P., Gervais, Y., and Valiere, J. C., 2004a, "Two-point laser Doppler velocimetry measurements in a Mach 1.2 cold supersonic jet for statistical aeroacoustic source model", *Experiments in Fluids*, Vol. 37, No. 3, pp. 419–437.

Kerhervé, F., Power, O., Fitzpatrick, J., and Jordan, P., 2004b, "Determination of Turbulent Scales in Subsonic and Supersonic Jets from LDV Measurements", *Presented at the 12th International Symposium on Applications of Laser Techniques to Fluid Mechanics, Lisbon*.

Kuo, C. W., Powers, R., and McLaughlin, D. K., 2011, "Space-time correlation of flow and acoustic field measurements in supersonic helium-air mixture jets using optical deflectometry", *17th AIAA/CEAS Aeroacoustics Conference (32nd AIAA Aeroacoustics Conference), Portland, Oregon*.

Lau, J. C., 1980, "Laser velocimeter correlation measurements in subsonic and supersonic jets", *Journal of Sound and Vibration*, Vol. 70, No. 1, pp. 85–101.

Lau, J. C., Morris, P. J., and Fisher, M. J., 1979, "Measurements in subsonic and supersonic free jets using a laser velocimeter", *Journal of Fluid Mechanics*, Vol. 93, pp. 1–27.

Lighthill, M. J., 1952, "On Sound Generated Aerodynamically. I. General Theory", *Proceedings of the Royal Society A: Mathematical, Physical and Engineering Sciences*, Vol. 211, No. 1107, pp. 564–587.

Lowe, K. T., Ng, W. F., and Ecker, T., 2012, "Early Development of Time-Resolved Volumetric Doppler Velocimetry for New Insights in Hot Supersonic Jet Noise", *Presented at the 18th AIAA/CEAS Aeroacoustics Conference (33rd AIAA Aeroacoustics Conference), Colorado Springs, CO*.

Ribner, H. S., 1969, "Quadrupole correlations governing the pattern of jet noise", *Journal of Fluid Mechanics*, Vol. 38, pp. 1–24.

Papamoschou, D., 1997, "Mach wave elimination in supersonic jets", *AIAA Journal*, Vol. 35, No. 10, pp. 1604-1611.

Papamoschou, D., Xiong, J., and Liu, F., 2014, "Reduction of Radiation Efficiency in High-Speed Jets", *Presented at the AIAA Aviation, 20th AIAACEAS Aeroacoustics Conference, Atlanta, GA*.

Plumblee, H. E., Jr., 1974, "The Generation and Radiation of Supersonic Jet Exhaust Noise: A Progress Report on Studies of Jet Noise Generation and Radiation, Turbulence Structure and Laser Velocimetry", Technical report AD0787192.

Pope, S. B., 2000, *Turbulent Flows*, Cambridge University Press.

Powers, R. W., and McLaughlin, D. K., 2012, "Acoustic measurements of scale models of military style supersonic beveled nozzle jets with interior corrugations", *Presented at the 18th AIAA/CEAS Aeroacoustics Conference (33rd AIAA Aeroacoustics Conference), Colorado Springs, CO*.

Thurow, B. S., 2005, *On the convective velocity of large-scale structures in compressible axisymmetric jets,* PhD Thesis, The Ohio State University, Columbus, OH.

Wallace, J. M., 2014, "Space-time correlations in turbulent flow: A review", *Theoretical and Applied Mechanics Letters*, Vol. 4, No. 2.

Wills, J. A. B., 1964, "On convection velocities in turbulent shear flows", *Journal of Fluid Mechanics*, Vol. 20, No. 3, pp. 417–432.

Part VII.

Conclusions and outlook

This dissertation has focused on two main contributions: The first is the development of new instrumentation capable of time-resolved measurements in high speed compressible shear layers. The second contribution is using this newly developed experimental capability to investigate heated supersonic jets at conditions relevant to tactical aircraft noise.

1. Conclusions

The first study in this dissertation focused on the development of a new velocimetry instrument. It has expanded the current state of the art of Doppler global velocimetry (DGV) technology. The time-shift multiplexing is a new approach which allows the reduction of required sensor devices while still providing data rates suitable for high speed applications and low mean uncertainties. The presented geometrical configuration in combination with time-shift multiplexing is of interest, because it can be easily extended to allow planar and volumetric operation. From a study of the data processing and its induced errors, it was found that next to the geometric configuration, the flow time scales are of largest impact on the instantaneous uncertainties for this instrument. For time scales prevalent in supersonic jets, the instantaneous velocity errors due to processing were found to be about $\pm$6.1 m/s for the streamwise and radial components and around $\pm$1.0 m/s for the azimuthal velocity component. Via a detailed heuristic uncertainty analysis, the uncertainties of the linearized DGV transfer function and the data processing were propagated into a total measurement uncertainty for the instrument. The uncertainties for the presented instrument are about $\pm$1.5 m/s for mean measurements and between $\pm$6.6 and $\pm$11.1 m/s for instantaneous measurement of the three-component velocity vector. This study demonstrates that using velocity multiplexing is an effective method to reduce the instrument cost without sacrificing uncertainties. Further, the uncertainties for the instantaneous velocity vectors are mainly characterized by random effects such as signal-to-noise ratio, as well as temporal averaging effects; both of these can be addressed relatively easily by evolving the current technology. Another significant and often overlooked property, the transmission line width, is analyzed with respect to associated uncertainties for flows with high mean velocities and high turbulence intensities. Mean flow velocity measurements at different supersonic jet operating conditions have been validated by comparing with a laser Doppler velocimeter and are within the expected uncertainty range for DGV. The detailed flow results of this study are from measurements at a supersonic over-expanded condition. Both mean flow vectors and full Reynolds stress tensors were obtained along the streamwise coordinate for one radial position. Global data rates of above 100 kHz with local data rates as high as 250 kHz allowed spectral analysis of the Reynolds

stress tensors, indicating the screech tone phenomena. The results reveal helical screech modes with a spatial extent fundamentally different from the structures at under-expanded conditions. Compared to under-expanded conditions, shock unsteadiness and vortical nonlinear instability growth cause a more rapid breakdown of the potential core. The screech tone phenomenon and its higher harmonics are present throughout the potential core, as well as in regions of increased turbulent mixing. The influence of the screech phenomenon on the normal stresses quickly diminishes, but the signature of the screech remains remains visible in the radial–azimuthal shear stresses, and that may be connected to its production. This study shows the benefits time-resolved DGV can provide for understanding dominant turbulent structures for noise generation in supersonic jets, and it provides the basis for the ongoing development of time-resolved multi-point DGV instrumentation.

In order to continue the development of the instrument used in the first study, a new kind of photomultiplier (PMT) camera was developed and presented. This camera is based on a commercially available 64-channel PMT array and integrated with a commercial field-programmable-gated-arrays (FPGA) data acquisition system and custom high-speed amplifiers. The technical study summarizes the working principles of FPGA and gives examples on how inline processing can be integrated in a measurement system. It is shown that FPGA units give an attractive capability for rapid development of velocimetry instrumentation. The new rapid response, 64-channel PMT camera is useful for optical time- (up to 10MHz) and space-resolved optical flow velocimetry.

In the second study the rapid response PMT camera is integrated into a new time-resolved, 32-point DGV instrument and applied to a perfectly expanded supersonic jet at two different total temperature conditions (1.6 and 2 times the ambient temperature). The resulting instrument is capable of time-resolved measurements at 250 kHz and enables long duration velocimetry at very low statistical errors in cross-correlation processing. The main goal of this study is to extract more information on the statistics of the turbulent velocity fluctuations within heated supersonic jet plumes. In addition to the data acquired with the DGV system, single-point LDV data were presented and analyzed with respect to fourth-order statistics. The kurtosis of the streamwise term indicated deviations from Gaussian statistics at the lip line as well as the edges of the shear layer indicating intermittency effects. Second- and fourth-order time cross-correlation data for both cross-correlations were presented and used to determine integral correlation time scales. The integral time scale estimates showed good agreement with previous studies in the same facility The time delay of the cross-correlation was used to calculate the streamwise integral eddy convective velocity throughout the developing shear layer, producing values between 54-58% of the jet exit velocity on the lip line. This is significantly lower than the values in literature for unheated supersonic jets, mainly due to the increased divergence of the shear line for heated jets. The convective velocity maps show similar axial distribution when compared to recent large eddy calculations of cold subsonic jets. The distribution of the acoustic Mach number within the shear layer indicates that flow heating

results in faster eddies relative to the ambient sound speed which indicates the occurrence of Mach wave radiations and increased radiation efficiency. In its conclusion, this study demonstrates the application of a novel DGV instrument, generating eddy convective data and correlations for heated jet pertinent to jet noise prediction applications.

In the third study, the previously acquired data is analyzed for the scaling of the eddy convective velocities. It is shown how the radial profiles of the convective velocity and previous data at different conditions show similarity by accounting for the differences in density ratio and symmetric convective Mach number. The presented data at several locations in the shear layer and near the centerline demonstrated the presence of high momentum, high velocity large-scale eddies downstream of the potential core. The difference in the radial diffusion of the mean velocity field and the integral eddy convective velocity along the streamwise coordinate creates regions of locally high convective Mach numbers leading to high convective amplification factors causing higher noise intensity. The regions surrounding the end of the potential core, as well as the region downstream of the potential core, are identified as the main zones of this phenomenon. Inn particular, the region at the end of the potential core has been established as a strongly sound-producing region with strong pressure fluctuations in previous studies. Based on the presented data, it is hypothesized that the intermittent presence of large-scale turbulent structures in regions of reduced mean velocity leads to an increase of radiation efficiency. Coupled with the emergence of Mach wave radiation, these eddy speeds are likely the key drivers of noise emission observed in heated supersonic jets.

2. Outlook

There are many opportunities to build upon the work presented, and some recommendations for further investigation are listed to follow:

- The current database on Reynolds stresses, even in cold supersonic jets, is sparse. Extensive surveys in heated supersonic jets could contribute to the experimental database to be used for validation purposes for numerical jet noise prediction tools.
- Application of the presented correlations in an acoustic analogy should be compared to far field measurements.
- The nozzle used in this research was a biconic design, which is more realistic for jet noise applications. However, the use of contoured nozzles designed from the methods of characteristics may lead to an easier interpretation of the fundamental physics involved.
- Variation of the convective Mach number by using nozzles with different design Mach numbers would greatly add to the current experimental database for supersonic heated jets.

- Experimental investigation of the nozzle exit conditions could enable a better understanding of the influence of the jet initial conditions on the shear layer turbulence properties.
- Scale up and testing in mid- (e.g NASA Glenn) and full-scale testing facilities with simultaneous far field noise level measurements

Appendix

A. Limitation of the spatial resolution by diffraction

The spot size on the measurement plane can be determined from the sensor size and the system magnification as:

$$d_{geometric} = \frac{d}{M} \tag{A.1}$$

where d is the sensor spot size, and M is the magnification.

$$NA = \frac{0.5}{(M-1)(f/\#)} \tag{A.2}$$

where NA is the numerical aperture and $f/\#$ the relative aperture of the lens (in this case $f/\# = 1.4$).

The diffraction limited spot size can then be estimated as:

$$d_{diffraction} = \frac{\lambda}{2NA} \tag{A.3}$$

where λ is the wavelength of the light (in this case $\lambda = 532nm$)

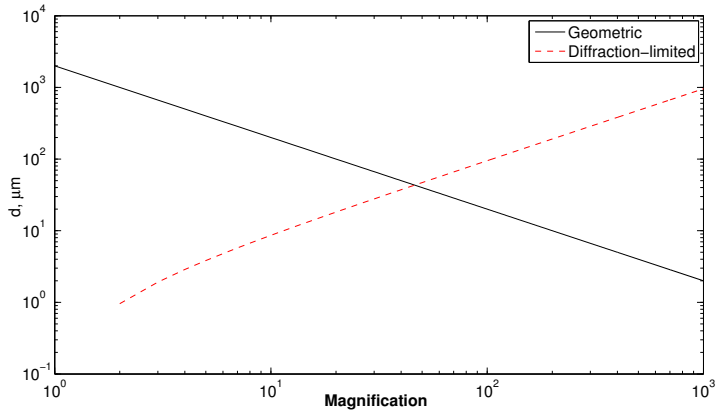

Figure A.1: Diffraction limited spot size compared to geometric spot size for different magnifications

The diffraction limited spot size for a $f/\# = 1.4$ optics as used in this research is about 36.5 µm (see figure A.1). Therefore the minimum spot size is 36.5 µm, where geometric magnification spot size equals the diffraction-limited spot size. As the magnification of the instrument used in this dissertation was much lower, the sensor spot was well resolved by geometric magnification.